Calhoun
Institutional Archive of the Naval Postgraduate School

Calhoun: The NPS Institutional Archive

DSpace Repository

Theses and Dissertations 1. Thesis and Dissertation Collection, all items

2008-09

Performance analysis of a Link-16/JTIDS compatible waveform transmitted over a channel with pulse-noise interference

Lekkakos, Dimitrios.

Monterey, California. Naval Postgraduate School

http://hdl.handle.net/10945/3889

This publication is a work of the U.S. Government as definedin Title 17, United States Code, Section 101. As such, it is in thepublic domain, and under the provisions of Title 17, United StatesCode, Section 105, is not copyrighted in the U.S.

Downloaded from NPS Archive: Calhoun

DUDLEY KNOX LIBRARY

Calhoun is the Naval Postgraduate School's public access digital repository for research materials and institutional publications created by the NPS community. Calhoun is named for Professor of Mathematics Guy K. Calhoun, NPS's first appointed -- and published -- scholarly author.

Dudley Knox Library / Naval Postgraduate School
411 Dyer Road / 1 University Circle
Monterey, California USA 93943

http://www.nps.edu/library

NAVAL POSTGRADUATE SCHOOL

MONTEREY, CALIFORNIA

THESIS

PERFORMANCE ANALYSIS OF A LINK-16/JTIDS COMPATIBLE WAVEFORM TRANSMITTED OVER A CHANNEL WITH PULSE-NOISE INTERFERENCE

by

Dimitrios Lekkakos

September 2008

Thesis Advisor:	Ralph C. Robertson
Second Reader:	Tri Ha

Approved for public release; distribution unlimited

THIS PAGE INTENTIONALLY LEFT BLANK

REPORT DOCUMENTATION PAGE	*Form Approved OMB No. 0704-0188*

Public reporting burden for this collection of information is estimated to average 1 hour per response, including the time for reviewing instruction, searching existing data sources, gathering and maintaining the data needed, and completing and reviewing the collection of information. Send comments regarding this burden estimate or any other aspect of this collection of information, including suggestions for reducing this burden, to Washington headquarters Services, Directorate for Information Operations and Reports, 1215 Jefferson Davis Highway, Suite 1204, Arlington, VA 22202-4302, and to the Office of Management and Budget, Paperwork Reduction Project (0704-0188) Washington DC 20503.

1. AGENCY USE ONLY *(Leave blank)*	**2. REPORT DATE** September 2008	**3. REPORT TYPE AND DATES COVERED** Master's Thesis

4. TITLE AND SUBTITLE: Performance Analysis of a Link-16/JTIDS Compatible Waveform Transmitted Over a Channel with Pulse-Noise Interference.	**5. FUNDING NUMBERS**
6. AUTHOR Dimitrios Lekkakos	
7. PERFORMING ORGANIZATION NAME(S) AND ADDRESS(ES) Naval Postgraduate School Monterey, CA 93943-5000	**8.PERFORMING ORGANIZATION REPORT NUMBER**
9. SPONSORING /MONITORING AGENCY NAME(S) AND ADDRESS(ES) N/A	**10. SPONSORING/MONITORING AGENCY REPORT NUMBER**

11. SUPPLEMENTARY NOTES The views expressed in this thesis are those of the author and do not reflect the official policy or position of the Department of Defense or the U.S. Government.

12a. DISTRIBUTION / AVAILABILITY STATEMENT Approved for public release; distribution unlimited	**12b. DISTRIBUTION CODE** A

13. ABSTRACT (maximum 200 words)

The Joint Tactical Information Distribution System (JTIDS) is a hybrid frequency-hoped, direct sequence spread spectrum system that utilizes a (31, 15) Reed-Solomon (RS) code and cyclical code-shift keying (CCSK) modulation for the data packets, where each encoded symbol consists of five bits. In this thesis, an alternative waveform consistent with the existing JTIDS channel waveform is analyzed. The system to be considered uses (31, 15) RS encoding as the original JTIDS, but each pair of five-bit symbols at the output of the RS encoder undergo serial-to-parallel conversion to two five-bit symbols, which are then independently transmitted on the in-phase (I) and quadrature (Q) component of the carrier using 32-ary orthogonal signaling with 32 chip baseband waveforms such as Walsh functions. This system is consistent with the direct sequence waveform generated by JTIDS. The performance obtained with alternative waveform is compared with that obtained with the existing JTIDS waveform for the relatively benign case where additive white Gaussian noise (AWGN) is the only noise present as well as when pulse-noise interference (PNI) is present. Errors-and-erasures decoding (EED) as well as errors only decoding is also considered. Based on the analyses, we conclude that the proposed alternative Link-16/JTIDS compatible waveform performs better than the existing Link-16/JTIDS waveform in AWGN as well as when PNI is present for both coherent and noncoherent demodulation. No significant advantage is obtained by using errors-and-erasures decoding (EED) for the alternative Link-16/JTIDS compatible waveform.

14. SUBJECT TERMS Link-16/JTIDS, (31, 15) Reed-Solomon (RS) coding, 32-ary Orthogonal signaling, Additive White Gaussian Noise (AWGN), Pulse-Noise Interference (PNI), Error-and-Erasures decoding (EED).	**15. NUMBER OF PAGES** 110
	16. PRICE CODE

17. SECURITY CLASSIFICATION OF REPORT Unclassified	**18. SECURITY CLASSIFICATION OF THIS PAGE** Unclassified	**19. SECURITY CLASSIFICATION OF ABSTRACT** Unclassified	**20. LIMITATION OF ABSTRACT** UU

NSN 7540-01-280-5500

Standard Form 298 (Rev. 2-89)
Prescribed by ANSI Std. 239-18

THIS PAGE INTENTIONALLY LEFT BLANK

Approved for public release; distribution unlimited

PERFORMANCE ANALYSIS OF A LINK-16/JTIDS COMPATIBLE WAVEFORM TRANSMITTED OVER A CHANNEL WITH PULSE-NOISE INTERFERENCE

Dimitrios Lekkakos
Lieutenant, Hellenic Navy
Bachelor of Naval Science, Hellenic Naval Academy, 1999

Submitted in partial fulfillment of the
requirements for the degrees of

MASTER OF SCIENCE IN ELECTRONIC WARFARE SYSTEM ENGINEERING

and

MASTER OF SCIENCE IN ELECTRICAL ENGINEERING

from the

NAVAL POSTGRADUATE SCHOOL
September 2008

Author:	Dimitrios Lekkakos
Approved by:	Ralph C. Robertson Thesis Advisor
	Tri Ha Second Reader
	Jeffrey B. Knorr Chairman, Department of Electrical and Computer Engineering
	Dan C. Boger Chairman, Department of Information Sciences

THIS PAGE INTENTIONALLY LEFT BLANK

ABSTRACT

The Joint Tactical Information Distribution System (JTIDS) is a hybrid frequency-hoped, direct sequence spread spectrum system that utilizes a (31, 15) Reed-Solomon (RS) code and cyclical code-shift keying (CCSK) modulation for the data packets, where each encoded symbol consists of five bits. In this thesis, an alternative waveform consistent with the existing JTIDS channel waveform is analyzed. The system to be considered uses (31, 15) RS encoding as the original JTIDS, but each pair of five-bit symbols at the output of the RS encoder undergo serial-to-parallel conversion to two five-bit symbols, which are then independently transmitted on the in-phase (I) and quadrature (Q) component of the carrier using 32-ary orthogonal signaling with 32 chip baseband waveforms such as Walsh functions. This system is consistent with the direct sequence waveform generated by JTIDS. The performance obtained with alternative waveform is compared with that obtained with the existing JTIDS waveform for the relatively benign case where additive white Gaussian noise (AWGN) is the only noise present as well as when pulse-noise interference (PNI) is present. Errors-and-erasures decoding (EED) as well as errors only decoding is also considered.

Based on the analyses, we conclude that the proposed alternative Link-16/JTIDS compatible waveform performs better than the existing Link-16/JTIDS waveform in AWGN as well as when PNI is present for both coherent and noncoherent demodulation. No significant advantage is obtained by using errors-and-erasures decoding (EED) for the alternative Link-16/JTIDS compatible waveform.

THIS PAGE INTENTIONALLY LEFT BLANK

TABLE OF CONTENTS

I. INTRODUCTION 1
  - A. OVERVIEW 1
  - B. THESIS OBJECTIVE 1
  - C. THESIS OUTLINE 2

II. BACKGROUND 3
  - A. *M*-ARY ORTHOGONAL SIGNALS 3
  - B. PERFORMANCE OF *M*-ARY ORTHOGONAL SIGNALING IN AWGN 6
  - C. PERFORMANCE IN AWGN WITH PULSED-NOISE INTERFERENCE 7
  - D. FORWARD ERROR CORRECTION CODING 8
  - E. ERRORS-AND-ERASURES DECODING 9
  - F. CHAPTER SUMMARY 10

III. PERFORMANCE ANALYSIS OF 32-ARY ORTHOGONAL SIGNALING WITH (31,15) RS ENCODING IN AWGN 11
  - A. COHERENT DEMODULATION 11
  - B. NONCOHERENT DEMODULATION 12
  - C. COMPARISON OF THE PERFORMANCE OBTAINED WITH COHERENT AND NONCOHERENT DEMODULATION 14
  - D. CHAPTER SUMMARY 15

IV. PERFORMANCE ANALYSIS OF 32-ARY ORTHOGONAL SIGNALING WITH (31,15) RS ENCODING IN AWGN AND PULSE-NOISE INTERFERENCE 17
  - A. COHERENT DEMODULATION 17
  - B. NONCOHERENT DEMODULATION 19
  - C. COMPARISON BETWEEN COHERENT AND NON-COHERENT DEMODULATION 21
  - D. CHAPTER SUMMARY 25

V. COMPARISON OF THE PERFORMANCE OF 32-ARY ORTHOGONAL SIGNALING WITH (31,15) RS ENCODING TO THAT OF THE JTIDS WAVEFORM 27
  - A. ORIGINAL JTIDS WAVEFORM IN AWGN 27
    - 1. Coherent Demodulation 27
    - 2. Noncoherent Demodulation 28
    - 3. Comparison Between Coherent and Noncoherent Demodulation for the Original JTIDS Waveform in AWGN 29
  - B. JTIDS WAVEFORM IN AWGN AND PNI 30
    - 1. Coherent Demodulation 30
    - 2. Noncoherent Demodulation 33

        - 3. Comparison Between Coherent and Noncoherent Demodulation for the Original JTIDS Waveform in AWGN and PNI with E_b / N_o =10 dB 36
        - 4. Comparison Between Coherent and Noncoherent Demodulation for the Original JTIDS Waveform in AWGN and PNI with Different Values of E_b / N_I 40
    - C. COMPARISON OF 32-ARY ORTHOGONAL SIGNALING WITH (31,15) ENCODING WITH THE JTIDS WAVEFORM IN AN AWGN ENVIRONMENT......44
        - 1. Coherent Demodulation 44
        - 2. Noncoherent Demodulation 45
    - D. COMPARISON OF 32-ARY ORTHOGONAL SIGNALING WITH (31, 15) ENCODING WITH THE JTIDS WAVEFORM IN BOTH AWGN AND PNI 46
        - 1. Coherent Demodulation 46
        - 2. Noncoherent Demodulation 49
    - E. CHAPTER SUMMARY......53
- VI. PERFORMANCE ANALYSIS OF 32-ARY ORTHOGONAL SIGNALING WITH (31,15) RS ENCODING IN AN AWGN AND PULSE-NOISE INTERFERENCE ENVIRONMENT WITH ERRORS-AND-ERASURES DECODING......55
    - A. COHERENT DEMODULATION IN AWGN 55
    - B. NONCOHERENT DEMODULATION IN AWGN 60
    - C. COHERENT DEMODULATION IN AWGN AND PNI......66
    - D. NONCOHERENT DEMODULATION IN AWGN AND PNI......75
    - E. CHAPTER SUMMARY......84
- VII. CONCLUSIONS AND FUTURE WORK 85
    - A. CONCLUSIONS 85
    - B. FUTURE RESEARCH AREAS 85
- LIST OF REFERENCES......87
- INITIAL DISTRIBUTION LIST 90

LIST OF FIGURES

Figure 1. Block diagram of a coherent *M*-ary orthogonal baseband waveform demodulator (From: [6]). 4
Figure 2. Block diagram of a noncoherent *M*-ary orthogonal baseband waveform demodulator (From: [6]). 6
Figure 3. Performance of 32-ary orthogonal signaling with (31, 15) RS encoding in AWGN for coherent demodulation. 12
Figure 4. Performance of 32-ary orthogonal signaling with (31, 15) RS encoding in AWGN for noncoherent demodulation. 13
Figure 5. Comparison of the performance of coherent and noncoherent demodulation for the alternative waveform in AWGN. 14
Figure 6. Performance of 32-ary orthogonal signaling with (31, 15) RS encoding for different values of ρ in both AWGN and PNI for coherent demodulation with $E_b / N_o = 10$ dB. 18
Figure 7. Performance of 32-ary orthogonal signaling with (31, 15) RS encoding for different values of ρ in both AWGN and PNI for noncoherent demodulation with $E_b / N_o = 10$ dB. 20
Figure 8. Comparison of the performance of the alternative waveform with both AWGN and BNI for coherent and noncoherent demodulation. 22
Figure 9. Comparison of the performance of the alternative waveform for $\rho = 0.2$ with both AWGN and PNI for coherent and noncoherent demodulation. 23
Figure 10. Comparison of the performance of the alternative waveform for $\rho = 0.1$ with both AWGN and PNI for coherent and noncoherent demodulation. 24
Figure 11. Performance of the original JTIDS waveform in AWGN for coherent demodulation. 28
Figure 12. Performance of the original JTIDS in AWGN for noncoherent demodulation. 29
Figure 13. Comparison of coherent and noncoherent demodulation of the original JTIDS waveform in AWGN. 30
Figure 14. Performance of the original JTIDS waveform with different values of ρ in both AWGN and PNI for coherent demodulation when E_b / N_o =10 dB. 32
Figure 15. Performance of the original JTIDS waveform with different values of ρ in both AWGN and PNI for noncoherent demodulation when E_b / N_o =10 dB. 35
Figure 16. Comparison of the performance of the original JTIDS waveform in both AWGN and PNI with $\rho = 1$ for coherent and noncoherent demodulation when E_b / N_o =10 dB. 36
Figure 17. Comparison of the performance of the original JTIDS waveform in both AWGN and PNI with $\rho = 0.2$ for coherent and noncoherent demodulation when E_b / N_o =10 dB. 37

Figure 18. Comparison of the performance of the original JTIDS waveform in both AWGN and PNI with $\rho = 0.1$ for coherent and noncoherent demodulation when E_b / N_o =10 dB.....38

Figure 19. Comparison of the performance of the original JTIDS waveform in both AWGN and PNI with $\rho = 0.05$ for coherent and noncoherent demodulation when E_b / N_o =10 dB.....39

Figure 20. Comparison of the performance of the original JTIDS waveform with $\rho = 1$ in both AWGN and PNI for coherent and noncoherent demodulation.....41

Figure 21. Comparison of the performance of the original JTIDS waveform with $\rho = 0.2$ in both AWGN and PNI for coherent and noncoherent demodulation.....42

Figure 22. Comparison of the performance of the original JTIDS waveform with $\rho = 0.1$ in both AWGN and PNI for coherent and noncoherent demodulation.....43

Figure 23. Comparison of 32-ary orthogonal signaling with (31, 15) RS encoding with the original JTIDS waveform in AWGN for coherent demodulation. 44

Figure 24. Comparison of 32-ary orthogonal signaling with (31, 15) RS encoding with the original JTIDS waveform in AWGN for noncoherent demodulation.....45

Figure 25. Comparison of 32-ary orthogonal signaling with (31, 15) encoding with the JTIDS waveform in both AWGN and PNI with $\rho = 1$ for coherent demodulation when E_b / N_o =10 dB.....46

Figure 26. Comparison of 32-ary orthogonal signaling with (31, 15) encoding with the JTIDS waveform in both AWGN and PNI with $\rho = 0.2$ for coherent demodulation when E_b / N_o =10 dB.....47

Figure 27. Comparison of 32-ary orthogonal signaling with (31, 15) encoding with the JTIDS waveform in both AWGN and PNI with $\rho = 0.1$ for coherent demodulation when E_b / N_o =10 dB.....48

Figure 28. Comparison of 32-ary orthogonal signaling with (31, 15) encoding with the JTIDS waveform in both AWGN and PNI with $\rho = 1$ for noncoherent demodulation when E_b / N_o =10 dB.....50

Figure 29. Comparison of 32-ary orthogonal signaling with (31, 15) encoding with the JTIDS waveform in both AWGN and PNI with $\rho = 0.2$ for noncoherent demodulation when E_b / N_o =10 dB.....51

Figure 30. Comparison of 32-ary orthogonal signaling with (31, 15) encoding with the JTIDS waveform in both AWGN and PNI with $\rho = 0.1$ for the noncoherent demodulation when E_b / N_o =10 dB.....52

Figure 31. The performance of 32-ary orthogonal signaling with a (31, 15) RS code and EED in AWGN for different values of α for coherent demodulation. 59

Figure 32. The performance of 32-ary orthogonal signaling with a (31, 15) RS code and EED in AWGN for different values of α for coherent demodulation. 60
Figure 33. The performance of 32-ary orthogonal signaling with a (31, 15) RS code and EED in AWGN for different values of α for noncoherent demodulation...65
Figure 34. The performance of 32-ary orthogonal signaling with a (31, 15) RS code and EED in AWGN for different values of α for noncoherent demodulation...66
Figure 35. The performance of 32-ary orthogonal signaling with EED in AWGN and PNI for different values of α with $\rho = 0.1$ for coherent demodulation when $E_b / N_0 = 10$ dB 68
Figure 36. The performance of 32-ary orthogonal signaling with EED in AWGN and PNI for different values of α with $\rho = 0.2$ for coherent demodulation when $E_b / N_0 = 10$ dB 69
Figure 37. The performance of 32-ary orthogonal signaling with EED in AWGN and PNI for different values of α with $\rho = 1$ for coherent demodulation when $E_b / N_0 = 10$ dB 70
Figure 38. The performance of 32-ary orthogonal signaling with EED in AWGN and PNI with $\alpha = 0.5$ and $E_b / N_0 = 10$ dB for different values of ρ for coherent demodulation..71
Figure 39. The performance of 32-ary orthogonal signaling with EED in AWGN and PNI for different values of α with $\rho = 0.1$ for coherent demodulation when $E_b / N_0 = 6.8$ dB 72
Figure 40. The performance of 32-ary orthogonal signaling with EED in AWGN and PNI for different values of α with $\rho = 0.2$ for coherent demodulation when $E_b / N_0 = 6.8$ dB 73
Figure 41. The performance of 32-ary orthogonal signaling with EED in AWGN and PNI for different values of α with $\rho = 1$ for coherent demodulation when $E_b / N_0 = 6.8$ dB 74
Figure 42. The performance of 32-ary orthogonal signaling with EED in AWGN and PNI with $\alpha = 0.3$ and $E_b / N_0 = 6.8$ dB for different values of ρ for coherent demodulation..75
Figure 43. The performance of 32-ary orthogonal signaling with EED in AWGN and PNI for different values of α with $\rho = 0.1$ and for noncoherent demodulation when $E_b / N_0 = 10$ dB 77
Figure 44. The performance of 32-ary orthogonal signaling with EED in AWGN and PNI for different values of α with $\rho = 0.2$ and for noncoherent demodulation when $E_b / N_0 = 10$ dB 78

Figure 45. The performance of 32-ary orthogonal signaling with EED in AWGN and PNI for different values of α with $\rho = 1$ and for noncoherent demodulation when $E_b / N_0 = 10$ dB 79
Figure 46. The performance of 32-ary orthogonal signaling with EED in AWGN and PNI with $\alpha = 0.3$ and $E_b / N_0 = 10$ dB for and different values of ρ for noncoherent demodulation. 80
Figure 47. The performance of 32-ary orthogonal signaling with EED in AWGN and PNI for different values of α with $\rho = 0.1$ and for noncoherent demodulation when $E_b / N_0 = 6.8$ dB 81
Figure 48. The performance of 32-ary orthogonal signaling with EED in AWGN and PNI for different values of α with $\rho = 0.2$ and for noncoherent demodulation when $E_b / N_0 = 6.8$ dB 82
Figure 49. The performance of 32-ary orthogonal signaling with EED in AWGN and PNI for different values of α with $\rho = 1$ and for noncoherent demodulation when $E_b / N_0 = 6.8$ dB 83
Figure 50. The performance of 32-ary orthogonal signaling with EED in AWGN and PNI with $\alpha = 0.3$ and $E_b / N_0 = 6.8$ dB for and different values of ρ for noncoherent demodulation. 84

LIST OF TABLES

Table 1. Performance of 32-ary orthogonal signaling with (31, 15) RS encoding for different values of ρ in both AWGN and PNI for coherent demodulation when $P_b = 10^{-5}$ 19
Table 2. Performance of 32-ary orthogonal signaling with (31, 15) RS encoding for different values of ρ in both AWGN and PNI for noncoherent demodulation when $P_b = 10^{-5}$ 21
Table 3. Comparison of the performance of the alternative waveform with both AWGN and BNI for coherent and noncoherent demodulation when $P_b = 10^{-5}$ 23
Table 4. Comparison of the performance of the alternative waveform for $\rho = 0.2$ with both AWGN and PNI for coherent and noncoherent demodulation when $P_b = 10^{-5}$ 24
Table 5. Comparison of the performance of the alternative waveform for $\rho = 0.1$ with both AWGN and PNI for coherent and noncoherent demodulation when $P_b = 10^{-5}$ 25
Table 6. Performance of the original JTIDS waveform with different values of ρ in both AWGN and PNI for coherent demodulation when $P_b = 10^{-5}$ and E_b / N_o =10 dB. 33
Table 7. Performance of the original JTIDS waveform with different values of ρ in both AWGN and PNI for noncoherent demodulation when $P_b = 10^{-5}$ and E_b / N_o =10 dB. 35
Table 8. Comparison of the performance of the original JTIDS waveform in both AWGN and PNI with $\rho = 1$ for coherent and noncoherent demodulation when $P_b = 10^{-5}$ and E_b / N_o =10 dB. 37
Table 9. Comparison of the performance of the original JTIDS waveform in both AWGN and PNI with $\rho = 0.2$ for coherent and noncoherent demodulation when $P_b = 10^{-5}$ and E_b / N_o =10 dB. 38
Table 10. Comparison of the performance of the original JTIDS waveform in both AWGN and PNI with $\rho = 0.1$ for coherent and noncoherent demodulation when $P_b = 10^{-5}$ and E_b / N_o =10 dB. 39
Table 11. Comparison of the performance of the original JTIDS waveform with $\rho = 1$ in both AWGN and PNI for coherent and noncoherent demodulation when $P_b = 10^{-5}$ 41

Table 12. Comparison of the performance of the original JTIDS waveform with $\rho = 0.2$ in both AWGN and PNI for coherent and noncoherent demodulation when $P_b = 10^{-5}$ 42
Table 13. Comparison of the performance of the original JTIDS waveform with $\rho = 0.1$ in both AWGN and PNI for coherent and noncoherent demodulation when $P_b = 10^{-5}$ 43
Table 14. Comparison of 32-ary orthogonal signaling with (31, 15) encoding with the JTIDS waveform in both AWGN and PNI with $\rho = 1$ for coherent demodulation when $P_b = 10^{-5}$ and E_b / N_o =10 dB. 47
Table 15. Comparison of 32-ary orthogonal signaling with (31, 15) encoding with the JTIDS waveform in both AWGN and PNI with $\rho = 0.2$ for coherent demodulation when $P_b = 10^{-5}$ and E_b / N_o =10 dB. 48
Table 16. Comparison of 32-ary orthogonal signaling with (31, 15) encoding with the JTIDS waveform in both AWGN and PNI with $\rho = 0.1$ for coherent demodulation when $P_b = 10^{-5}$ and E_b / N_o =10 dB. 49
Table 17. Comparison of 32-ary orthogonal signaling with (31, 15) encoding with the JTIDS waveform in both AWGN and PNI with $\rho = 1$ for noncoherent demodulation when $P_b = 10^{-5}$ and E_b / N_o =10 dB. 50
Table 18. Comparison of 32-ary orthogonal signaling with (31, 15) encoding with the JTIDS waveform in both AWGN and PNI with $\rho = 0.2$ for noncoherent demodulation when $P_b = 10^{-5}$ and E_b / N_o =10 dB. 51
Table 19. Comparison of 32-ary orthogonal signaling with (31,15) encoding with the JTIDS waveform in both AWGN and PNI with $\rho = 0.1$ for noncoherent demodulation when $P_b = 10^{-5}$ and E_b / N_o =10 dB. 52

EXECUTIVE SUMMARY

Tactical data links (TDL) have played a vital role in modern military strategy and have attracted much attention since they form the basis of technology that supports Network Centric Warfare. In order to provide a real-time exchange of tactical data to all participants, tactical data links must be able to effectively achieve and manage all of the battle information in a modern warfare battlefield.

The Joint Tactical Information Distribution System (JTIDS)/Link-16 is a message tactical data link which is used by naval, joint service and NATO units from different countries around the world. It provides digital communication of both data and voice for command and control, relative positioning, identification, navigation, and situational awareness.

Link-16/JTIDS operates in the L-band and is a hybrid frequency-hopped, direct sequence spread spectrum system that utilizes a (31, 15) Reed-Solomon (RS) code and cyclical code-shift keying (CCSK) modulation for the data packets, where each encoded symbol consists of five bits. In this thesis, an alternative waveform consistent with the existing JTIDS channel waveform was analyzed. The system considered uses (31, 15) RS encoding as the original JTIDS, but each pair of five-bit symbols at the output of the RS encoder undergo serial-to-parallel conversion to two five-bit symbols, which are then independently transmitted on the in-phase (I) and quadrature (Q) component of the carrier using 32-ary orthogonal signaling with 32 chip baseband waveforms such as Walsh functions. This system is consistent with the direct sequence waveform generated by JTIDS. The performance obtained with the alternative waveform was compared with that obtained with the existing JTIDS waveform for the relatively benign case where additive white Gaussian noise (AWGN) is the only noise present as well as when pulse-noise interference (PNI) is present. Errors-and-erasures decoding (EED) as well as errors only decoding was also considered.

Based on the analyses and results of this thesis, we conclude that the proposed alternative Link-16/JTIDS compatible waveform performs 1.7 dB and 1.4 dB better than the existing Link-16/JTIDS waveform in AWGN for coherent and noncoherent demodulation, respectively. When PNI is present, the alternative waveform outperforms the existing waveform by 2.8 dB and 3.1 dB for coherent and noncoherent demodulation, respectively, when $E_b / N_0 = 10$ dB. No significant advantage is obtained by using errors-and-erasures decoding (EED) for the alternative Link-16/JTIDS compatible waveform.

ACKNOWLEDGMENTS

I dedicate this work to my beloved mother, Styliani Dermanoutsou, for the educational enlightenment and the generous support she has given me during my educational and military career.

I would also like to devote this work to my lovely wife, Despoina Karagiannidou, and my wonderful daughter, Kyriaki Lekkakou for their continuous loving support and the happiness that they bring to my life.

Also, I would like to extend my sincere appreciation to Professor Clark Robertson for his constant support, guidance and encouragement in order to complete this work and thank Professor Tri Ha as my second reader for reviewing this thesis.

Finally, I am grateful to the Hellenic Navy for giving me the opportunity to expand my educational horizons at Naval Postgraduate School.

THIS PAGE INTENTIONALLY LEFT BLANK

I. INTRODUCTION

A. OVERVIEW

Tactical data links (TDL) have played a vital role in modern military strategy and attracted much attention since they form the basis of technology that supports Network Centric Warfare. In order to provide a real-time exchange of tactical data to all participants, tactical data links must be able to manage all battle information in today's modern warfare battlefield.

Link-16/Joint Tactical Information Distribution System (JTIDS) operates in the L-band and is a good example of a waveform designed to resist interference. Link-16/JTIDS uses a combination of time-division multiple access, frequency-hopping, direct sequence spread spectrum, Reed Solomon (RS) encoding and cyclical code-shift keying (CCSK) modulation. Link-16/JTIDS produces a 32-chip sequence with CCSK modulation to represent each 5-bit symbol, and the individual chips are transmitted using minimum-shift keying (MSK) modulation.

A primary drawback to JTIDS is the limited data throughput which makes it ill suited for the transmission of large blocks of data. This constrains its usage to situational awareness functions, command and control, and derivative functions such as weapon guidance [1].

B. THESIS OBJECTIVE

Some enhancements to JTIDS have been introduced to alleviate problems arising from its basic design. One enhancement is Link-16 Enhanced Throughput (LET), which leads to increased throughput. For LET, the spread spectrum and RS encoding of the original JTIDS waveform are replaced with a combined RS and convolutional coding scheme which can adapt to required link capability much in the manner of the variable throughput design of the IEEE 802.11a and g waveforms. LET provides 3.33, 5.08, 7.75, 9.0, or 10.25 times more throughput than the basic JTIDS modulation but does so at the expense of both link robustness and transmission range. The highest data rate LET mode is probably insufficiently robust for most combat environments [1]. In [2] the performance of a CCSK waveform is compared with an orthogonal waveform. In [3] an analysis of different forward error correction (FEC) techniques for high-rate direct sequence spread spectrum is examined. In [4], an analytical approximation for the probability of symbol error of CCSK is derived, but the performance obtained is optimistic by about 2 dB [5]. In this thesis, an alternative waveform consisting of (31, 15) RS encoding and 32-ary orthogonal signaling with 32 chip baseband waveforms is analyzed. The alternative waveform is consistent with the existing JTIDS channel waveform. The effects of both additive white Gaussian noise (AWGN) and pulse-noise interference (PNI) are investigated. To the best of the author's knowledge, the effect of PNI on this waveform has not been previously investigated.

C. THESIS OUTLINE

This thesis is organized into the introduction, background (Chapter II) and five additional chapters. Chapter III contains an analysis of the performance of 32-ary orthogonal signaling with (31, 15) RS encoding in an AWGN environment. In Chapter IV, the performance of 32-ary orthogonal signaling with (31, 15) RS encoding in both AWGN and PNI environment is analyzed. Chapter V contains a comparison of the performance of 32-ary orthogonal signaling with (31, 15) RS encoding with the JTIDS waveform both for AWGN only as well as both AWGN and PNI. In Chapter VI, the performance of 32-ary orthogonal signaling with (31, 15) RS encoding in both AWGN and PNI environment with errors-and-erasures decoding is analyzed. Finally, in Chapter VII the conclusions based on the results obtained from the analysis in the previous chapters are presented.

II. BACKGROUND

In this chapter, some of the background knowledge and concepts required for subsequent analysis of the alternative JTIDS/Link-16 waveform considered in this thesis are introduced.

A. *M*-ARY ORTHOGONAL SIGNALS

For *M*-ary communication systems, one of M unique signals, $s_m(t), m = 1, 2, ..., M$, is transmitted in order to represent symbol m. Each symbol represents k bits where $M = 2^k$. An *M*-ary orthogonal signal can be received either coherently (the receiver requires the phase of the received signal) or noncoherently (the receiver does not require the phase of the received signal). This type of receiver can be implemented either with a bank of M multipliers and low pass filters or with a bank of M matched filters [6].

The waveform of an *M*-ary orthogonal signal when AWGN is present can be represented by

$$s_T(t) = \sqrt{2} A_c c_m(t) \cos\left(2\pi f_c t + \theta_i\right) + n(t) \tag{2.1}$$

where $n(t)$ is AWGN noise with PSD $N_0 / 2$, the phase difference is known for coherent detection and $c_m(t)$, $m = 1, 2, ..., M$, is a baseband waveform that represents symbol m. A block diagram of a coherent *M*-ary orthogonal baseband waveform demodulator is shown in Figure 1.

It can be shown that the integrator outputs $x_m(iT_S)$ for each branch of the receiver can be represented as the independent Gaussian random variables $X_m, m = 1, 2, ..., M$. The conditional probability density functions for the random variables X_m, $m = 1, 2, ..., M$, that represent the integrator outputs when the noise is modeled as Gaussian are [6]

$$f_{X_m}\left(x_m \mid m\right) = \frac{1}{\sqrt{2\pi}\sigma_{x_m}} \exp\left[\frac{-\left(x_m - \sqrt{2}A_c\right)^2}{2\sigma_{x_m}{}^2}\right] \text{ for } m \le M \tag{2.2}$$

and

$$f_{X_n}\left(x_n \mid n,\, n \ne m\right) = \frac{1}{\sqrt{2\pi}\sigma_{x_m}} \exp\left[\frac{-x_n{}^2}{2\sigma_{x_m}{}^2}\right] \tag{2.3}$$

when the signal corresponding to symbol m is transmitted and

$$\sigma_{X_1}{}^2 = \sigma_{X_2}{}^2 = \ldots = \sigma_{X_M}{}^2 = \sigma^2 = N_0 / T_s\,. \tag{2.4}$$

The mean of X_m is given by

$$\overline{X_m} = \frac{2\sqrt{2}A_c}{T_s} \int_0^{T_s} c_m(t) c_n(t) \cos^2\left(2\pi f_c t + \theta_i\right) dt = \begin{cases} \sqrt{2}A_c & for, n=m \\ 0 & for, n\ne m \end{cases}\,. \tag{2.5}$$

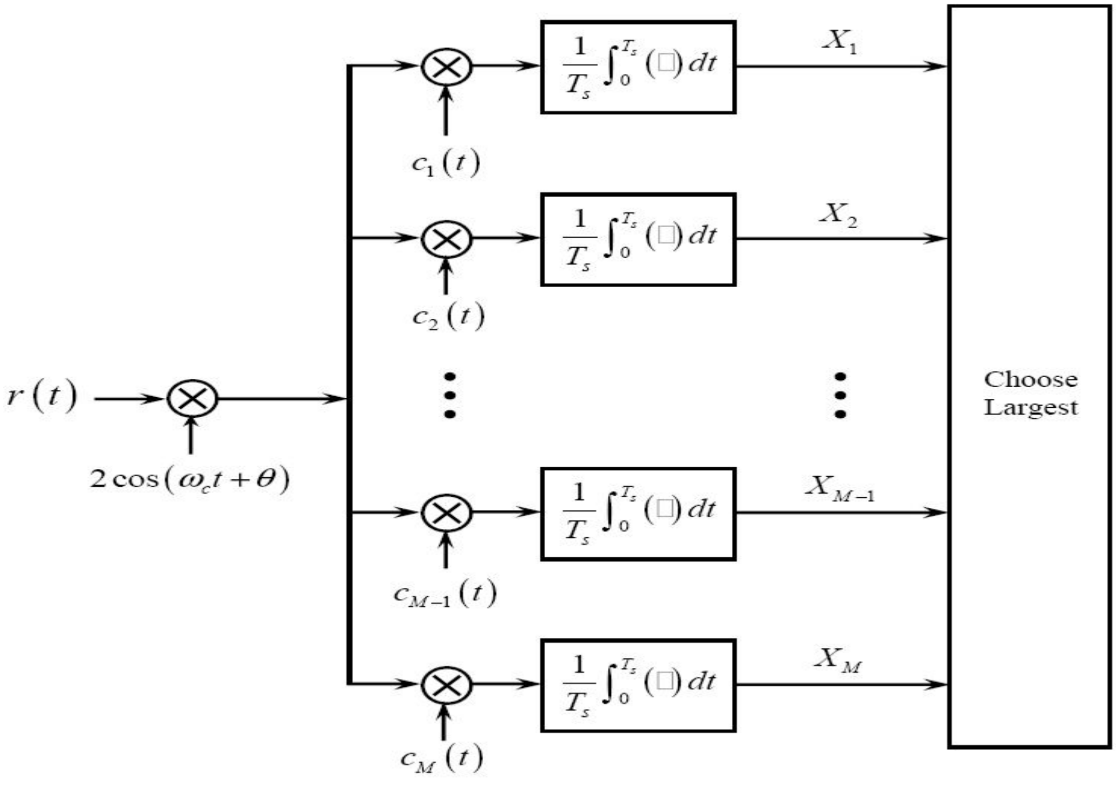

Figure 1. Block diagram of a coherent *M*-ary orthogonal baseband waveform demodulator (From: [6]).

The signal is the same for noncoherent detection of *M*-ary orthogonal signals when AWGN is present, but the phase difference is not known. A block diagram of a noncoherent *M*-ary orthogonal baseband waveform demodulator is shown in Figure 2.

When AWGN is present, it can be shown that the integrator outputs $x_m\left(iT_S\right)$ for each branch of the receiver can be represented as the independent Gaussian random variables $X_{m_i}, X_{m_q}, m = 1, 2, ..., M$, where for the in-phase integrator outputs

$$\begin{aligned}\overline{X_{m_i}} &= \frac{2\sqrt{2}A_c}{T_s}\int_0^{T_s} c_m(t)c_n(t)\cos\left(2\pi f_c t + \theta_i\right)\cos\left(2\pi f_c t\right)dt \\ &= \begin{cases}\sqrt{2}A_c\cos\theta_i & for, n=m \\ 0 & for, n\neq m\end{cases}\end{aligned}, \tag{2.6}$$

and for the quadrature integrator outputs

$$\begin{aligned}\overline{X_{m_q}} &= \frac{2\sqrt{2}A_c}{T_s}\int_0^{T_s} c_m(t)c_n(t)\cos\left(2\pi f_c t + \theta_i\right)\cos\left(2\pi f_c t\right)dt \\ &= \begin{cases}-\sqrt{2}A_c\sin\theta_i & for, n=m \\ 0 & for, n\neq m\end{cases}\end{aligned}, \tag{2.7}$$

where

$$\begin{aligned}&\sigma_{X_{1_i}}{}^2 = \sigma_{X_{2_i}}{}^2 = \ldots = \sigma_{X_{M_i}}{}^2 \\ &\quad = \sigma_{X_{1q}}{}^2 = \sigma_{X_{2_q}}{}^2 = \ldots = \sigma_{X_{Mq}}{}^2 = \sigma^2 = N_0 / T_s\end{aligned}. \tag{2.8}$$

The conditional probability density functions for the random variables V_m , $m = 1, 2, ..., M$, that represent the output of the m^{th} branch when the signal corresponding to symbol m is transmitted is given by the non-central chi-squared probability density function with two degrees of freedom when the noise is modeled as Gaussian [6]. Hence,

$$f_{V_m}\left(v_m \mid m\right) = \frac{1}{2\sigma^2}\exp\left[\frac{-\left(v_m + 2A_c{}^2\right)}{2\sigma^2}\right] \times I_0\left(\frac{A_c\sqrt{2v_m}}{\sigma^2}\right) \tag{2.9}$$

where $I_0(\bullet)$ is the modified Bessel function of the first kind and order zero, and

$$f_{V_n}\left(v_n \mid n,\, n \neq m\right) = \frac{1}{2\sigma^2} \exp\left[\frac{-v_n}{2\sigma^2}\right] \tag{2.10}$$

since $I_0(0) = 1$.

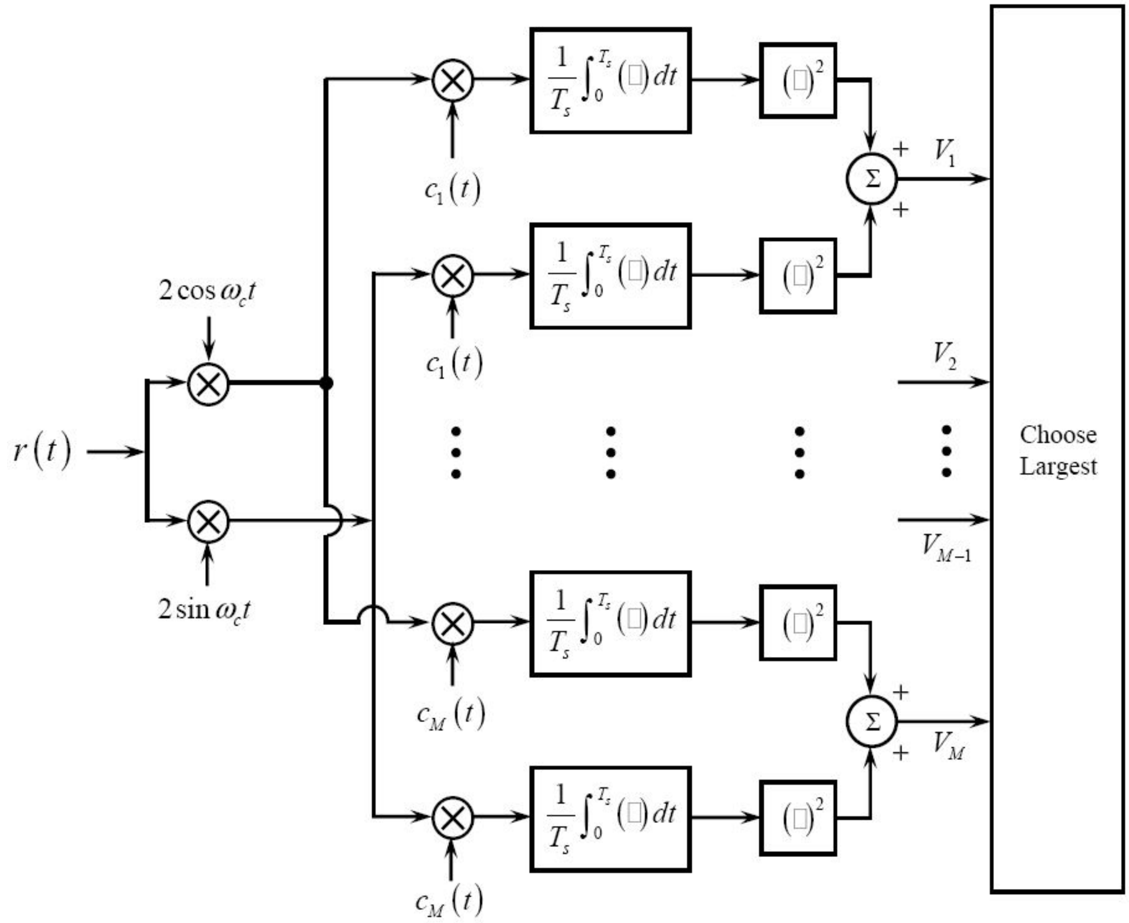

Figure 2. Block diagram of a noncoherent *M*-ary orthogonal baseband waveform demodulator (From: [6]).

B. PERFORMANCE OF *M*-ARY ORTHOGONAL SIGNALING IN AWGN

When AWGN is present with power spectral density $N_0/2$, the probability of channel symbol error for coherent *M*-ary orthogonal signaling in AWGN is [6]

$$p_s = \frac{1}{\sqrt{2\pi}} \int_{-\infty}^{\infty} e^{\left(\frac{-u^2}{2}\right)} \times \left\{ 1 - \left[1 - Q(u + \sqrt{\frac{2E_s}{N_0}}) \right]^{M-1} \right\} du \tag{2.11}$$

and for noncoherent *M*-ary orthogonal signaling in AWGN is [6]

$$p_s = \sum_{n=1}^{M-1} \frac{\left(-1\right)^{n+1}}{n+1} \binom{M-1}{n} \exp\left[\frac{-nrmE_b}{\left(n+1\right) N_o} \right] \tag{2.12}$$

where E_s is the average energy per channel symbol, $E_s = A_c{}^2 T_s$, where $A_c{}^2$ is the average received signal power, T_s is the symbol duration, and $Q(\bullet)$ is the Q-function. Equations (2.10) and (2.11) will be used to obtain the probability of symbol and bit error for the alternative JTIDS/Link-16 system in the next chapter.

C. PERFORMANCE IN AWGN WITH PULSED-NOISE INTERFERENCE

We have also to consider the effect of PNI on the performance of the system. In this thesis, we consider the performance of the alternative JTIDS/Link-16 system in both AWGN and PNI.

When a channel is affected by AWGN, the noise signal that arrives at the receiver is assumed to be uniformly spread across the spectrum and time-independent, but those assumptions may not be valid if PNI is present. In this thesis, the AWGN and PNI are assumed to be statistically independent, and the PNI is modeled as Gaussian noise. When AWGN and PNI are both present the total noise power at the receiver integrator outputs is given by

$$\sigma_X^2 = \sigma_{WG}^2 + \sigma_I^2 \tag{2.13}$$

where $\sigma_{WG}^2 = N_0 / T_b$ and $\sigma_I^2 = N_I / \rho T_b$, and ρ is a fraction of time that an interferer is switched on. When $\rho = 1$, the interferer is continuously on and is referred to as barrage noise interference.

When PNI is present, the probability of symbol error can be expressed as

$$P_s = \Pr(\text{Interferer is ON})\ p_s(\text{AWGN+PNI}) + \Pr(\text{Interferer is OFF})\ p_s(\text{AWGN}) \quad (2.14)$$

where we assume that a symbol is either completely free of PNI or the entire symbol is affected by PNI. Since $\Pr(\text{Interferer is ON}) = \rho$,

$$P_s = \rho\ p_s(\text{AWGN+PNI}) + (1-\rho)\ p_s(\text{AWGN}), \quad (2.15)$$

where $p_s(x)$ represent the probability of symbol error for condition as it is defined by x.

D. FORWARD ERROR CORRECTION CODING

For JTIDS/Link-16, the FEC used is (31, 15) RS coding, a linear, non-binary code. To maintain consistency with the JTIDS/Link-16 waveform, the alternative JTIDS/Link-16 waveform also employs (31, 15) RS coding for error detection and correction. For non-binary codes, symbols are generated instead of bits where each symbol represents *m* bits and the number of different symbols required are $M = 2^m$. An (n, k) RS encoder, takes *k* information symbols (mk information bits) and generates *n* coded symbols (mn coded bits) [7].

The probability of decoder, or block, error for a *t*-symbol error correcting, nonbinary block code with maximum likelihood decoding is upper bounded by [7]

$$P_E \le \sum_{i=t+1}^{n} \binom{n}{i} p_s^{\,i} \left(1-p_s\right)^{n-i} \quad (2.16)$$

or

$$P_E \le 1 - \sum_{i=0}^{t} \binom{n}{i} p_s^{\,i} \left(1-p_s\right)^{n-i} \quad (2.17)$$

where the inequality holds for either a perfect code or a bounded distance decoder, and p_s is the probability of coded, or channel, symbol error.

For RS codes and *M*-ary orthogonal modulation with $M = 2^m$ and hard decision decoding, we obtain the probability of information bit error as [7]

$$P_b \approx \frac{n+1}{2n^2} \sum_{i=t+1}^{n} i \binom{n}{i} p_s^{\,i} \left(1-p_s\right)^{n-i}. \quad (2.18)$$

E. ERRORS-AND-ERASURES DECODING

Error-and-erasures decoding (EED) is the simplest form of soft decision decoding and an alternative to hard decision decoding that is easily implemented. In binary erasure decoding, the output of the demodulator is not binary but ternary, and the three possible outputs are bit 1, bit 0, and erasure (e). Suppose that a received code word has a single erased bit. Now all valid code words are separated by a Hamming distance of at least $d_{\min} - 1$. In general, given e erasures in a received code word, all valid code words are separated by a Hamming distance of at least $d_{\min} - e$. Hence, the effective free distance is [7]

$$d_{\min_{eff}} = d_{\min} - e. \tag{2.19}$$

Therefore, the number of errors in the non-erased bits of the code word that can be corrected is [7]

$$t_e = \frac{1}{2}\left[d_{\min} - e - 1\right]. \tag{2.20}$$

A total of t_e errors and e erasures can be corrected as long as

$$2t_e + e < d_{\min}. \tag{2.21}$$

Hence, twice as many erasures as errors can be corrected. Intuitively, this makes sense because we have more information about the erasures; the locations of the erasures are known, but the locations of the errors are not.

For error-and-erasures decoding, the probability that there are a total of i errors and j erasures in a block of n symbols is given by [7]

$$\Pr(i, j) = \binom{n}{i}\binom{n-i}{j} p_s^i p_e^j p_c^{n-i-j} \tag{2.22}$$

where each symbol is assumed to be received independently, p_e is the probability of channel symbol erasure, p_s is the probability of channel symbol error, and the probability of correct channel symbol detection is [7]

$$p_s = 1 - p_e - p_c. \tag{2.23}$$

Since a block error does not occur as long as $d_{\min} > 2i + j$, then the probability of correct block decoding is given by

$$P_C = \sum_{i=0}^{t} \binom{n}{i} p_s^i \sum_{j=0}^{d_{\min}-1-2i} \binom{n-i}{j} p_e^j p_c^{n-i-j} \tag{2.24}$$

In this case, the probability of block error is given by

$$P_E = 1 - P_C \tag{2.25}$$

Substituting (2.24) into (2.25), we get

$$P_E = 1 - \sum_{i=0}^{t} \binom{n}{i} p_s^i \sum_{j=0}^{d_{\min}-1-2i} \binom{n-i}{j} p_e^j p_c^{n-i-j}. \tag{2.26}$$

Using the average of the upper and lower bound on the probability of symbol error given that a *block* error has occurred, we can approximate the probability of symbol error as [7]

$$P_s \approx \frac{k+1}{2k} P_E. \tag{2.27}$$

Finally, an approximation for the probability of *bit* error is obtained by taking the average of the upper and lower bound on the probability of bit error given that a symbol error has occurred to get

$$P_b \approx \frac{m+1}{2m} P_s. \tag{2.28}$$

F. CHAPTER SUMMARY

In this chapter, *M*-ary orthogonal signals were introduced and the background and concepts necessary to examine the performance of an alternative JTIDS/Link-16 waveform which consists of 32-ary orthogonal signaling with (31, 15) RS coding both for coherent and noncoherent demodulations were addressed. The concept of forward error correction (FEC) coding as well as the concept of errors-and-erasures (EE) decoding was also introduced. In the next chapter, the performance of an alternative JTIDS waveform that utilizes (31, 15) RS coding with *M*-ary orthogonal modulation transmitted over a channel with only AWGN is examined.

III. PERFORMANCE ANALYSIS OF 32-ARY ORTHOGONAL SIGNALING WITH (31,15) RS ENCODING IN AWGN

In this chapter we examine the performance of 32-ary orthogonal signaling with (31, 15) RS encoding in an AWGN environment.

We first examine the performance for coherent demodulation in AWGN, noise which is present for all communications systems even when there are no other types of noise present. Second, the performance of the alternative waveform for noncoherent demodulation is examined. Finally, the results obtained with coherent and noncoherent demodulation are examined.

A. COHERENT DEMODULATION

For the alternative JTIDS waveform with 32-ary orthogonal modulation, the probability of channel symbol error is upper bounded by [6]

$$p_s \le (M-1)Q\left(\sqrt{\frac{rE_s}{N_0}}\right), \tag{3.1}$$

where $r = k/n$, is the code rate.

Expressed in terms of bit energy E_b, (3.1) is given by

$$p_s \le (M-1)Q\left(\sqrt{\frac{rmE_b}{N_0}}\right), \tag{3.2}$$

where m is the number of bits per symbol.

In this thesis, we only consider $M = 32$ and $m = 5$, so (3.2) reduces to

$$p_s \le 31Q\left(\sqrt{\frac{5rE_b}{N_0}}\right). \tag{3.3}$$

Substituting (3.3) into (2.18), we get the results are shown in Figure 3 for 32-ary orthogonal signaling with (31, 15) RS encoding (the alternative JTIDS waveform) in AWGN for coherent demodulation. As can be seen, in order to achieve $P_b = 10^{-5}$, the alternative waveform requires $E_b / No = 5.3$ dB.

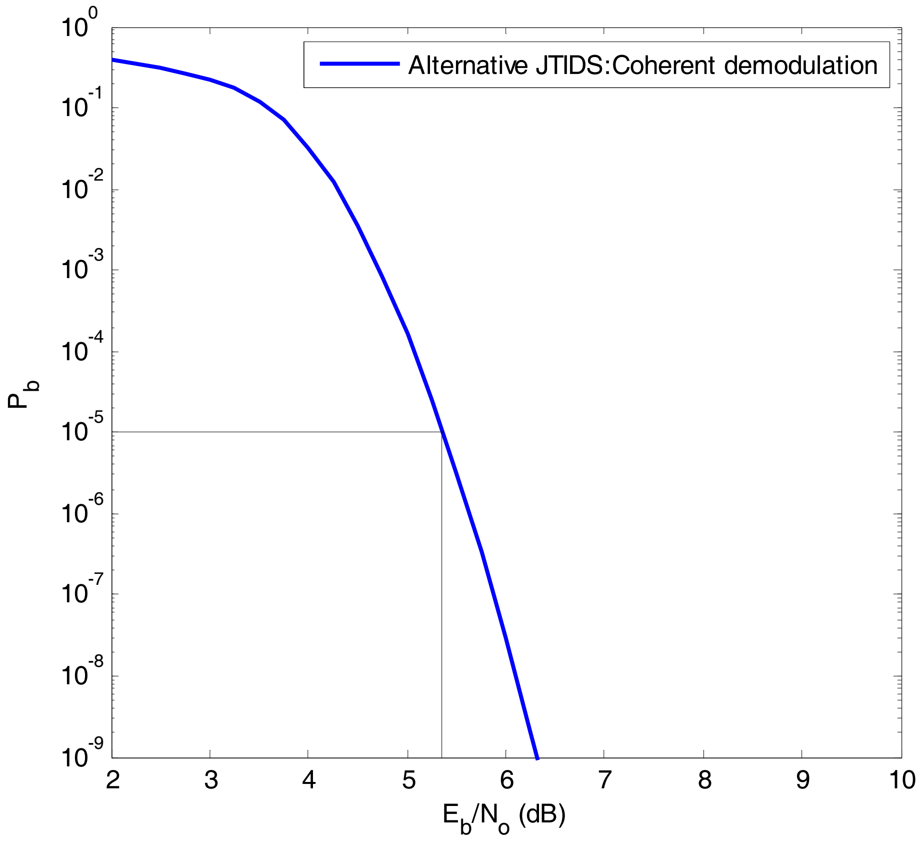

Figure 3. Performance of 32-ary orthogonal signaling with (31, 15) RS encoding in AWGN for coherent demodulation.

B. NONCOHERENT DEMODULATION

The probability of channel symbol error for 32-ary orthogonal signaling with noncoherent demodulation is upper bounded by [6]

$$p_s \le \frac{(M-1)}{2}\exp\left(-\frac{rE_s}{2N_0}\right). \tag{3.4}$$

Expressed in terms of bit energy E_b, (3.4) is given by

$$p_s = \frac{(M-1)}{2}\exp\left(-\frac{rmE_b}{2N_0}\right). \tag{3.5}$$

For $M = 32$ and $m = 5$, (3.5) simplifies to

$$p_s = 15.5\exp\left(-\frac{5rE_b}{2N_0}\right). \tag{3.6}$$

As for coherent demodulation, the probability of bit error is obtained by substituting (3.5) into (2.18). The results are shown in Figure 4 for 32-ary orthogonal signaling with (31, 15) RS encoding. As can be seen, in order to achieve $P_b = 10^{-5}$, the alternative waveform requires $E_b / No = 6.6$ dB for noncoherent demodulation.

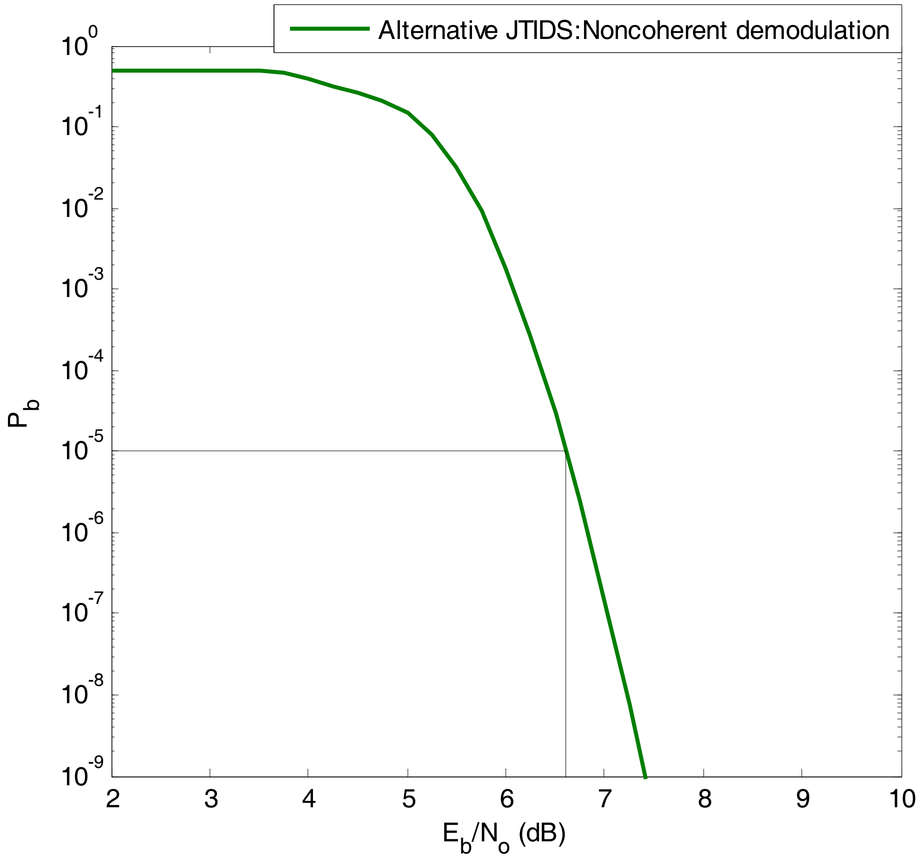

Figure 4. Performance of 32-ary orthogonal signaling with (31, 15) RS encoding in AWGN for noncoherent demodulation.

C. COMPARISON OF THE PERFORMANCE OBTAINED WITH COHERENT AND NONCOHERENT DEMODULATION

For purposes of comparison, the performances obtained for both coherent and noncoherent demodulation of the alternative waveform are plotted in Figure 5. As previously mentioned, at $P_b = 10^{-5}$ the alternative waveform requires $E_b / N_0 = 5.3$ dB and $E_b / N_0 = 6.6$ dB for coherent and noncoherent demodulation, respectively. Hence, there is a gain of 1.3 dB at $P_b = 10^{-5}$ with coherent as opposed to noncoherent demodulation.

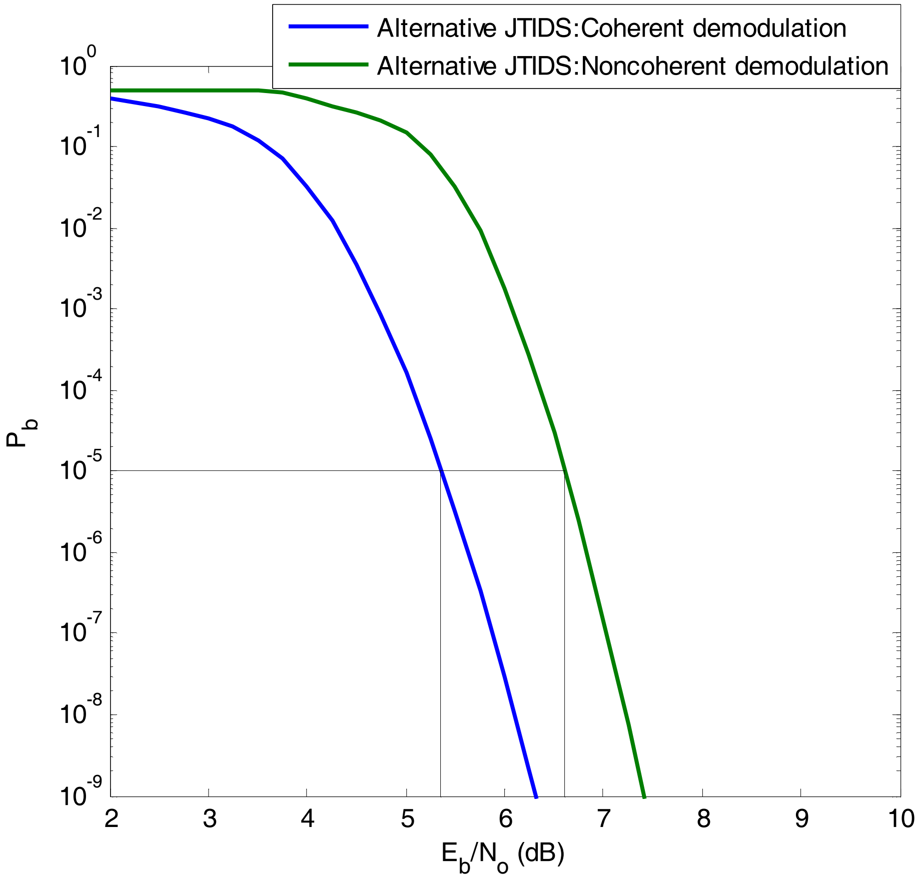

Figure 5. Comparison of the performance of coherent and noncoherent demodulation for the alternative waveform in AWGN.

D. CHAPTER SUMMARY

In this chapter, the effects of AWGN on the performances for both coherent and noncoherent demodulation of the alternative JTIDS waveform were examined. In the next chapter, the performance of the alternative JTIDS waveform for both coherent and noncoherent demodulation in both AWGN and PNI are examined.

THIS PAGE INTENTIONALLY LEFT BLANK

IV. PERFORMANCE ANALYSIS OF 32-ARY ORTHOGONAL SIGNALING WITH (31,15) RS ENCODING IN AWGN AND PULSE-NOISE INTERFERENCE

We now examine the performance of the receiver in the presence of PNI and AWGN. With PNI, we assume that the communications system is attacked by a noise-like signal that is turned on and off periodically. If ρ represents the fraction of time that the PNI is turned on, then $(1 - \rho)$ represents the fraction of time that the PNI is turned off where $0 < \rho \leq 1$. In this kind of noisy environment, received symbols are affected by two different levels of noise power since some of the symbols are affected only by AWGN and the rest by both AWGN and PNI. If the one-sided power spectral density (PSD) of the AWGN is N_o and the one-sided PSD of barrage noise interference is N_I, then N_I/ρ is the PSD of the PNI since we assume that average interference power is independent of ρ .

A. COHERENT DEMODULATION

For the alternative JTIDS waveform, the probability of channel symbol error for the coherent demodulation is obtained by combining (2.11), (2.13) and (2.15) to get

$$\begin{aligned} p_s = {} & \rho \frac{1}{\sqrt{2\pi}} \int_{-\infty}^{\infty} e^{\left(\frac{-u^2}{2}\right)} \times \left\{ 1 - \left[1 - Q\left(u + \sqrt{\frac{2rm}{\frac{N_0}{E_b} + \frac{N_I}{\rho E_b}}}\right) \right]^{M-1} \right\} du \\ & + (1-\rho) \frac{1}{\sqrt{2\pi}} \int_{-\infty}^{\infty} e^{\left(\frac{-u^2}{2}\right)} \times \left\{ 1 - \left[1 - Q\left(u + \sqrt{\frac{2E_s}{N_0}}\right) \right]^{M-1} \right\} du \end{aligned} \quad . \tag{4.1}$$

Defining $\gamma_b = E_b / N_o$, $\gamma_I = E_b / N_I$, and $\gamma_T = \left[1 / \left(\gamma_b^{-1} + \left(\rho \gamma_I \right)^{-1} \right) \right]$, we obtain from (4.1)

$$p_s = \rho \frac{1}{\sqrt{2\pi}} \int_{-\infty}^{\infty} e^{\left(\frac{-u^2}{2}\right)} \times \left\{ 1 - \left[1 - Q(u + \sqrt{10 r \gamma_T}) \right]^{31} \right\} du$$
$$+ (1-\rho) \frac{1}{\sqrt{2\pi}} \int_{-\infty}^{\infty} e^{\left(\frac{-u^2}{2}\right)} \times \left\{ 1 - \left[1 - Q(u + \sqrt{10 r \gamma_b}) \right]^{31} \right\} du \quad (4.2)$$

The probability of bit error is obtained by substituting (4.2) into (2.18).

The performance of the alternative waveform for different values of ρ in both AWGN and PNI for coherent demodulation is shown in Figure 6. The plot is obtained for $E_b / N_o = 10$ dB, and we see that PNI degrades the performance of the system relative to barrage-noise interference (BNI).

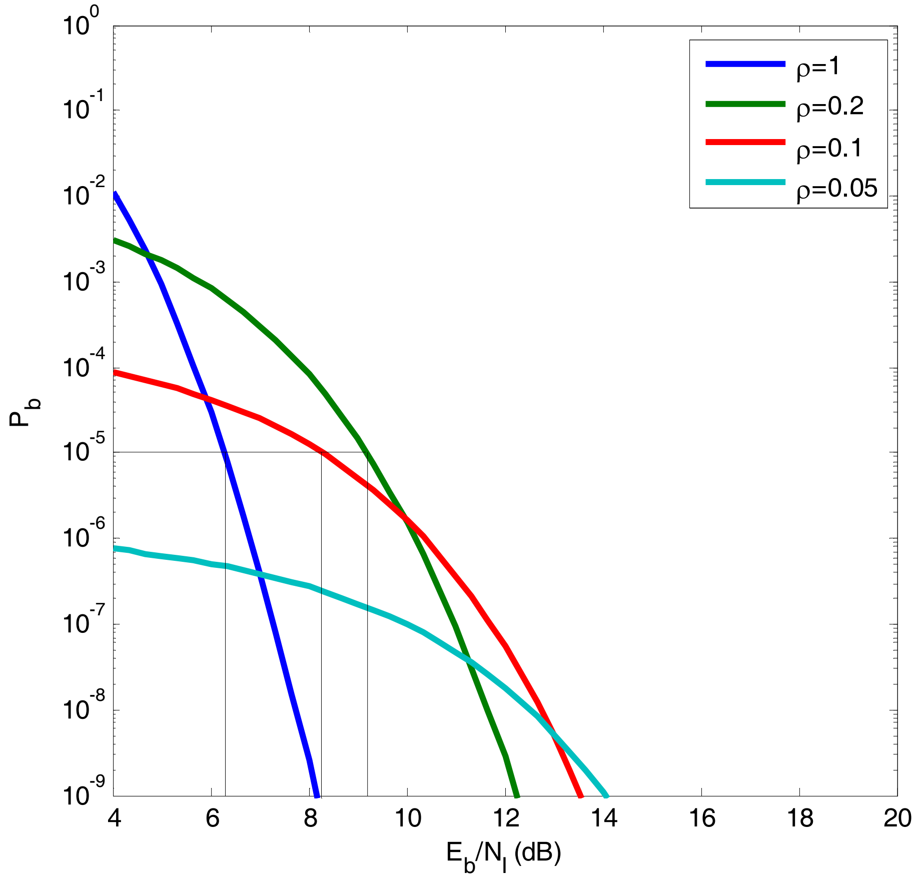

Figure 6. Performance of 32-ary orthogonal signaling with (31, 15) RS encoding for different values of ρ in both AWGN and PNI for coherent demodulation with $E_b / N_o = 10$ dB.

From Table 1 we can see that PNI degrades the performance of the system relative to barrage-noise interference ($\rho = 1$) when $P_b = 10^{-5}$ by almost 3.0 dB. For $\rho < 0.1$, performance is not affected for $P_b \geq 10^{-5}$.

Table 1. Performance of 32-ary orthogonal signaling with (31, 15) RS encoding for different values of ρ in both AWGN and PNI for coherent demodulation when $P_b = 10^{-5}$.

ρ	E_b / N_I (dB)
1	6.3
0.2	9.1
0.1	8.3

B. NONCOHERENT DEMODULATION

When AWGN and PNI are both present, the probability of channel symbol error for 32-ary orthogonal signaling with noncoherent demodulation is obtained by combining (2.12), (2.13) and (2.15) to get

$$p_s = \rho \sum_{n=1}^{M-1} \frac{(-1)^{n+1}}{n+1} \binom{M-1}{n} \exp\left[\frac{-nrm}{(n+1)\left(\frac{N_0}{E_b} + \frac{N_I}{\rho E_b} \right)} \right] + (1-\rho) \sum_{n=1}^{M-1} \frac{(-1)^{n+1}}{n+1} \binom{M-1}{n} \exp\left[\frac{-nrmE_b}{(n+1) N_o} \right] \tag{4.3}$$

Making the same substitutions in (4.3) that were made in (4.2), we get

$$p_s = \rho \sum_{n=1}^{31} \frac{(-1)^{n+1}}{n+1} \binom{31}{n} \exp\left[\frac{-n5r}{(n+1)\left(\frac{N_0}{E_b} + \frac{N_I}{\rho E_b} \right)} \right] + (1-\rho) \sum_{n=1}^{31} \frac{(-1)^{n+1}}{n+1} \binom{31}{n} \exp\left[\frac{-n5rE_b}{(n+1) N_o} \right] \tag{4.4}$$

Substituting (4.4) into (2.18), we get the performance of the alternative waveform for different values of ρ in both AWGN and PNI for noncoherent demodulation. The results are shown in Figure 7. The plot is obtained for $E_b / N_o = 10$ dB, and we see that PNI degrade the performance of the system relative to barrage-noise interference (BNI) just as in the case of coherent demodulation.

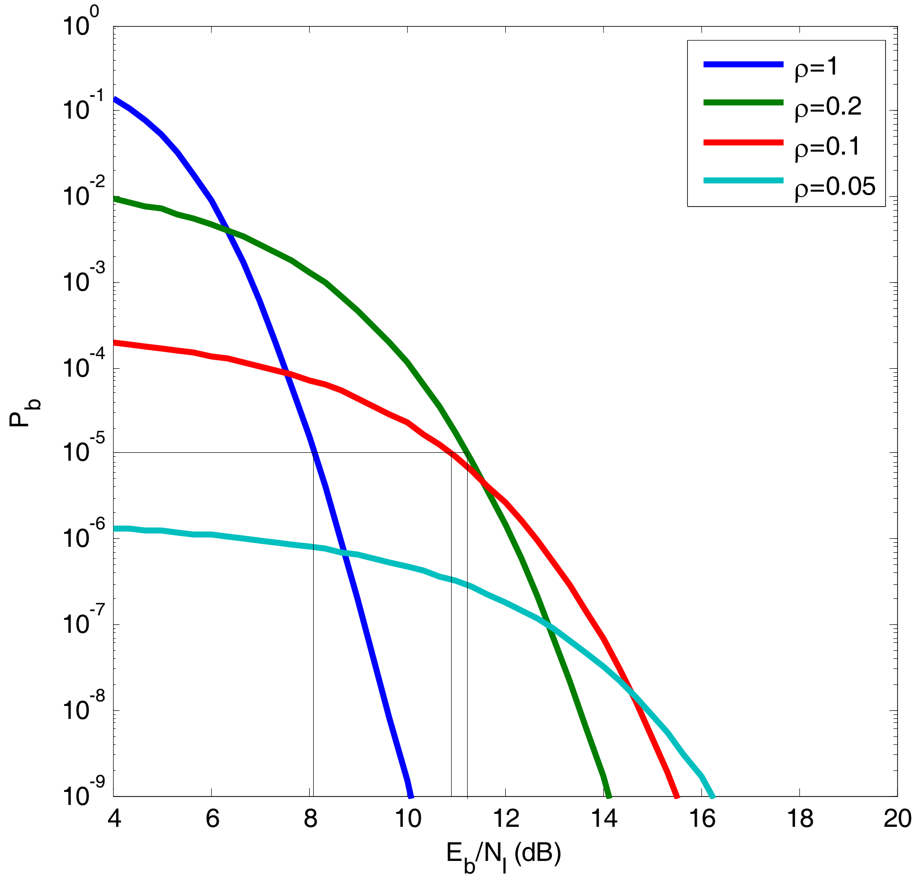

Figure 7. Performance of 32-ary orthogonal signaling with (31, 15) RS encoding for different values of ρ in both AWGN and PNI for noncoherent demodulation with $E_b / N_o = 10$ dB.

From Table 2 we can see that PNI degrades the performance of the system relative to barrage-noise interference when $P_b = 10^{-5}$ by 3.1 dB. For $\rho < 0.1$, performance is not affected for $P_b \geq 10^{-5}$, just as in the case of coherent detection.

Table 2. Performance of 32-ary orthogonal signaling with (31, 15) RS encoding for different values of ρ in both AWGN and PNI for noncoherent demodulation when $P_b = 10^{-5}$.

ρ	E_b / N_I (dB)
1	8.1
0.2	11.2
0.1	10.9

C. COMPARISON BETWEEN COHERENT AND NON-COHERENT DEMODULATION

For purposes of comparison, the performance for both coherent and noncoherent demodulation of the alternative waveform for $\rho = 1$, $\rho = 0.2$, and $\rho = 0.1$ are plotted in Figures 8, 9 and 10, respectively. In each figure, E_b / N_o =10 dB, and we see that in this case PNI degrades the performance of the system relative to BNI. Also in each figure, performance with E_b / N_o =6.8 dB, which results in $P_b = 10^{-8}$ for noncoherent demodulation when E_b / N_I >>1, is compared with those for coherent demodulation when E_b / N_o =6.8 dB. The E_b / N_I required for $P_b = 10^{-5}$ when E_b / N_o =10 dB and when E_b / N_o =6.8 dB for $\rho = 1$, $\rho = 0.2$, and $\rho = 0.1$, respectively, are listed in Tables 3, 4 and 5.

From Figures 8, 9 and 10, we see that for E_b / N_o =6.8 dB, which leads asymptotically to $P_b = 10^{-8}$ for noncoherent demodulation, the E_b / N_I required for $P_b = 10^{-5}$ increases as ρ decreases. Additionally, for E_b / N_o =10 dB and $P_b = 10^{-5}$, as ρ decreases, the difference in performance between coherent and noncoherent demodulation increases from 1.7 dB for BNI to 2.6 dB for $\rho = 0.1$. Note that a reduction of E_b / N_o requires an increase in E_b / N_I in order to maintain $P_b = 10^{-5}$. In the case of noncoherent detection, an approximately 3 dB decrease of E_b / N_o leads to a greater than 3 dB increase in required E_b / N_I. The increase is the most extreme for BNI, when E_b / N_I must increase by more than 5 dB. In the case of coherent detection, an approximately 3 dB decrease in E_b / N_o also leads to an increase in required E_b / N_I, but in this case the increase is less than 3 dB. As in the noncoherent case, the increase is the most extreme for BNI, when E_b / N_I must increase by 2.6 dB. For both coherent and noncoherent demodulation, as ρ decreases, the increase in required E_b / N_I also decreases.

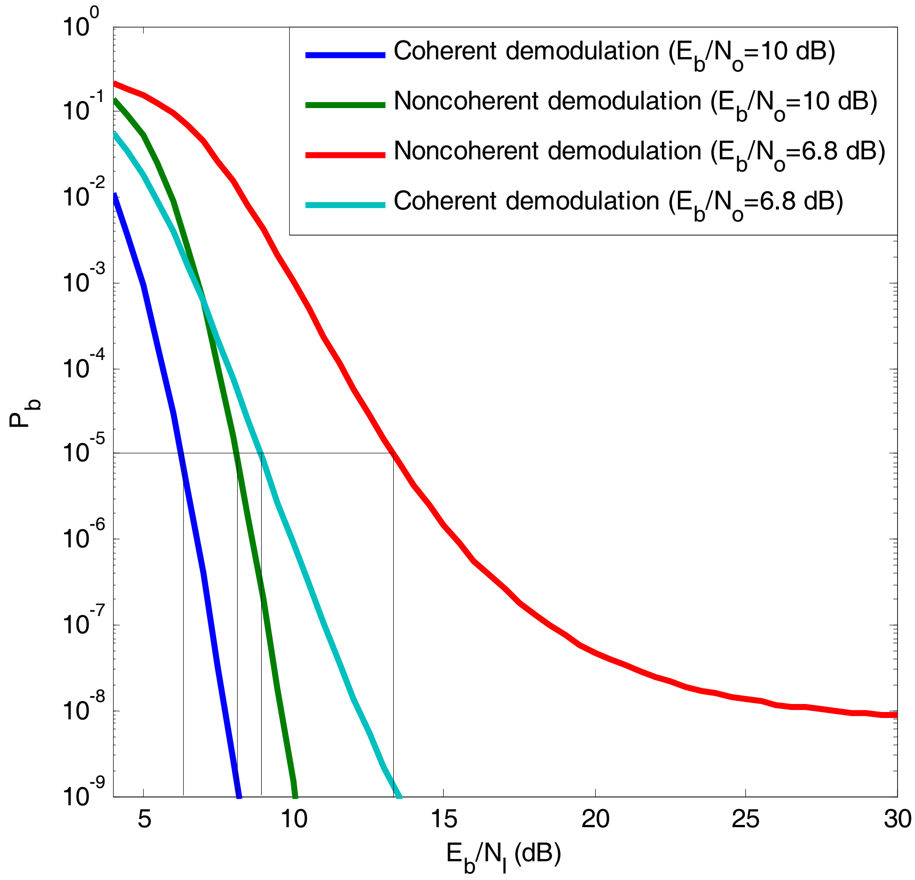

Figure 8. Comparison of the performance of the alternative waveform with both AWGN and BNI for coherent and noncoherent demodulation.

Table 3. Comparison of the performance of the alternative waveform with both AWGN and BNI for coherent and noncoherent demodulation when $P_b = 10^{-5}$.

E_b / N_o (dB)	Demodulation	E_b / N_I (dB)
10	Coherent	6.3
10	Noncoherent	8.1
6.8	Coherent	8.9
6.8	Noncoherent	13.3

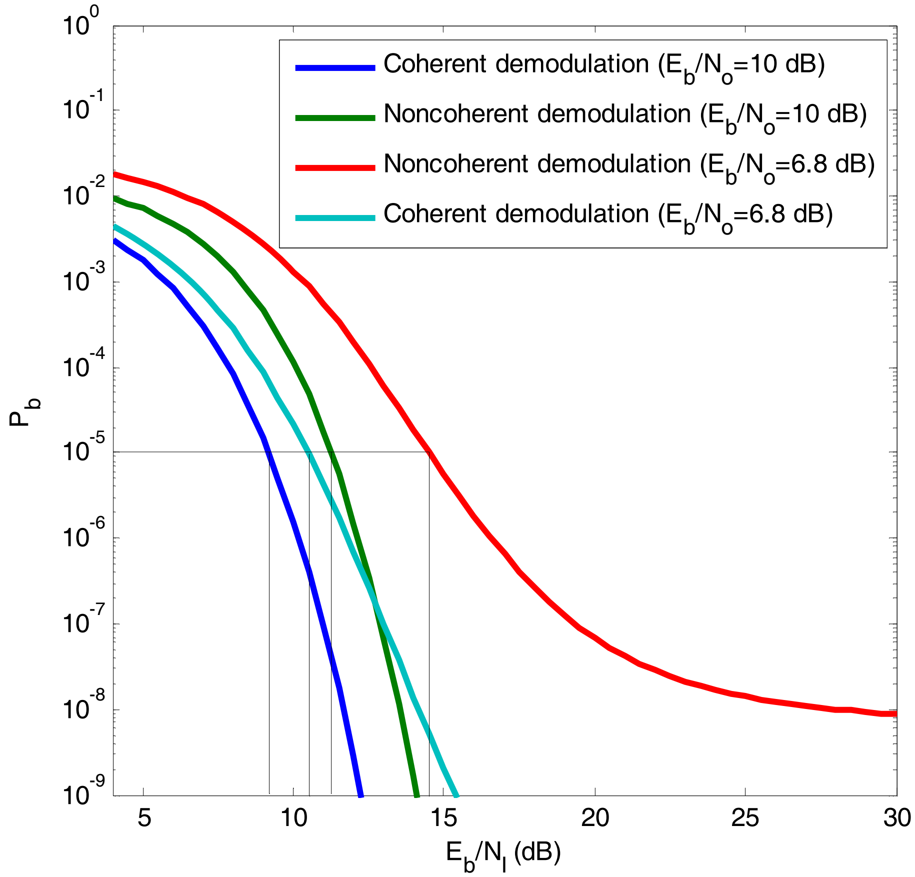

Figure 9. Comparison of the performance of the alternative waveform for $\rho = 0.2$ with both AWGN and PNI for coherent and noncoherent demodulation.

Table 4. Comparison of the performance of the alternative waveform for $\rho = 0.2$ with both AWGN and PNI for coherent and noncoherent demodulation when $P_b = 10^{-5}$.

E_b / N_o (dB)	Demodulation	E_b / N_I (dB)
10	Coherent	9.1
10	Noncoherent	11.2
6.8	Coherent	10.4
6.8	Noncoherent	14.4

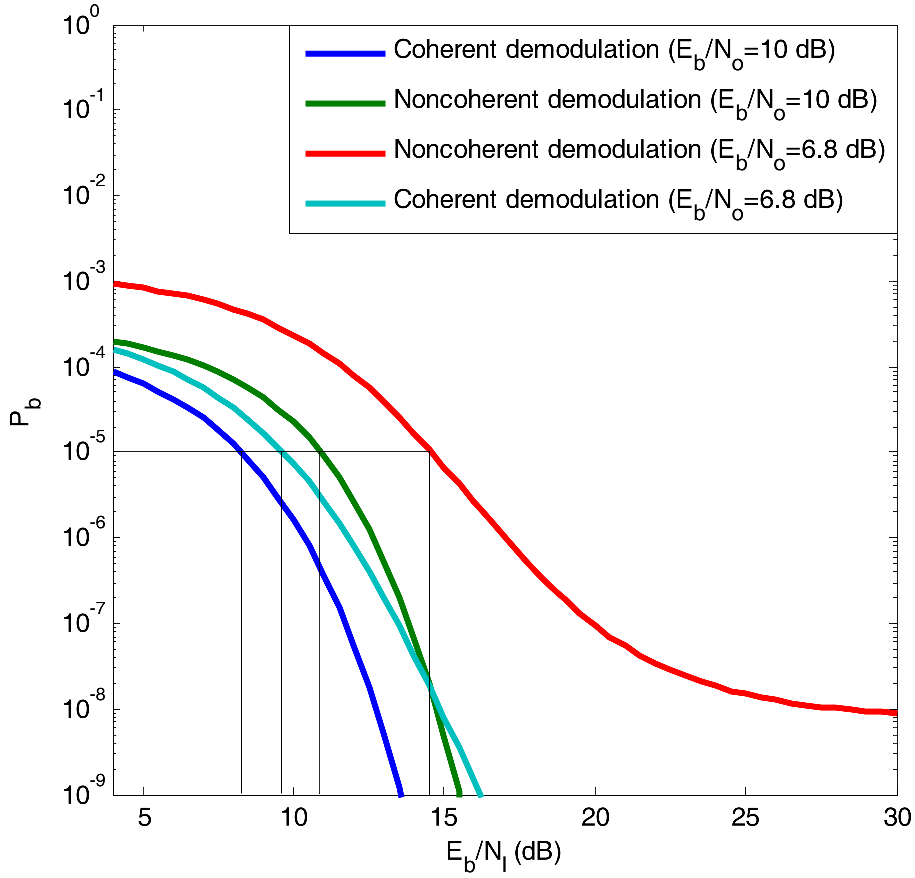

Figure 10. Comparison of the performance of the alternative waveform for $\rho = 0.1$ with both AWGN and PNI for coherent and noncoherent demodulation.

Table 5. Comparison of the performance of the alternative waveform for $\rho = 0.1$ with both AWGN and PNI for coherent and noncoherent demodulation when $P_b = 10^{-5}$.

E_b / N_o (dB)	Demodulation	E_b / N_I (dB)
10	Coherent	8.3
10	Noncoherent	10.9
6.8	Coherent	9.6
6.8	Noncoherent	14.5

D. CHAPTER SUMMARY

In this chapter, the effects of AWGN and PNI on the performance of the alternative JTIDS waveform for both coherent and noncoherent demodulation were examined. In the next chapter, the performance of the original JTIDS waveform for both coherent and noncoherent demodulation is examined for AWGN as well as for both AWGN and PNI. The performance of the alternative waveform is then compared to the original JTIDS waveform for both coherent and noncoherent detection.

THIS PAGE INTENTIONALLY LEFT BLANK

V. COMPARISON OF THE PERFORMANCE OF 32-ARY ORTHOGONAL SIGNALING WITH (31,15) RS ENCODING TO THAT OF THE JTIDS WAVEFORM

In this chapter, the performance of the alternative JTIDS/Link-16 waveform is compared with that of the original JTIDS/Link-16 waveform. Results from [5] are used to obtain the performance of the original JTIDS/Link-16 waveform.

A. ORIGINAL JTIDS WAVEFORM IN AWGN

1. Coherent Demodulation

For the original JTIDS/Link-16 waveform, the FEC used is (31, 15) RS coding, and the modulation is CCSK, which is demodulated at the chip level. In AWGN, the probability of channel chip error with coherent detection is [5]

$$p_c = Q\left(\sqrt{\frac{10rLE_b}{32N_0}}\right) \tag{5.1}$$

where r is the code rate, $L=1$ for the single-pulse structure, $r = k/n$, and E_b is the average energy per bit in a pulse.

An analytic expression for the probability of channel symbol error for the CCSK sequence used in JTIDS is [5]

$$p_s = \sum_{j=0}^{32} \zeta_j \binom{32}{j} p_c^j \left(1-p_c\right)^{32-j} \tag{5.2}$$

where ζ_j is the conditional probability of channel symbol error given that j chip errors have occurred at the output of MSK chip demodulator. The values of ζ_j are derived in [5].

As in the previous chapters, (5.2) is used in

$$P_s \approx \frac{1}{n}\sum_{i=t+1}^{n} i \binom{n}{i} p_s^{\,i} \left(1-p_s\right)^{n-i} \tag{5.3}$$

and (2.28) to obtain an estimate of the probability of bit error.

The performance of the original JTIDS waveform with coherent demodulation in AWGN is shown in Figure 11.

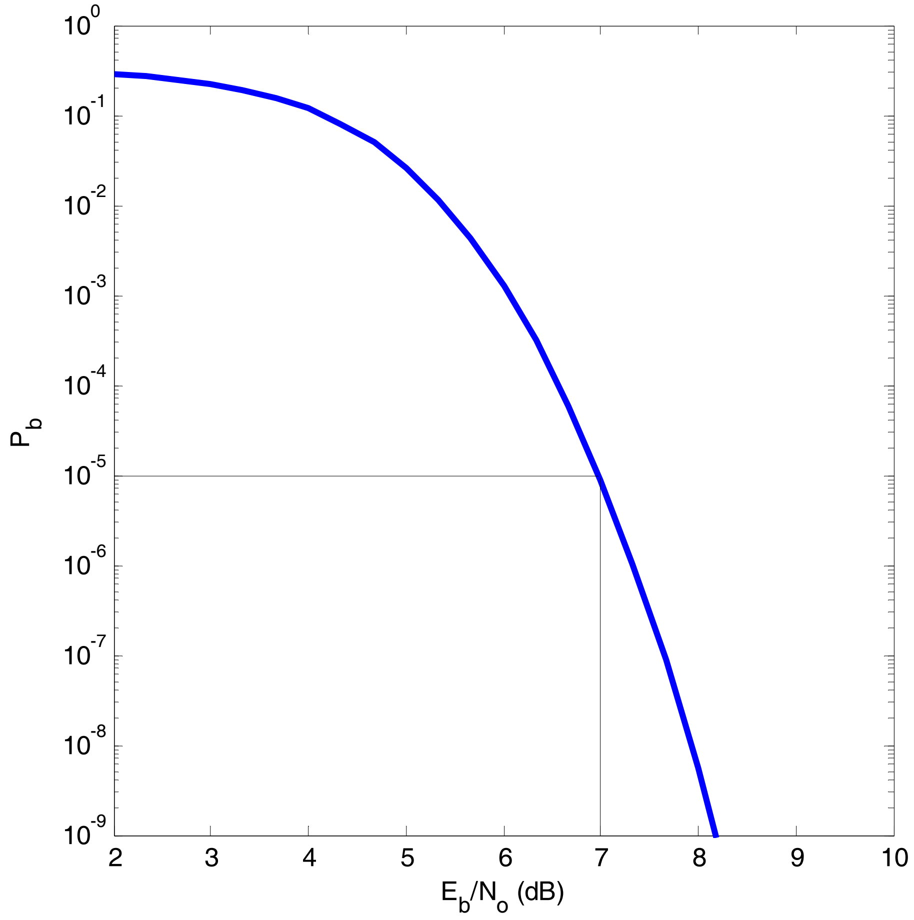

Figure 11. Performance of the original JTIDS waveform in AWGN for coherent demodulation.

2. Noncoherent Demodulation

For the original JTIDS/Link-16 waveform, in AWGN the probability of channel chip error is

$$p_c = \frac{1}{2}\exp\left(-\frac{10rE_b}{32N_0}\right). \tag{5.4}$$

Again, equations (5.2), (5.4) and (2.28) are used to obtain the probability of bit error.

The performance of the original JTIDS waveform in AWGN with noncoherent demodulation is shown in Figure 12.

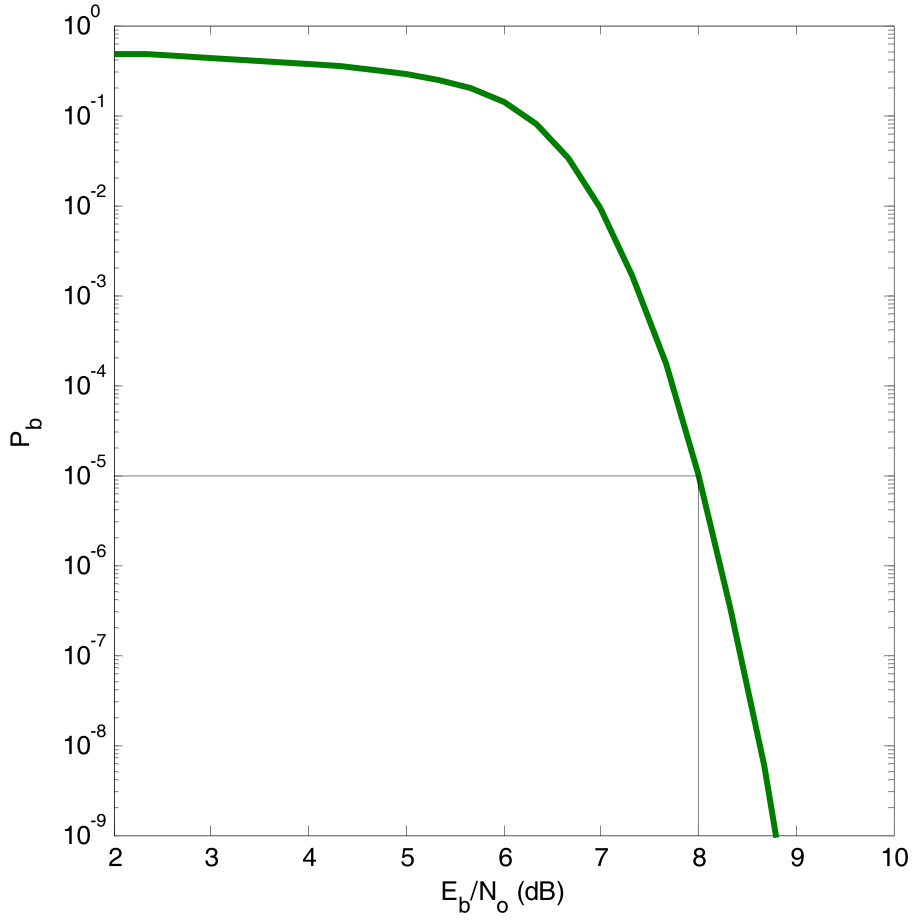

Figure 12. Performance of the original JTIDS in AWGN for noncoherent demodulation.

3. Comparison Between Coherent and Noncoherent Demodulation for the Original JTIDS Waveform in AWGN

For purpose of comparison, the performance for both coherent and noncoherent demodulation of the original JTIDS waveform is plotted in Figure 13. For $P_b = 10^{-5}$ the original JTIDS waveform with coherent demodulation requires $E_b / N_0 = 7$ dB, while noncoherent demodulation requires $E_b / N_0 = 8$ dB. Hence, at $P_b = 10^{-5}$ the noncoherent system requires 1.0 dB more than the coherent system.

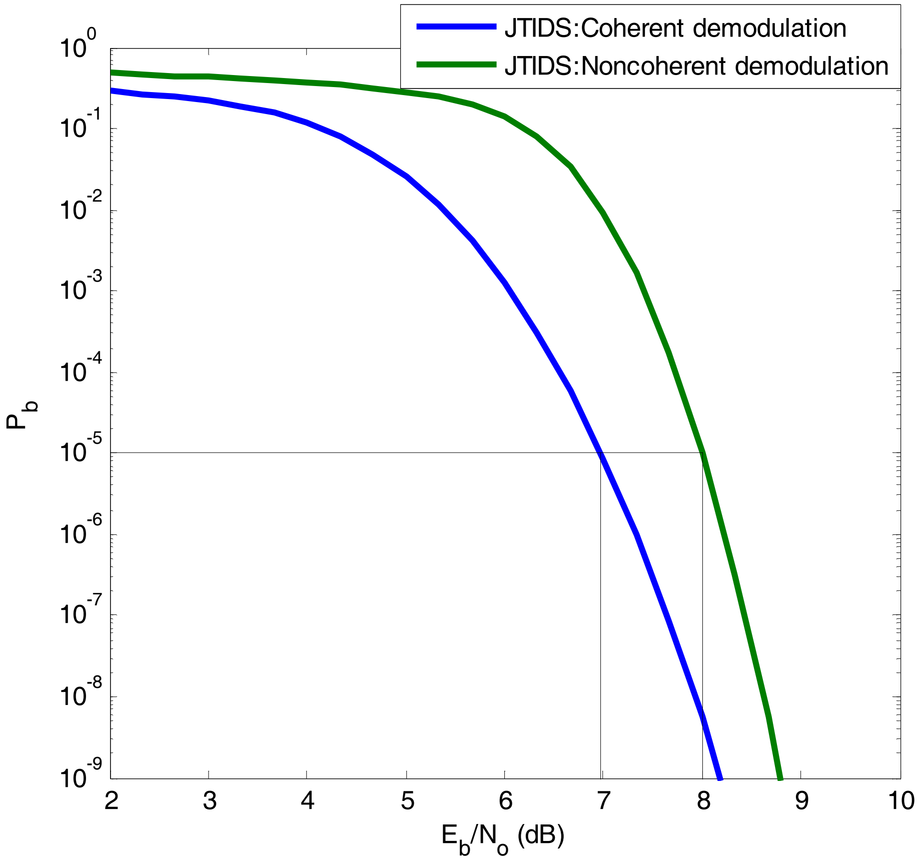

Figure 13. Comparison of coherent and noncoherent demodulation of the original JTIDS waveform in AWGN.

B. JTIDS WAVEFORM IN AWGN AND PNI

1. Coherent Demodulation

For the original JTIDS/Link-16 waveform in AWGN and PNI, the probability of channel chip error is [5]

$$p_{cI} = Q\left(\sqrt{\frac{10rL}{32\left(\frac{N_0}{E_b}+\frac{N_I}{\rho E_b}\right)}}\right) \tag{5.5}$$

where $\gamma_b = E_b / N_o$ and $\gamma_I = E_b / N_I$.

Defining $\gamma_T = \left[1/\left(\gamma_b{}^{-1} + \left(\rho\gamma_I\right)^{-1}\right)\right]$ in (5.5), we obtain

$$p_{cI} = Q\left(\sqrt{\frac{10r\gamma_T}{32}}\right). \tag{5.6}$$

In AWGN, the probability of channel chip error is given by (5.1), which can be expressed as

$$p_{cWN} = Q\left(\sqrt{\frac{10r\gamma_b}{32}}\right) \tag{5.7}$$

Substituting (5.6) into (5.2), we obtain the probability of channel symbol error for both AWGN and PNI from

$$p_{sI} = \sum_{j=0}^{32}\zeta_j\binom{32}{j}p_{cI}^{j}\left(1-p_{cI}\right)^{32-j}. \tag{5.8}$$

Substituting (5.7) into (5.2), we get

$$p_{sWN} = \sum_{j=0}^{32}\zeta_j\binom{32}{j}p_{cWN}^{j}\left(1-p_{cWN}\right)^{32-j}. \tag{5.9}$$

Now substituting (5.8) and (5.9) into (2.15), we get

$$\begin{aligned} p_s = \rho&\sum_{j=0}^{32}\zeta_j\binom{32}{j}p_{cI}^{j}\left(1-p_{cI}\right)^{32-j} \\ &+\left(1-\rho\right)\sum_{j=0}^{32}\zeta_j\binom{32}{j}p_{cWN}^{j}\left(1-p_{cWN}\right)^{32-j} \end{aligned} \tag{5.10}$$

Substituting (5.10) into (5.3) we approximate the probability of bit error by taking the average of the upper and lower bound on the probability of bit error given that a symbol error has occurred.

The performance of the original JTIDS waveform with different values of ρ for both AWGN and PNI is shown in Figure 14. The plot is obtained for E_b / N_o =10 dB. From Figure 14, we see that PNI degrades the performance of the system relative to BNI by a maximum of 2.2 dB. We also see that $\rho < 0.1$ is not effective in degrading performance. The E_b / N_I required for $P_b = 10^{-5}$ when E_b / N_o =10 dB for $\rho = 1$, $\rho = 0.2$ and $\rho = 0.1$, respectively, are listed in Table 6.

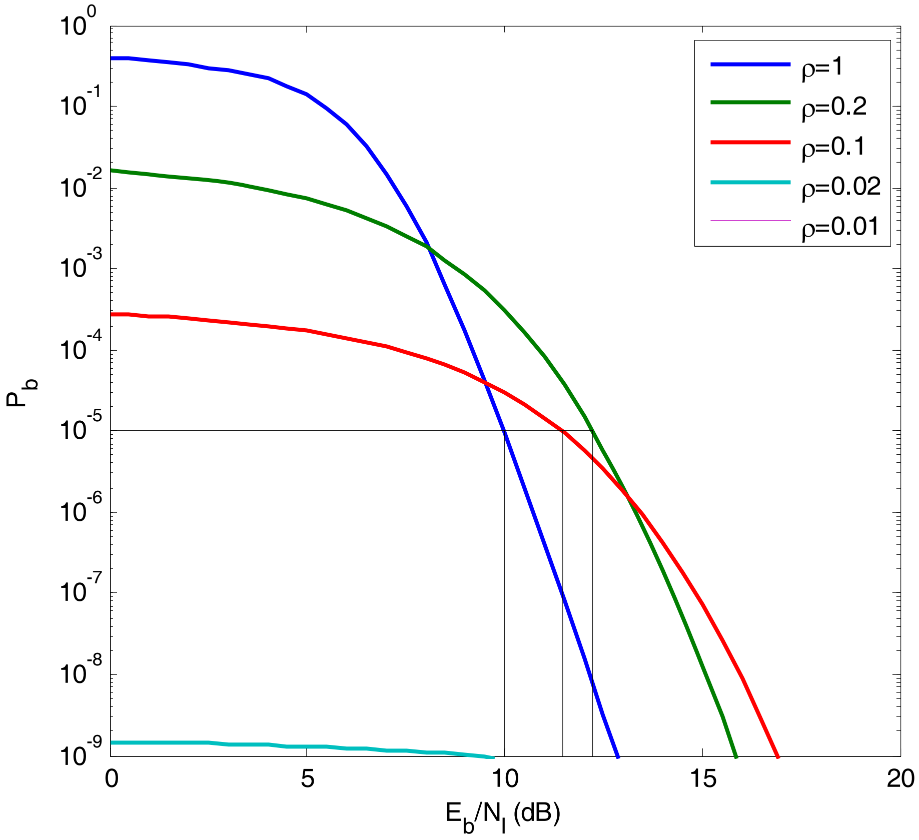

Figure 14. Performance of the original JTIDS waveform with different values of ρ in both AWGN and PNI for coherent demodulation when E_b / N_o =10 dB.

Table 6. Performance of the original JTIDS waveform with different values of ρ in both AWGN and PNI for coherent demodulation when $P_b = 10^{-5}$ and E_b / N_o =10 dB.

ρ	E_b / N_I (dB)
1	10.0
0.2	12.2
0.1	11.4

2. Noncoherent Demodulation

For noncoherent demodulation, the probability of channel chip error for the original JTIDS/Link-16 waveform in AWGN and PNI is [7]

$$p_{cI} = \frac{1}{2}\exp\left(-\frac{10r}{32\left(\frac{N_0}{E_b}+\frac{N_I}{\rho E_b}\right)}\right) \tag{5.11}$$

for the single-pulse structure.

As before defining $\gamma_T = \left[1/\left(\gamma_b^{-1} + \left(\rho\gamma_I\right)^{-1}\right)\right]$ in (5.11), we obtain

$$p_{cI} = \frac{1}{2}\exp\left(-\frac{10r\gamma_T}{32}\right) \tag{5.12}$$

In AWGN, the probability of channel chip error is

$$p_{cWN} = \frac{1}{2}\exp\left(-\frac{10rE_b}{32N_0}\right) \tag{5.13}$$

for the single-pulse structure. Since $\gamma_b = E_b / N_o$, we obtain from (5.13)

$$p_{cWN} = \frac{1}{2}\exp\left(-\frac{10r\gamma_b}{32}\right) \tag{5.14}$$

Substituting (5.12) and (5.14) into (2.15), we get

$$
\begin{aligned}
p_s = {} & \rho \sum_{j=0}^{32} \zeta_j \binom{32}{j} p_{cI}^{j} \left(1 - p_{cI}\right)^{32-j} \\
& + \left(1-\rho\right) \sum_{j=0}^{32} \zeta_j \binom{32}{j} p_{cWN}^{j} \left(1 - p_{cWN}\right)^{32-j}
\end{aligned}
\tag{5.15}
$$

Substituting (5.15) into (5.3), we approximate the probability of bit error by taking the average of the upper and lower bound on the probability of bit error given that a symbol error has occurred.

The performance of the original JTIDS waveform with different values of ρ for both AWGN and PNI is shown in Figure 15. The plot is obtained for E_b / N_o =10 dB. From Figure 15, we see that PNI degrades the performance of the system relative to BNI by 3.3 dB. As with coherent demodulation, $\rho < 0.1$ is not effective in degrading performance.

The E_b / N_I required for $P_b = 10^{-5}$ when E_b / N_o =10 dB for $\rho = 1$, $\rho = 0.2$ and $\rho = 0.1$, respectively, are listed in Table 7.

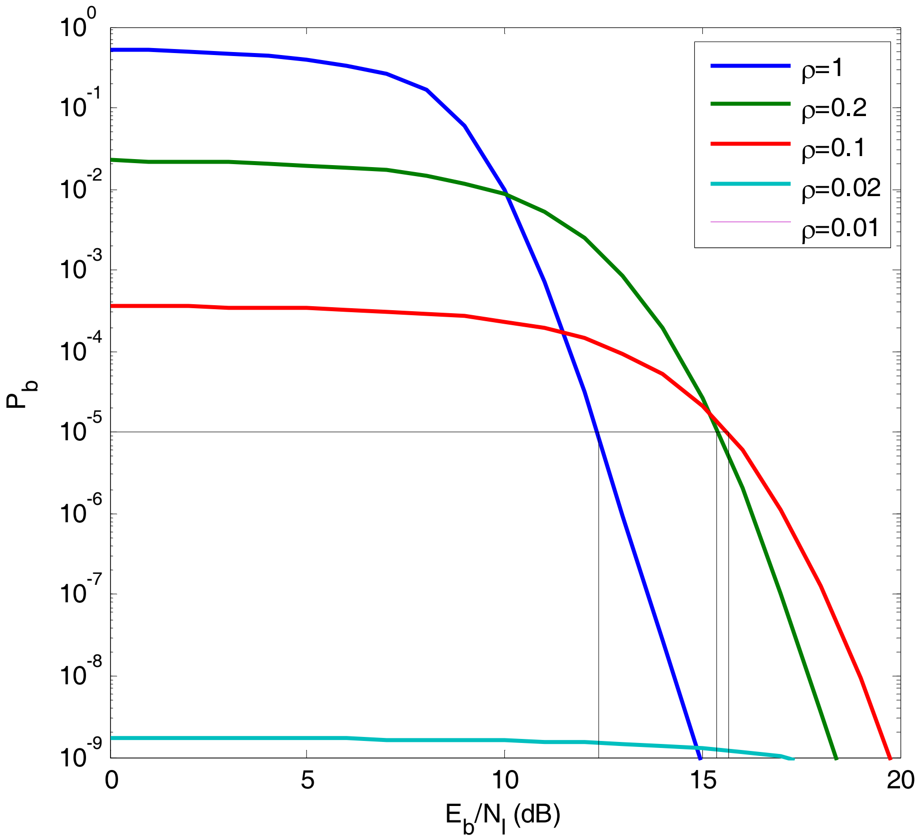

Figure 15. Performance of the original JTIDS waveform with different values of ρ in both AWGN and PNI for noncoherent demodulation when E_b / N_o =10 dB.

Table 7. Performance of the original JTIDS waveform with different values of ρ in both AWGN and PNI for noncoherent demodulation when $P_b = 10^{-5}$ and E_b / N_o =10 dB.

ρ	E_b / N_I (dB)
1	12.3
0.2	15.4
0.1	15.6

3. Comparison Between Coherent and Noncoherent Demodulation for the Original JTIDS Waveform in AWGN and PNI with E_b / N_o =10 dB

For purposes of comparison, both coherent and noncoherent demodulation of the original JTIDS waveform with $\rho = 1$, $\rho = 0.2$, $\rho = 0.1$ and $\rho = 0.05$ for E_b / N_o =10 dB are plotted in Figures 16, 17, 18 and 19, respectively. The performance for coherent demodulation is superior to that of noncoherent demodulation, and the relative benefit of coherent demodulation increases as ρ decreases for $\rho \geq 0.1$. For $\rho < 0.1$, $P_b < 10^{-5}$ for all E_b / N_I when E_b / N_o =10 dB. For comparison purposes, the E_b / N_I required for $P_b = 10^{-5}$ when E_b / N_o =10 dB for $\rho = 1$, $\rho = 0.2$, $\rho = 0.1$ and $\rho = 0.05$, respectively, are listed in Tables 8, 9 and 10.

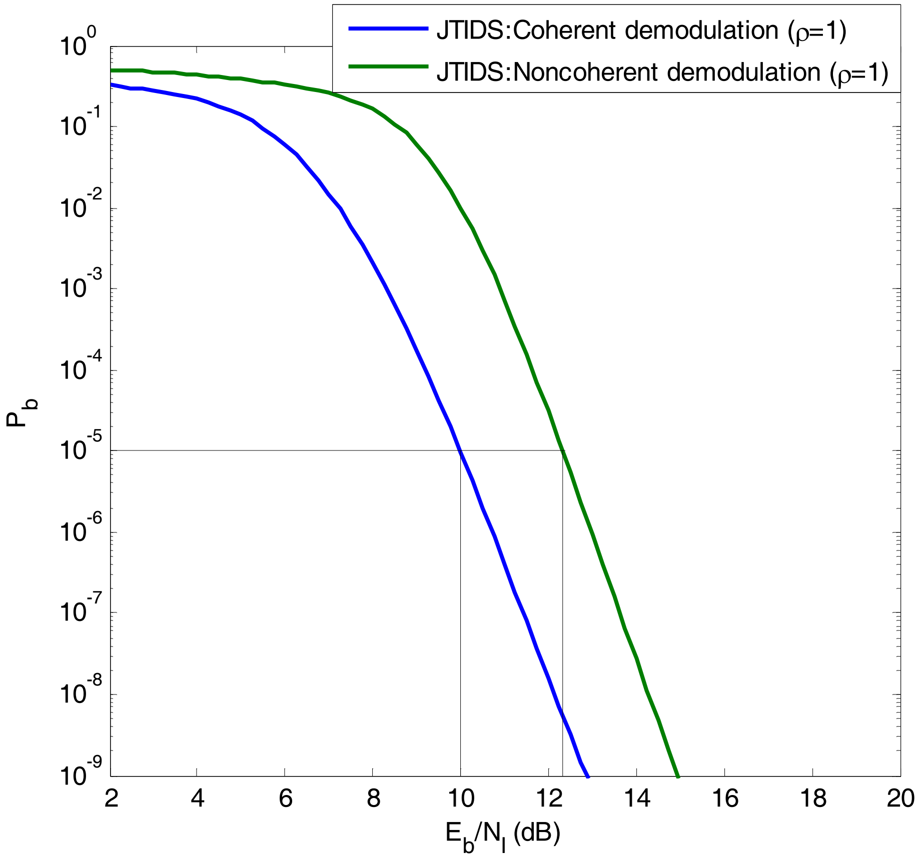

Figure 16. Comparison of the performance of the original JTIDS waveform in both AWGN and PNI with $\rho = 1$ for coherent and noncoherent demodulation when E_b / N_o =10 dB.

Table 8. Comparison of the performance of the original JTIDS waveform in both AWGN and PNI with $\rho = 1$ for coherent and noncoherent demodulation when $P_b = 10^{-5}$ and E_b / N_o =10 dB.

Demodulation	E_b / N_I (dB)
Coherent	10.0
Noncoherent	12.3

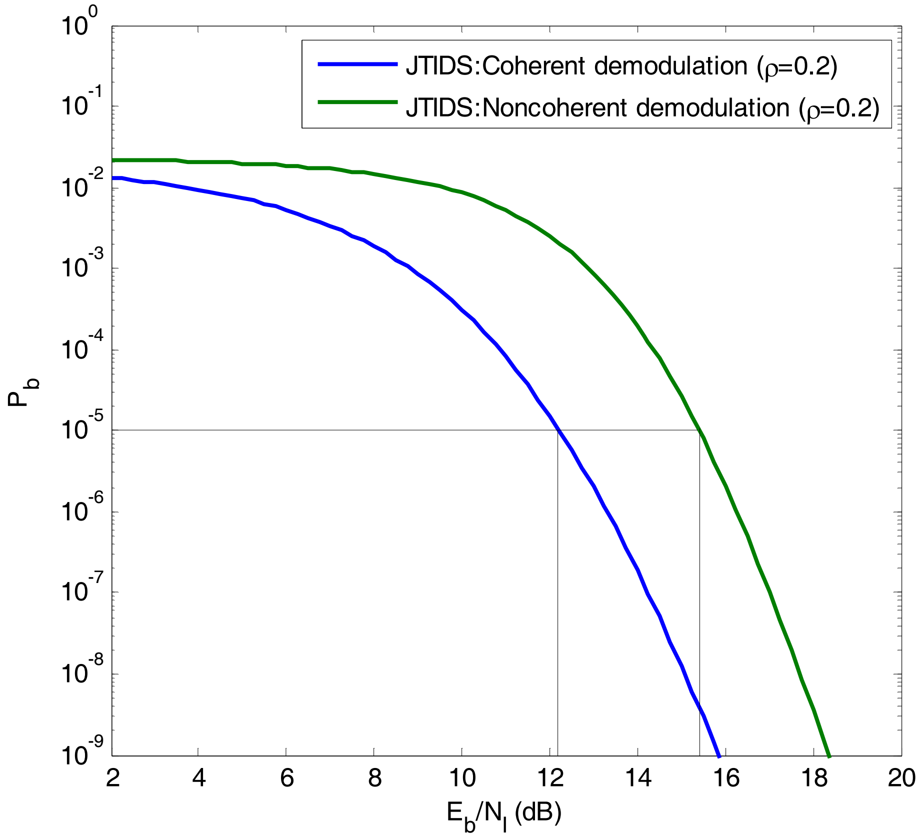

Figure 17. Comparison of the performance of the original JTIDS waveform in both AWGN and PNI with $\rho = 0.2$ for coherent and noncoherent demodulation when E_b / N_o =10 dB.

Table 9. Comparison of the performance of the original JTIDS waveform in both AWGN and PNI with $\rho = 0.2$ for coherent and noncoherent demodulation when $P_b = 10^{-5}$ and E_b / N_o =10 dB.

Demodulation	E_b / N_I (dB)
Coherent	12.2
Noncoherent	15.4

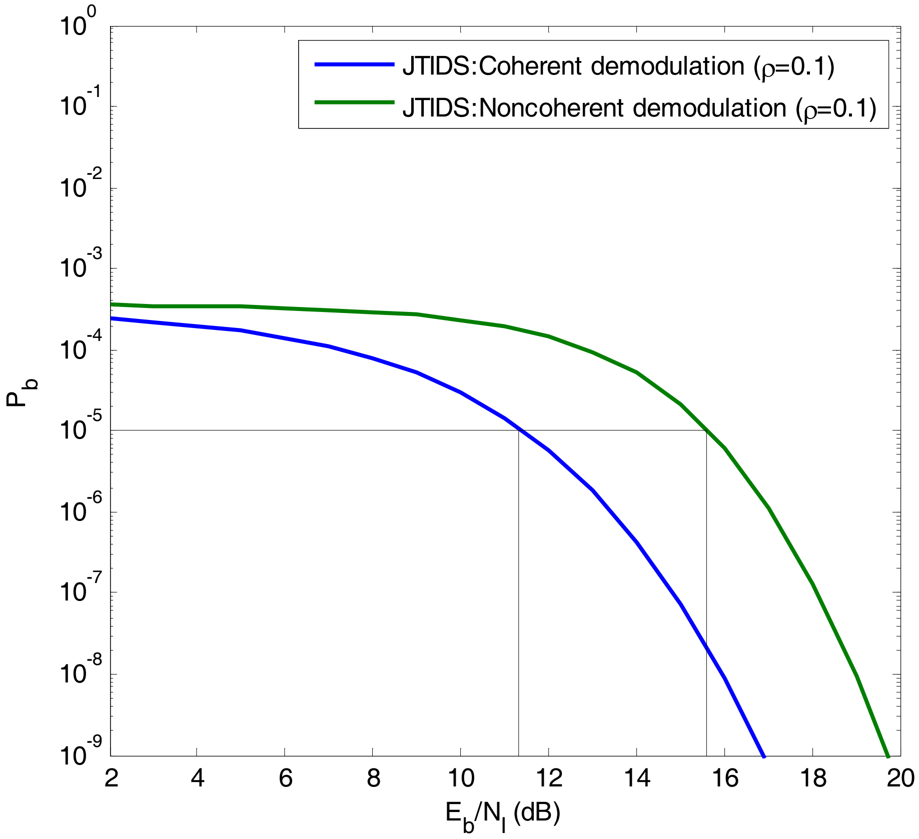

Figure 18. Comparison of the performance of the original JTIDS waveform in both AWGN and PNI with $\rho = 0.1$ for coherent and noncoherent demodulation when E_b / N_o =10 dB.

Table 10. Comparison of the performance of the original JTIDS waveform in both AWGN and PNI with $\rho = 0.1$ for coherent and noncoherent demodulation when $P_b = 10^{-5}$ and E_b / N_o =10 dB.

Demodulation	E_b / N_I (dB)
Coherent	11.4
Noncoherent	15.6

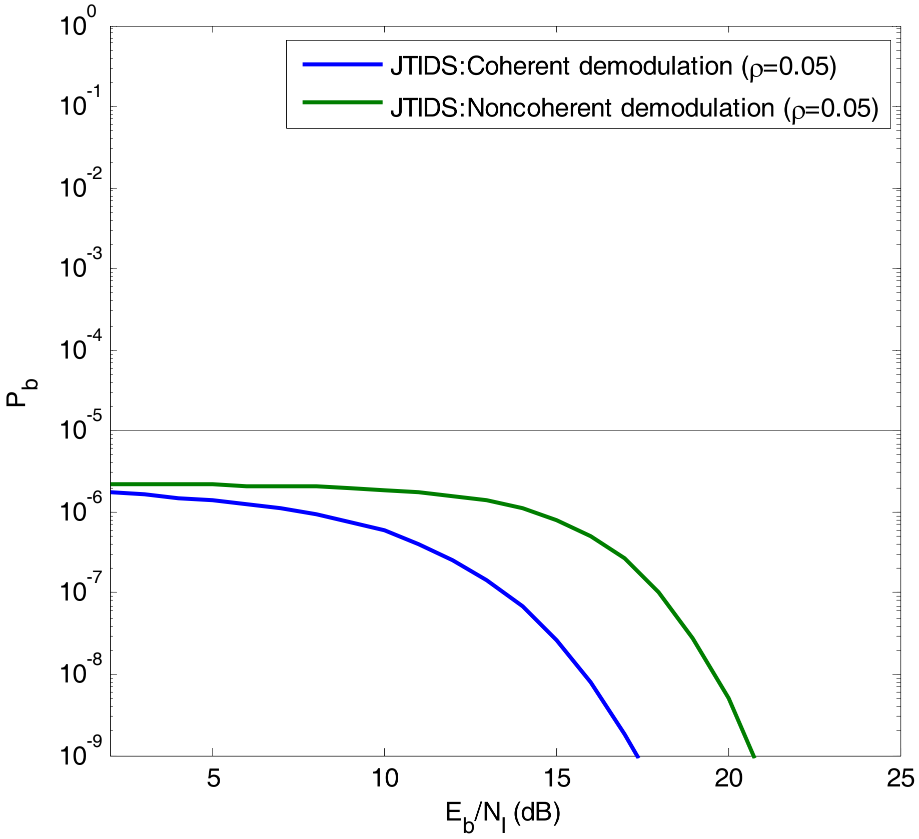

Figure 19. Comparison of the performance of the original JTIDS waveform in both AWGN and PNI with $\rho = 0.05$ for coherent and noncoherent demodulation when E_b / N_o =10 dB.

4. Comparison Between Coherent and Noncoherent Demodulation for the Original JTIDS Waveform in AWGN and PNI with Different Values of E_b / N_I

For purposes of comparison, both coherent and noncoherent demodulation of the original JTIDS waveform with $\rho = 1$, $\rho = 0.2$ and $\rho = 0.1$ in both AWGN and PNI are plotted in Figures 20, 21 and 22, respectively. In each figure, the performance for both coherent and noncoherent demodulation for E_b / N_o =10 dB as well as for E_b / N_o =8.7 dB, which leads to $P_b = 10^{-8}$ for noncoherent demodulation when E_b/N_I>>1, is plotted. The E_b / N_I required for $P_b = 10^{-5}$ when E_b / N_o =10 dB as well as when E_b / N_o =8.7 dB for $\rho = 1$, $\rho = 0.2$ and $\rho = 0.1$ are listed in Tables 11, 12 and 13, respectively.

As for the alternative JTIDS waveform, the comparison between coherent and noncoherent demodulation for the original waveform lead to similar conclusions. From Figures 20, 21 and 22, we see that for E_b / N_o =8.7 dB which leads asymptotically to $P_b = 10^{-8}$ for noncoherent demodulation, the E_b / N_I required for $P_b = 10^{-5}$ increases as ρ decreases. Finally, for E_b / N_o =10 dB and $P_b = 10^{-5}$, as ρ decreases, the difference in performance between coherent and noncoherent demodulation increases from 2.3 dB for BNI to 4.2 dB for $\rho = 0.1$.

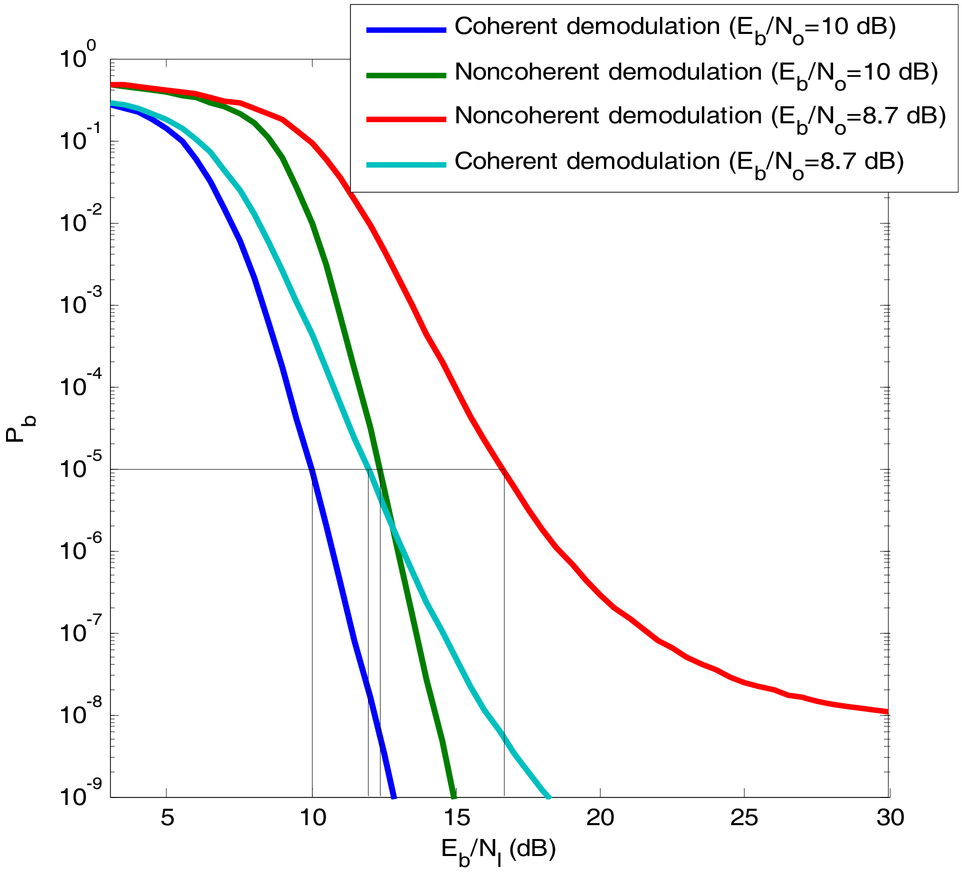

Figure 20. Comparison of the performance of the original JTIDS waveform with $\rho = 1$ in both AWGN and PNI for coherent and noncoherent demodulation.

Table 11. Comparison of the performance of the original JTIDS waveform with $\rho = 1$ in both AWGN and PNI for coherent and noncoherent demodulation when $P_b = 10^{-5}$.

E_b / N_o (dB)	Demodulation	E_b / N_I (dB)
10	Coherent	10.0
10	Noncoherent	12.3
8.7	Coherent	12.0
8.7	Noncoherent	16.6

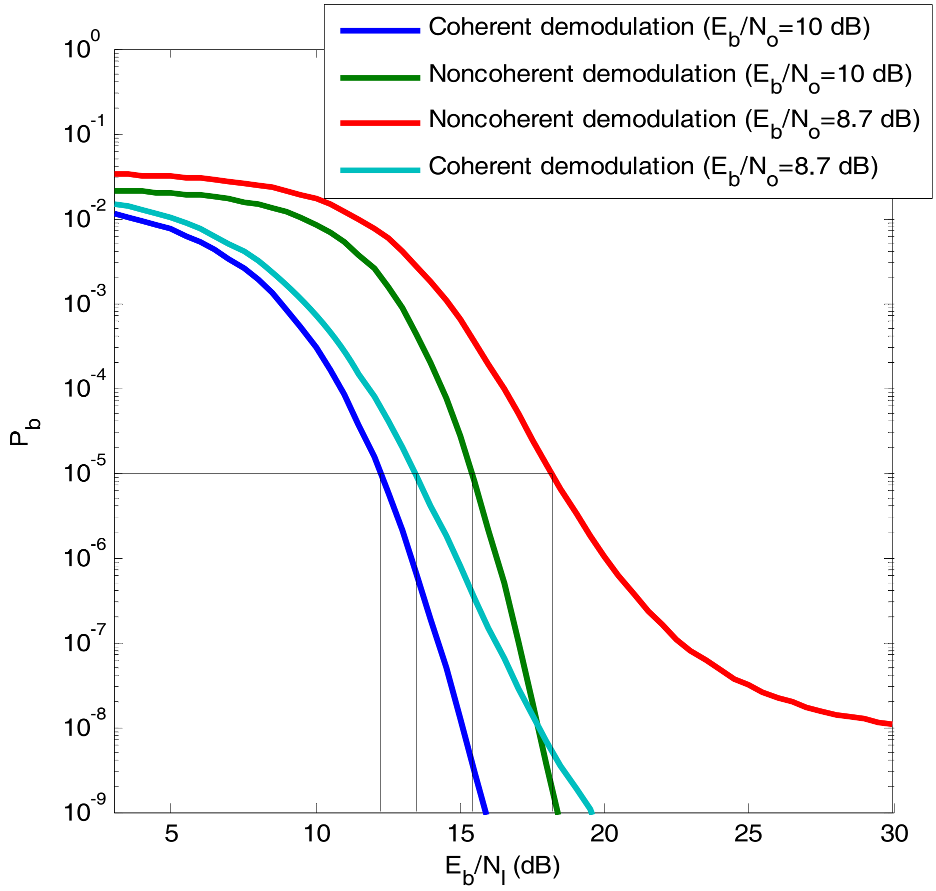

Figure 21. Comparison of the performance of the original JTIDS waveform with $\rho = 0.2$ in both AWGN and PNI for coherent and noncoherent demodulation.

Table 12. Comparison of the performance of the original JTIDS waveform with $\rho = 0.2$ in both AWGN and PNI for coherent and noncoherent demodulation when $P_b = 10^{-5}$.

E_b / N_o (dB)	Demodulation	E_b / N_I (dB)
10	Coherent	12.2
10	Noncoherent	15.4
8.7	Coherent	13.5
8.7	Noncoherent	18.2

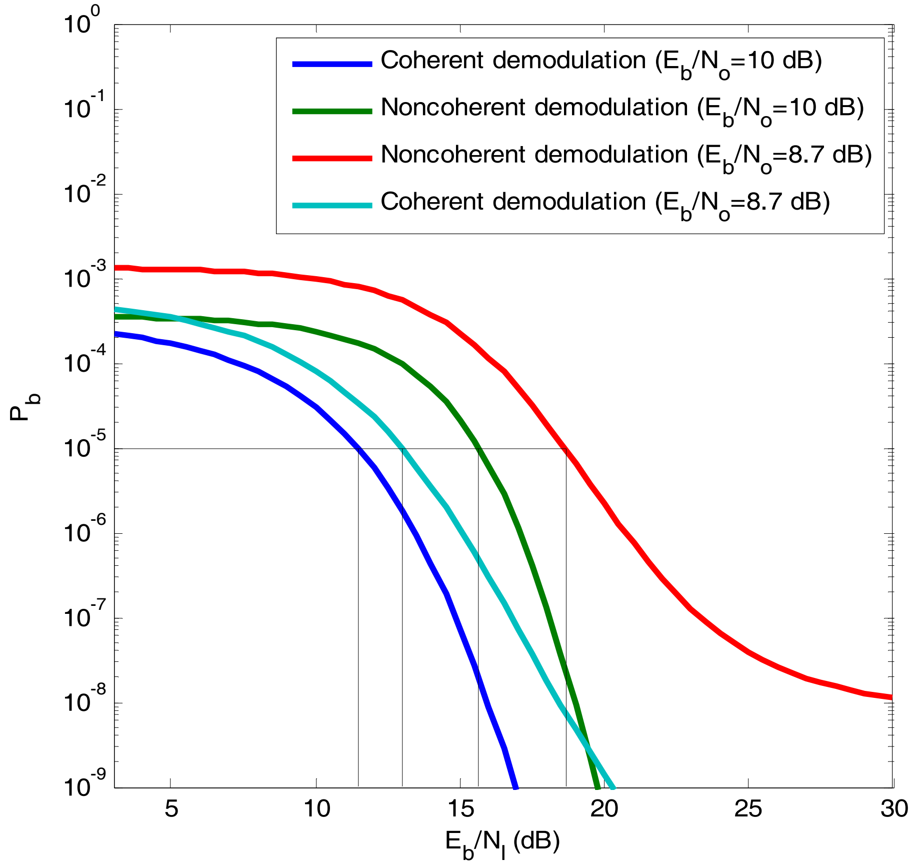

Figure 22. Comparison of the performance of the original JTIDS waveform with $\rho = 0.1$ in both AWGN and PNI for coherent and noncoherent demodulation.

Table 13. Comparison of the performance of the original JTIDS waveform with $\rho = 0.1$ in both AWGN and PNI for coherent and noncoherent demodulation when $P_b = 10^{-5}$.

E_b / N_o (dB)	Demodulation	E_b / N_I (dB)
10	Coherent	11.4
10	Noncoherent	15.6
8.7	Coherent	13.0
8.7	Noncoherent	18.6

C. COMPARISON OF 32-ARY ORTHOGONAL SIGNALING WITH (31,15) ENCODING WITH THE JTIDS WAVEFORM IN AN AWGN ENVIRONMENT

In this section, we compare the performance of the alternative JTIDS/Link-16 waveform and the original JTIDS/Link-16 waveform for both coherent and noncoherent demodulation in AWGN.

1. Coherent Demodulation

The probability of information bit error for the alternative JTIDS/Link-16 waveform and the JTIDS/Link-16 waveform in AWGN are plotted in Figure 23. For $P_b = 10^{-5}$, $E_b / N_0 = 5.3$ dB and $E_b / N_0 = 7$ dB for the alternative JTIDS/Link-16 waveform and the existing JTIDS/Link-16 waveform, respectively. This gives a 1.7 dB gain for the proposed JTIDS/Link-16 waveform as compared to the JTIDS/Link-16 waveform.

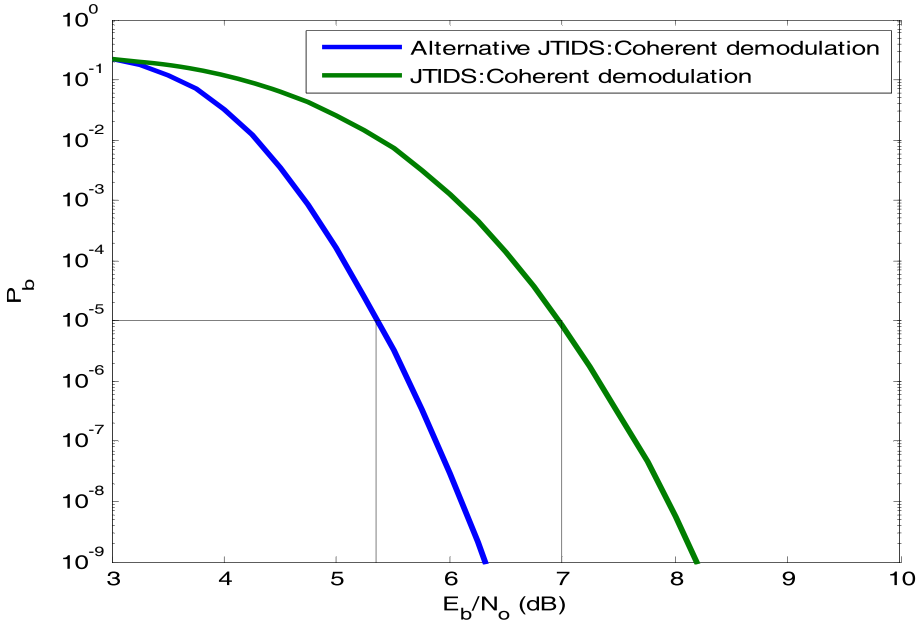

Figure 23. Comparison of 32-ary orthogonal signaling with (31, 15) RS encoding with the original JTIDS waveform in AWGN for coherent demodulation.

2. Noncoherent Demodulation

The probability of information bit error for the alternative JTIDS/Link-16 waveform and the JTIDS/Link-16 waveform in AWGN are plotted in Figure 24. For $P_b = 10^{-5}$, $E_b / N_0 = 6.6$ dB and $E_b / N_0 = 8$ dB for the alternative JTIDS/Link-16 waveform and the existing JTIDS/Link-16 waveform, respectively. This gives a 1.4 dB gain for the proposed JTIDS/Link-16 waveform as compared to the JTIDS/Link-16 waveform.

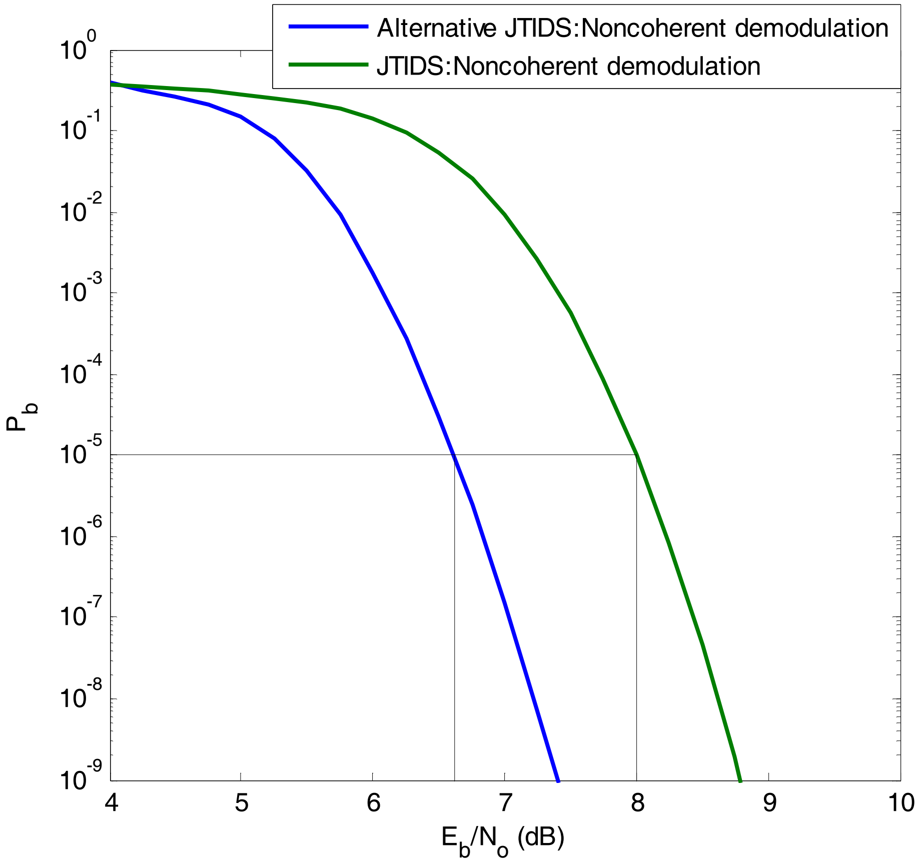

Figure 24. Comparison of 32-ary orthogonal signaling with (31, 15) RS encoding with the original JTIDS waveform in AWGN for noncoherent demodulation.

D. COMPARISON OF 32-ARY ORTHOGONAL SIGNALING WITH (31, 15) ENCODING WITH THE JTIDS WAVEFORM IN BOTH AWGN AND PNI

In this section, we compare the performance of the alternative JTIDS/Link-16 waveform and the original JTIDS/Link-16 waveform for both coherent and noncoherent demodulation when both AWGN and PNI are present.

1. Coherent Demodulation

We see in Figures 25, 26 and 27 and from Tables 14, 15 and 16 that for $P_b = 10^{-5}$ and for $0.1 \le \rho \le 1$ the original JTIDS waveform has a substantially inferior performance if the two waveforms are compared on an equal E_b / N_0 basis, where the difference is most pronounced for BNI but is 3.1 dB for $\rho = 0.1$.

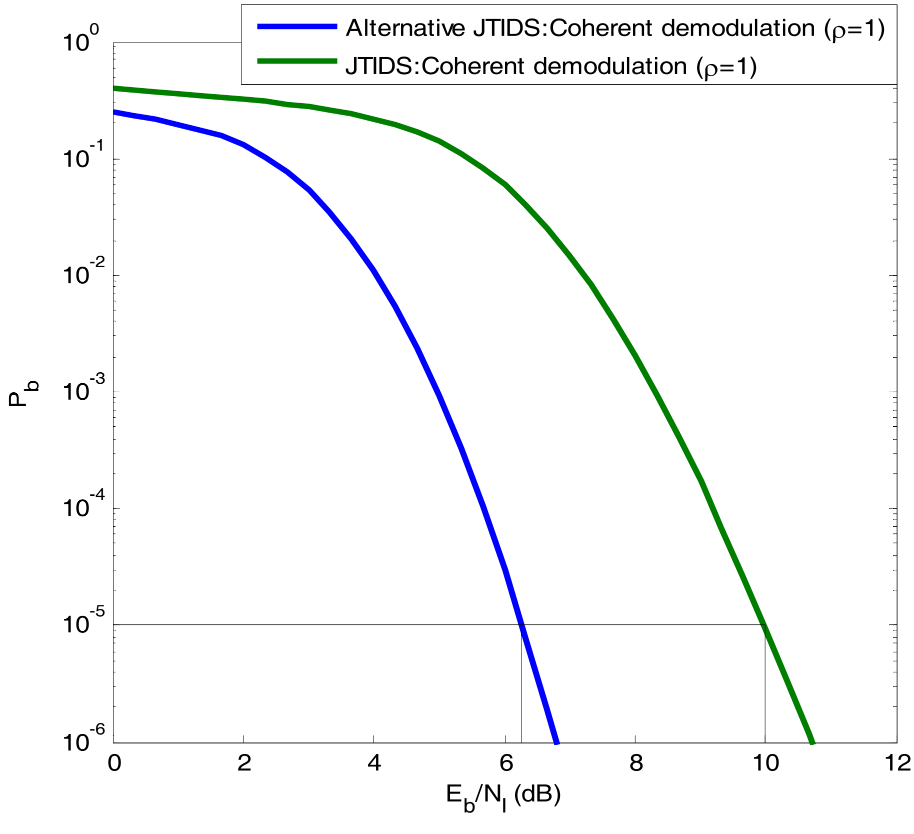

Figure 25. Comparison of 32-ary orthogonal signaling with (31, 15) encoding with the JTIDS waveform in both AWGN and PNI with $\rho = 1$ for coherent demodulation when E_b / N_o =10 dB.

Table 14. Comparison of 32-ary orthogonal signaling with (31, 15) encoding with the JTIDS waveform in both AWGN and PNI with $\rho = 1$ for coherent demodulation when $P_b = 10^{-5}$ and E_b / N_o =10 dB.

JTIDS (waveform)	E_b / N_I (dB)
Alternative	6.3
Original	10.0

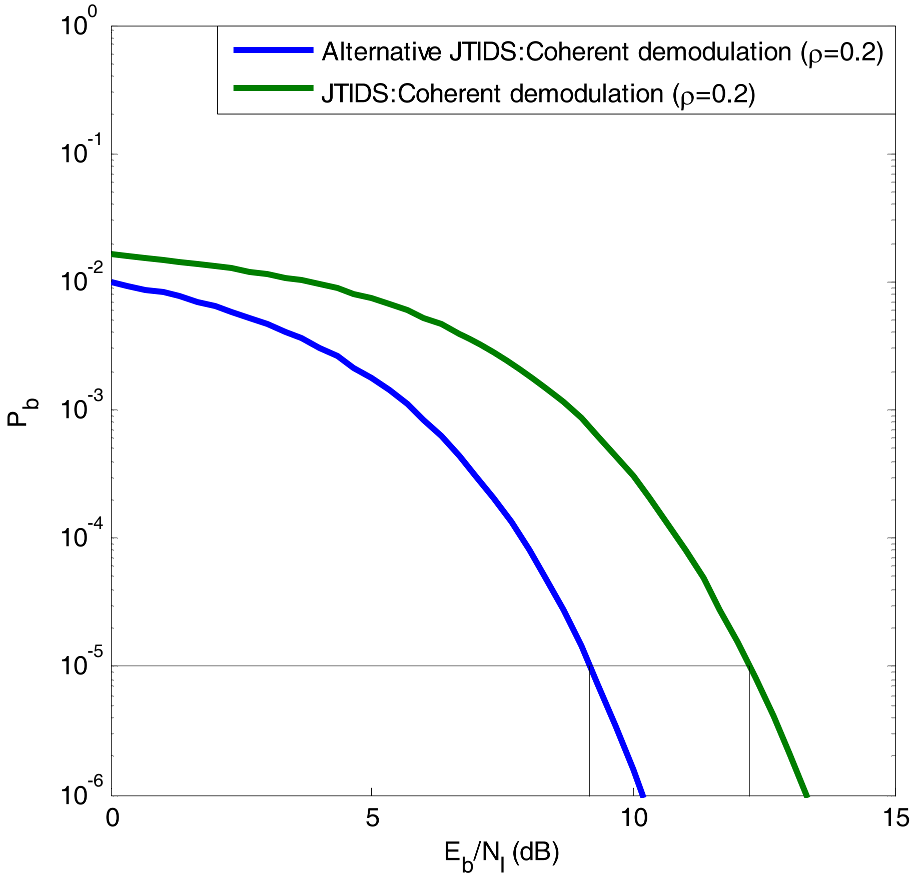

Figure 26. Comparison of 32-ary orthogonal signaling with (31, 15) encoding with the JTIDS waveform in both AWGN and PNI with $\rho = 0.2$ for coherent demodulation when E_b / N_o =10 dB.

Table 15. Comparison of 32-ary orthogonal signaling with (31, 15) encoding with the JTIDS waveform in both AWGN and PNI with $\rho = 0.2$ for coherent demodulation when $P_b = 10^{-5}$ and E_b / N_o =10 dB.

JTIDS (waveform)	E_b / N_I (dB)
Alternative	9.1
Original	12.2

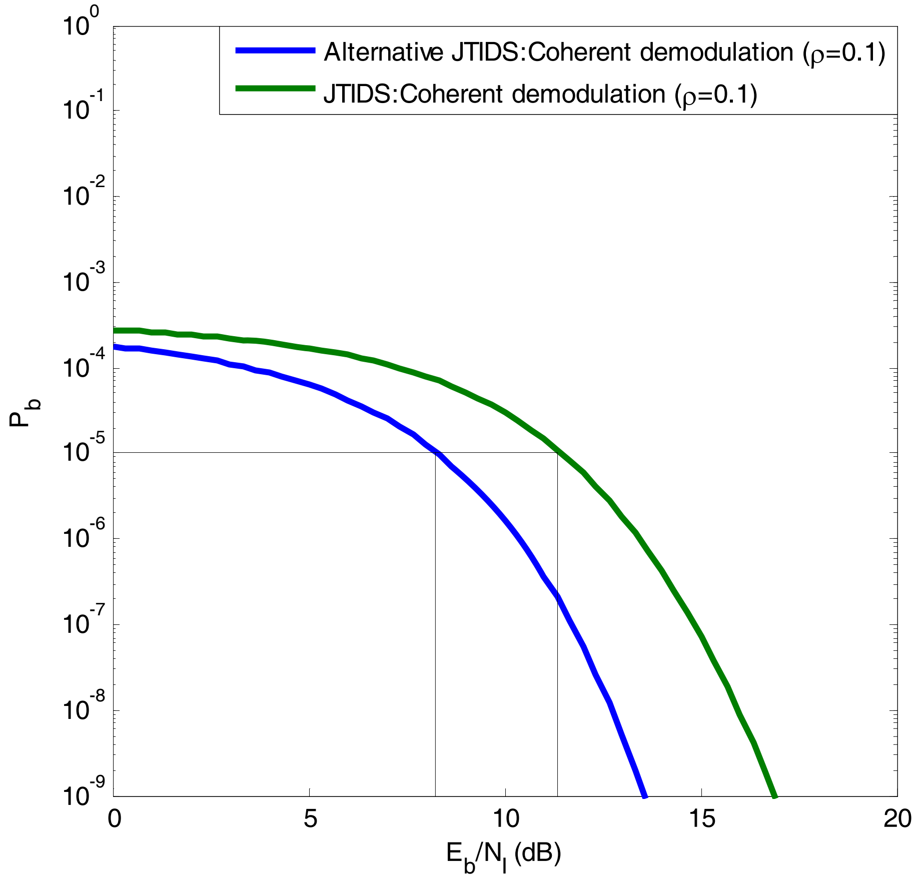

Figure 27. Comparison of 32-ary orthogonal signaling with (31, 15) encoding with the JTIDS waveform in both AWGN and PNI with $\rho = 0.1$ for coherent demodulation when E_b / N_o =10 dB.

Table 16. Comparison of 32-ary orthogonal signaling with (31, 15) encoding with the JTIDS waveform in both AWGN and PNI with $\rho = 0.1$ for coherent demodulation when $P_b = 10^{-5}$ and E_b / N_o =10 dB.

JTIDS (waveform)	E_b / N_I (dB)
Alternative	8.3
Original	11.4

2. Noncoherent Demodulation

In this subsection, the alternative and the original waveform in both AWGN and PNI for different values of ρ for noncoherent demodulation are compared.

As with coherent demodulation, we see in Figures 28, 29 and 30 and from Tables 17, 18 and 19 that, at $P_b = 10^{-5}$ and for $0.1 \le \rho \le 1$, the original JTIDS waveform is inferior if the two waveforms are compared on an equal E_b / N_0 basis. In this case, the difference exceeds 4 dB, and the maximum difference of 4.7 dB occurs for $\rho = 0.1$.

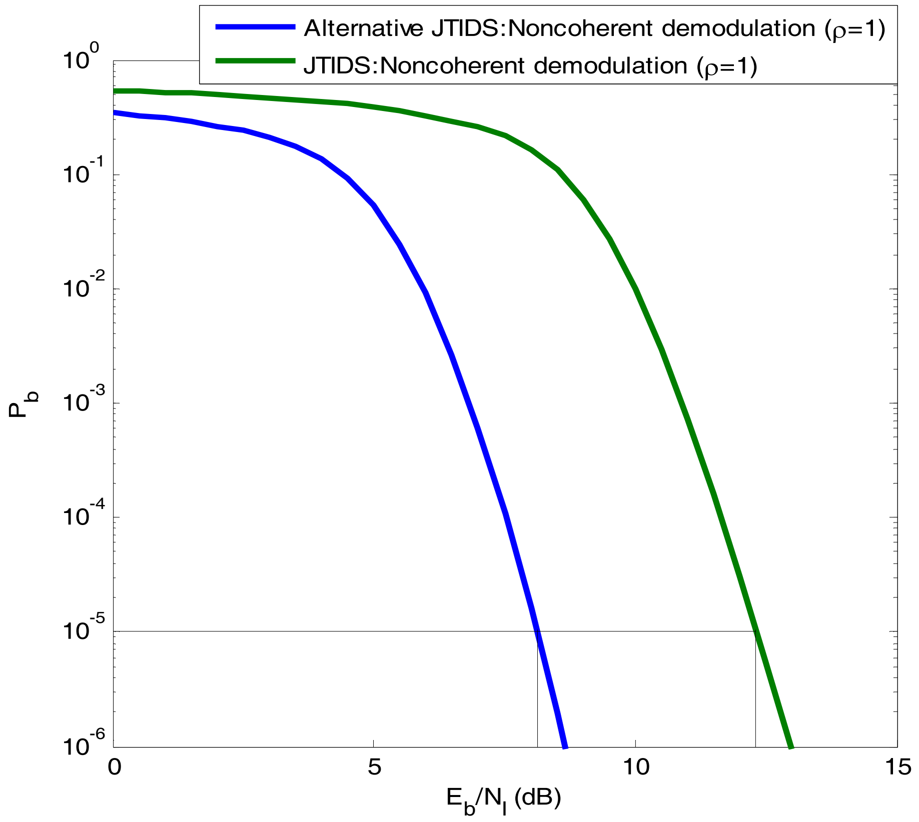

Figure 28. Comparison of 32-ary orthogonal signaling with (31, 15) encoding with the JTIDS waveform in both AWGN and PNI with $\rho = 1$ for noncoherent demodulation when E_b / N_o =10 dB.

Table 17. Comparison of 32-ary orthogonal signaling with (31, 15) encoding with the JTIDS waveform in both AWGN and PNI with $\rho = 1$ for noncoherent demodulation when $P_b = 10^{-5}$ and E_b / N_o =10 dB.

JTIDS (waveform)	E_b / N_I (dB)
Alternative	8.1
Original	12.4

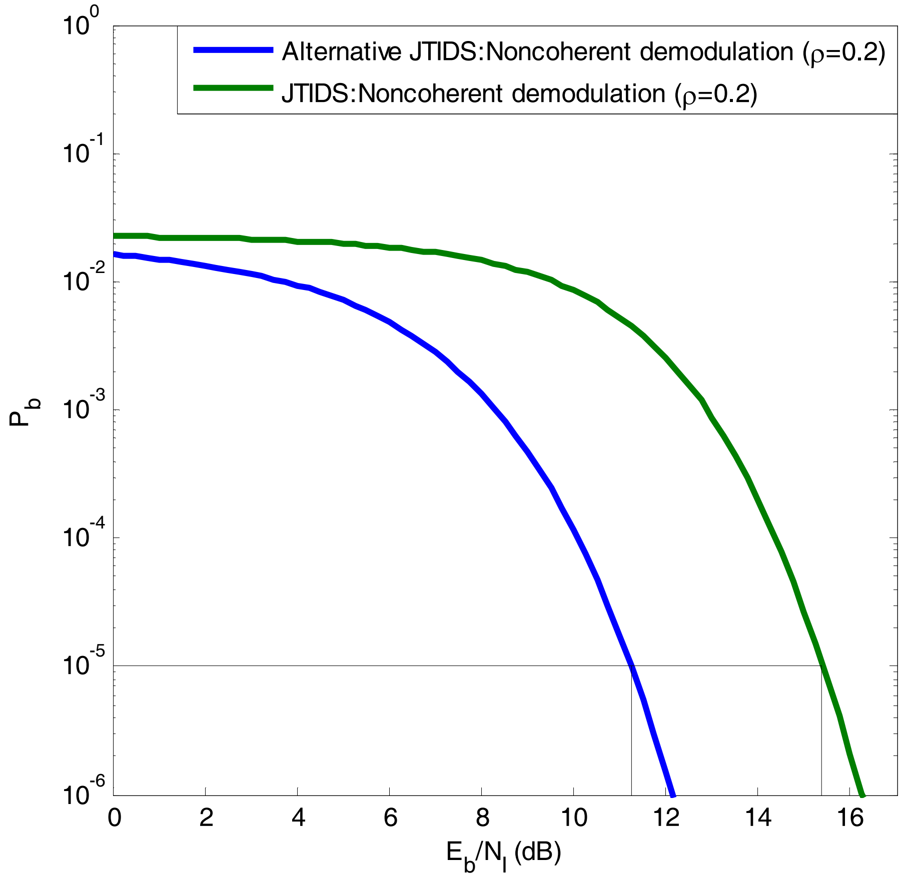

Figure 29. Comparison of 32-ary orthogonal signaling with (31, 15) encoding with the JTIDS waveform in both AWGN and PNI with $\rho = 0.2$ for noncoherent demodulation when E_b / N_o =10 dB.

Table 18. Comparison of 32-ary orthogonal signaling with (31, 15) encoding with the JTIDS waveform in both AWGN and PNI with $\rho = 0.2$ for noncoherent demodulation when $P_b = 10^{-5}$ and E_b / N_o =10 dB.

JTIDS (waveform)	E_b / N_I (dB)
Alternative	11.2
Original	15.4

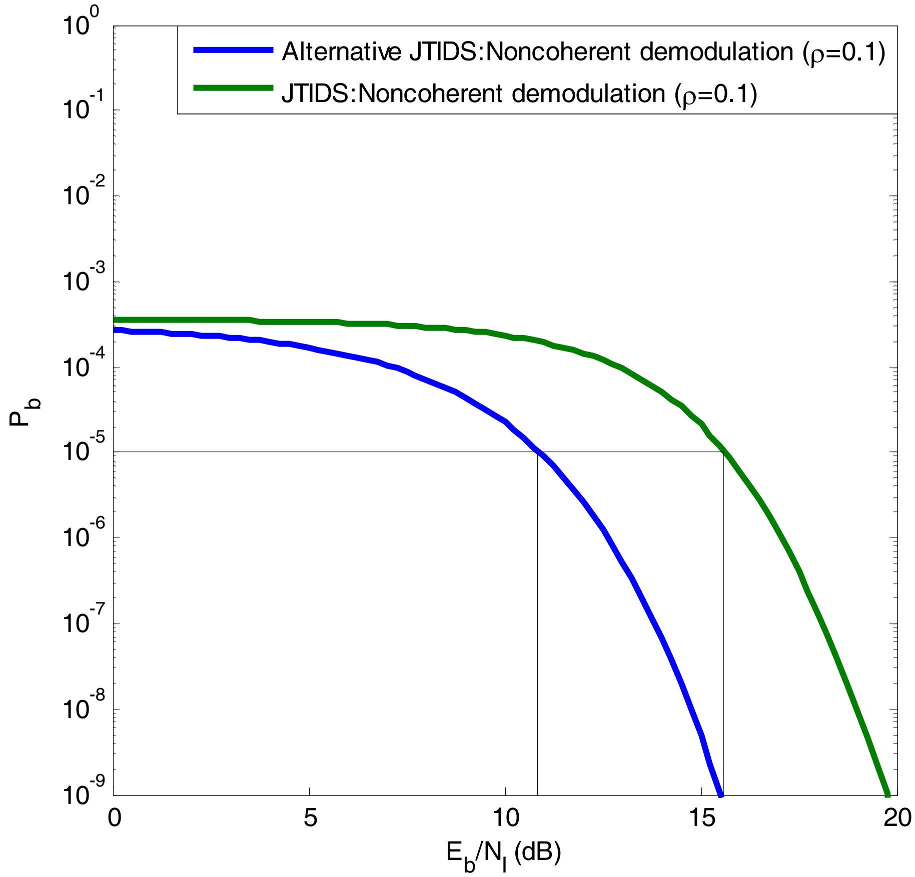

Figure 30. Comparison of 32-ary orthogonal signaling with (31, 15) encoding with the JTIDS waveform in both AWGN and PNI with $\rho = 0.1$ for the noncoherent demodulation when E_b / N_o =10 dB.

Table 19. Comparison of 32-ary orthogonal signaling with (31,15) encoding with the JTIDS waveform in both AWGN and PNI with $\rho = 0.1$ for noncoherent demodulation when $P_b = 10^{-5}$ and E_b / N_o =10 dB.

JTIDS (waveform)	E_b / N_I (dB)
Alternative	10.9
Original	15.6

E. CHAPTER SUMMARY

In this chapter, the performance of the original JTIDS waveform was compared to that of the alternative JTIDS waveform for both coherent and noncoherent demodulation in AWGN only as well as both AWGN and PNI. The results show a significant improvement over the original JTIDS waveform for $\rho \leq 1$. In the next chapter, the performance of the alternative JTIDS waveform with EED in AWGN only as well as both AWGN and PNI is investigated for both coherent and noncoherent demodulation.

THIS PAGE INTENTIONALLY LEFT BLANK

VI. PERFORMANCE ANALYSIS OF 32-ARY ORTHOGONAL SIGNALING WITH (31,15) RS ENCODING IN AN AWGN AND PULSE-NOISE INTERFERENCE ENVIRONMENT WITH ERRORS-AND-ERASURES DECODING

In this chapter the performance of 32-ary orthogonal signaling with (31, 15) RS encoding in AWGN as well as both AWGN and PNI is examined for errors-and-erasures decoding. Both coherent and noncoherent demodulation are considered.

A. COHERENT DEMODULATION IN AWGN

We first examine the effect of errors-and-erasures decoding for coherent demodulation in AWGN, noise which is present for all communication systems even when there are no other types of noise present.

The receiver has to decide which of the M symbols was received or decide that it cannot make a decision with sufficient confidence. If the output of each integrator $V_T > X_i,\ i = 1, 2, ..., M$, then the receiver cannot decide with sufficient confidence, and the symbol is erased.

Without loss of generality, we assume that the original signal representing symbol ‘1’ is transmitted. With errors-and-erasures demodulation, if symbol ‘1’ is transmitted, then the probability of channel symbol erasure p_e and probability of correct symbol detection p_c are [6]

$$p_e = \Pr(V_T > X_1 \cap V_T > X_2 \cap V_T > X_3 \cap ... \cap V_T > X_M \,|1) \qquad (6.1)$$

and

$$p_c = \Pr(X_1 > X_2 \cap X_1 > X_3 \cap ... \cap X_1 > X_M \,|1, X_1 > V_T), \qquad (6.2)$$

respectively. The probability of channel symbol error can be obtained by substituting (6.1) and (6.2) into

$$p_s = 1 - p_e - p_c\,. \qquad (6.3)$$

From (6.1), the probability of symbol erasure is given by [6]

$$p_e = \int_{-\infty}^{V_T}\int_{-\infty}^{V_T}\int_{-\infty}^{V_T}\ldots\int_{-\infty}^{V_T} f_{X_1X_2\ldots X_M}\left(x_1, x_2, \ldots, x_M \mid 1\right) dx_1 dx_2 dx_3 \ldots dx_M \tag{6.4}$$

where $f_{X_1X_2\ldots X_M}\left(x_1, x_2, \ldots, x_M \mid 1\right)$ represents the joint probability density function of the random variables that model the branch outputs. Since the random variables that model the branch outputs are independent, (6.4) can be written as

$$\begin{aligned} p_e = & \int_{-\infty}^{V_T} f_{X_1}\left(x_1 \mid 1\right) dx_1 \int_{-\infty}^{V_T} f_{X_2}\left(x_2 \mid 1\right) dx_2 \\ & \times \int_{-\infty}^{V_T} f_{X_3}\left(x_3 \mid 1\right) dx_3 \ldots \int_{-\infty}^{V_T} f_{X_M}\left(x_M \mid 1\right) dx_M . \end{aligned} \tag{6.5}$$

Since $\int_{-\infty}^{V_T} f_{X_2}\left(x_2 \mid 1\right) dx_2 = \int_{-\infty}^{V_T} f_{X_3}\left(x_3 \mid 1\right) dx_3 = \ldots = \int_{-\infty}^{V_T} f_{X_M}\left(x_M \mid 1\right) dx_M$, (6.6)

(6.5) simplifies to

$$p_e = \left[\int_{-\infty}^{V_T} f_{X_1}\left(x_1 \mid 1\right) dx_1\right]\left[\int_{-\infty}^{V_T} f_{X_2}\left(x_2 \mid 1\right) dx_2\right]^{M-1} . \tag{6.7}$$

The conditional probability density functions for the random variables X_m, where $m = 1, 2, \ldots, M$ that represent the integrator outputs when the noise is modeled as Gaussian noise are [6]

$$f_{X_m}\left(x_m \mid m\right) = \frac{1}{\sqrt{2\pi}\sigma}\exp\left[\frac{-\left(x_m - \sqrt{2}A_c\right)^2}{2\sigma^2}\right] \quad \text{for } m \le M , \tag{6.8}$$

and

$$f_{X_n}\left(x_n \mid n,\, n \ne m\right) = \frac{1}{\sqrt{2\pi}\sigma}\exp\left[\frac{-x_n^{\ 2}}{2\sigma^2}\right] \tag{6.9}$$

where $\sigma^2 = N_0 / T_s$. Substituting (6.8) and (6.9) into (6.7), we obtain

$$p_e = \left[\int_{-\infty}^{V_T} \frac{1}{\sqrt{2\pi}\sigma}\exp\left[\frac{-\left(x_1 - \sqrt{2}A_c\right)^2}{2\sigma^2}\right] dx_1\right]\left[\int_{-\infty}^{V_T} \frac{1}{\sqrt{2\pi}\sigma}\exp\left[\frac{-x_2^{\ 2}}{2\sigma^2}\right] dx_2\right]^{M-1} \tag{6.10}$$

which can be evaluated to obtain

$$p_e = \left[1 - Q\left(\frac{V_T - \sqrt{2}A_c}{\sigma}\right)\right]\left[1 - Q\left(\frac{V_T}{\sigma}\right)\right]^{M-1} . \tag{6.11}$$

Defining $V_T = \alpha\sqrt{2}A_c$, where $0 < \alpha < 1$, we get

$$p_e = \left[1 - Q\left(\frac{\alpha\sqrt{2}A_c - \sqrt{2}A_c}{\sigma}\right)\right]\left[1 - Q\left(\frac{\alpha\sqrt{2}A_c}{\sigma}\right)\right]^{M-1} . \tag{6.12}$$

Hence,

$$p_e = \left[1 - Q\left((\alpha - 1)\sqrt{\frac{2E_s}{N_o}}\right)\right]\left[1 - Q\left(\alpha\sqrt{\frac{2E_s}{N_o}}\right)\right]^{M-1} . \tag{6.13}$$

From (6.13), the probability of channel erasure with (*n*, *k*) RS coding with code rate r is

$$p_e = \left[1 - Q\left((\alpha - 1)\sqrt{\frac{2rE_s}{N_o}}\right)\right]\left[1 - Q\left(\alpha\sqrt{\frac{2rE_s}{N_o}}\right)\right]^{M-1} . \tag{6.14}$$

Expressed in terms of E_b / N_o, (6.14) is given by

$$p_e = \left[1 - Q\left((\alpha - 1)\sqrt{\frac{2rmE_b}{N_o}}\right)\right]\left[1 - Q\left(\alpha\sqrt{\frac{2rmE_b}{N_o}}\right)\right]^{M-1} . \tag{6.15}$$

Similarly, we can derive an expression for the probability of correct symbol detection [6]. From (6.2), we get

$$p_c = \int_{V_T}^{\infty}\left[\int_{-\infty}^{x_1}\int_{-\infty}^{x_1}\cdots\int_{-\infty}^{x_1} f_{X_1X_2\ldots X_M}\left(x_1, x_2, \ldots, x_M \mid 1\right)dx_2dx_3\ldots dx_M\right]dx_1 . \tag{6.16}$$

Since the random variables X_m, where $m = 1, 2, \ldots, M$, are independent, (6.16) can be written as

$$p_c = \int_{V_T}^{\infty} f_{X_1}\left(x_1 \mid 1\right)\times\left[\int_{-\infty}^{x_1} f_{X_2}\left(x_2 \mid 1\right)dx_2\int_{-\infty}^{x_1} f_{X_3}\left(x_3 \mid 1\right)dx_3\ldots\int_{-\infty}^{x_1} f_{X_M}\left(x_M \mid 1\right)dx_M\right]dx_1 \tag{6.17}$$

Using (6.6), we see that (6.17) simplifies to

$$p_c = \int_{V_T}^{\infty} f_{X_1}\left(x_1 \mid 1\right)\times\left[\int_{-\infty}^{x_1} f_{X_2}\left(x_2 \mid 1\right)dx_2\right]^{M-1}dx_1 . \tag{6.18}$$

Substituting (6.8) and (6.9) into (6.18), we get

$$p_c = \int_{V_T}^{\infty} \frac{1}{\sqrt{2\pi}\sigma} \exp\left[\frac{-\left(x_1 - \sqrt{2}A_c\right)^2}{2\sigma^2}\right] \times \left[\int_{-\infty}^{x_1} \frac{1}{\sqrt{2\pi}\sigma} \exp\left(\frac{-x_2{}^2}{2\sigma^2}\right) dx_2\right]^{M-1} dx_1 \qquad (6.19)$$

which can be evaluated to obtain

$$p_c = \int_{V_T}^{\infty} \frac{1}{\sqrt{2\pi}\sigma} \exp\left[\frac{-\left(x_1 - \sqrt{2}A_c\right)^2}{2\sigma^2}\right] \times \left[1 - Q\left(\frac{x_1}{\sigma}\right)\right]^{M-1} dx_1 \qquad (6.20)$$

Letting $u = \left(x_1 - \sqrt{2}A_c\right) / \sigma$, we get

$$p_c = \int_{\frac{V_T - \sqrt{2}A_c}{\sigma}}^{\infty} \frac{1}{\sqrt{2\pi}} e^{\left(\frac{-u^2}{2}\right)} \times \left[1 - Q\left(u + \frac{\sqrt{2}A_c}{\sigma}\right)\right]^{M-1} du \qquad (6.21)$$

Finally, with $V_T = \alpha\sqrt{2}A_c$ and $\sigma = N_o / T_s$, we obtain the probability of correct channel detection as

$$p_c = \frac{1}{\sqrt{2\pi}} \int_{-(1-\alpha)\sqrt{\frac{2E_s}{N_o}}}^{\infty} e^{\left(\frac{-u^2}{2}\right)} \left[1 - Q\left(u + \sqrt{\frac{2E_s}{N_o}}\right)\right]^{M-1} du \qquad (6.22)$$

The probability of correct channel detection can be expressed in terms of E_b / N_o and code rate *r* as

$$p_c = \frac{1}{\sqrt{2\pi}} \int_{-(1-\alpha)\sqrt{\frac{2rmE_b}{N_o}}}^{\infty} e^{\left(\frac{-u^2}{2}\right)} \left[1 - Q\left(u + \sqrt{\frac{2rmE_b}{N_o}}\right)\right]^{M-1} du\,. \qquad (6.23)$$

With errors-and-erasures decoding, the probability of block error is given by [6]

$$P_E = 1 - \left[\sum_{i=0}^{t} \binom{n}{i} p_s^i \sum_{j=0}^{d_{\min}-1-2i} \binom{n-i}{j} p_e^j p_c^{n-i-j}\right] \qquad (6.24)$$

where (6.3), (6.15) and (6.23) are used in (6.24).

The performance for 32-ary orthogonal signaling with a (31, 15) RS code and EED in AWGN for different values of α is shown in Figures 31 and 32. From Figures 31 and 32, we see that performance degrades for large α $(\alpha \geq 0.8)$, and there is not much difference in performance for $\alpha < 0.5$. At $P_b = 10^{-5}$, there is a very small improvement in performance when $\alpha = 0.6$ relative to $\alpha = 0.0$. Since $\alpha = 0.0$ implies no EED, we conclude that there is only a small improvement in performance using EED for the alternative JTIDS/Link-16 waveform in the presence of AWGN. If α is too large, EED degrades performance.

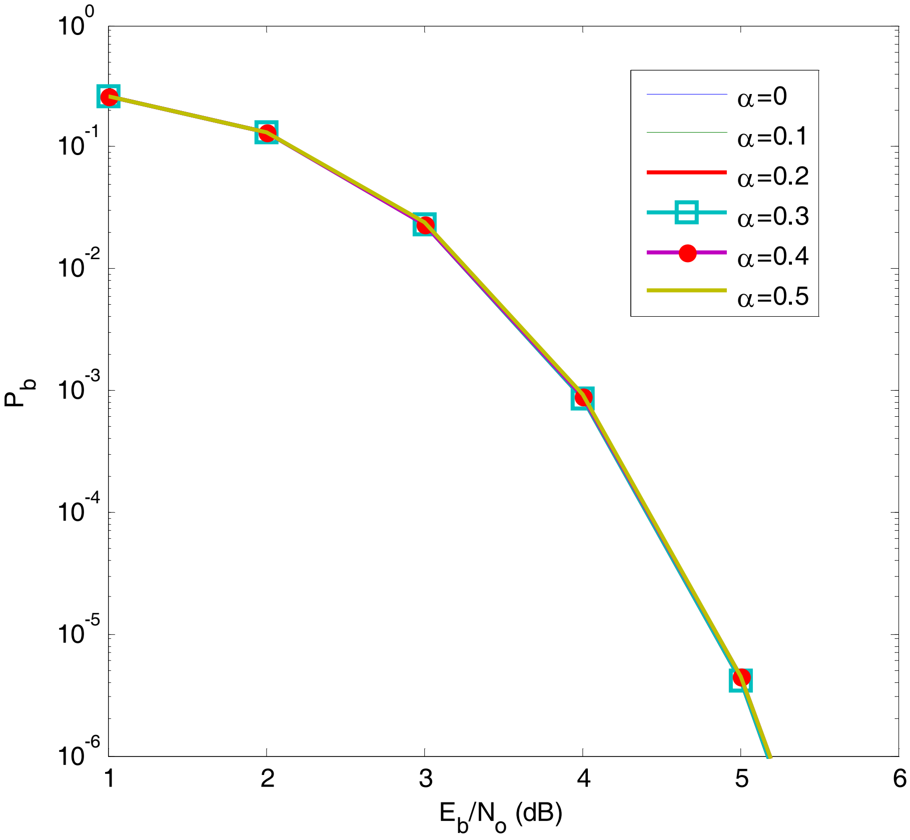

Figure 31. The performance of 32-ary orthogonal signaling with a (31, 15) RS code and EED in AWGN for different values of α for coherent demodulation.

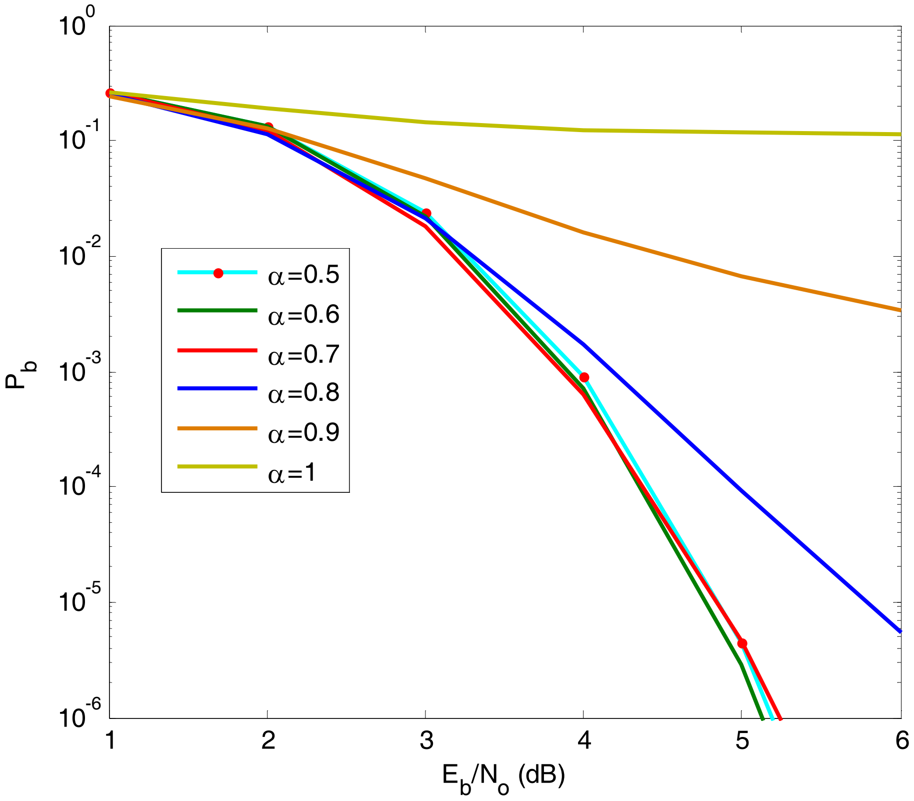

Figure 32. The performance of 32-ary orthogonal signaling with a (31, 15) RS code and EED in AWGN for different values of α for coherent demodulation.

B. NONCOHERENT DEMODULATION IN AWGN

With errors-and-erasures demodulation, if symbol '1' is transmitted, then the probability of channel symbol erasure p_e and probability of correct symbol detection p_c are [6]

$$p_e = \Pr(V_T > X_1 \cap V_T > X_2 \cap V_T > X_3 \cap \ldots \cap V_T > X_M \,|\, 1) \tag{6.25}$$

and

$$p_c = \Pr(X_1 > X_2 \cap X_1 > X_3 \cap \ldots \cap X_1 > X_M \,|\, 1, X_1 > V_T), \tag{6.26}$$

respectively. The probability of channel symbol error can be obtained by substituting (6.25) and (6.26) into

$$p_s = 1 - p_e - p_c. \tag{6.27}$$

From (6.25), the probability of symbol erasure is given by [6]

$$p_e = \int_0^{V_T}\int_0^{V_T}\int_0^{V_T}\ldots\int_0^{V_T} f_{V_1V_2\ldots V_M}\left(v_1, v_2, \ldots, v_M \mid 1\right) dv_1 dv_2 dv_3 \ldots dv_M \tag{6.28}$$

where $f_{V_1V_2\ldots V_M}\left(v_1, v_2, \ldots, v_M \mid 1\right)$ represents the joint probability density function of the random variables that model the detector outputs. Since the random variables that model the branch outputs are independent, (6.28) can be written as

$$\begin{aligned} p_e &= \int_0^{V_T} f_{V_1}\left(v_1 \mid 1\right) dv_1 \int_0^{V_T} f_{V_2}\left(v_2 \mid 1\right) dv_2 \\ &\times \int_0^{V_T} f_{V_3}\left(v_3 \mid 1\right) dv_3 \ldots \int_0^{V_T} f_{V_M}\left(v_M \mid 1\right) dv_M . \end{aligned} \tag{6.29}$$

Since $\int_0^{V_T} f_{V_2}\left(v_2 \mid 1\right) dv_2 = \int_0^{V_T} f_{V_3}\left(v_3 \mid 1\right) dv_3 = \ldots = \int_0^{V_T} f_{V_M}\left(v_M \mid 1\right) dv_M$, (6.30)

(6.29) simplifies to

$$p_e = \left[\int_0^{V_T} f_{V_1}\left(v_1 \mid 1\right) dv_1\right]\left[\int_0^{V_T} f_{V_2}\left(v_2 \mid 1\right) dv_2\right]^{M-1}. \tag{6.31}$$

The conditional probability density functions for the random variables V_m, where $m = 1, 2, \ldots, M$, that represent the branch outputs when the signal representing symbol m is transmitted is the non-central chi-squared probability density function with two degrees of freedom when the noise is modeled as Gaussian noise [6]. Hence,

$$f_{V_m}\left(v_m \mid m\right) = \frac{1}{2\sigma^2}\exp\left[\frac{-\left(v_m + 2A_c^{\,2}\right)}{2\sigma^2}\right] I_0\left(\frac{A_c\sqrt{2v_m}}{\sigma^2}\right) \quad \text{for } m \le M , \tag{6.32}$$

and

$$f_{V_n}\left(v_n \mid n,\, n \ne m\right) = \frac{1}{2\sigma^2}\exp\left[\frac{-v_n}{2\sigma^2}\right]. \tag{6.33}$$

Substituting (6.32) and (6.33) into (6.31), we get

$$p_e = \left[\int_0^{V_T} \frac{1}{2\sigma^2}\exp\left[\frac{-\left(v_1 + 2A_c^{\,2}\right)}{2\sigma^2}\right] I_0\left(\frac{A_c\sqrt{2v_1}}{\sigma^2}\right) dv_1\right]\left[\int_0^{V_T} \frac{1}{2\sigma^2}\exp\left[\frac{-v_2}{2\sigma^2}\right] dv_2\right]^{M-1} \tag{6.34}$$

Equation (6.34) can be rewritten as

$$\begin{aligned} p_e = & \left[\int_0^{\infty} \frac{1}{2\sigma^2} \exp\left[\frac{-\left(v_1 + 2A_c{}^2\right)}{2\sigma^2} \right] I_0\left(\frac{A_c\sqrt{2v_1}}{\sigma^2} \right) dv_1 - \int_{V_T}^{\infty} \frac{1}{2\sigma^2} \exp\left[\frac{-\left(v_1 + 2A_c{}^2\right)}{2\sigma^2} \right] I_0\left(\frac{A_c\sqrt{2v_1}}{\sigma^2} \right) dv_1 \right] \\ & \times \left[\int_0^{V_T} \frac{1}{2\sigma^2} \exp\left[\frac{-v_2}{2\sigma^2} \right] dv_2 \right]^{M-1}. \end{aligned} \tag{6.35}$$

Since

$$\int_0^{\infty} \frac{1}{2\sigma^2} \exp\left[\frac{-\left(v_1 + 2A_c{}^2\right)}{2\sigma^2} \right] I_0\left(\frac{A_c\sqrt{2v_1}}{\sigma^2} \right) dv_1 = 1 \tag{6.36}$$

then (6.35) is given by

$$\begin{aligned} p_e = & \left[1 - \int_{V_T}^{\infty} \frac{1}{2\sigma^2} \exp\left[\frac{-\left(v_1 + 2A_c{}^2\right)}{2\sigma^2} \right] I_0\left(\frac{A_c\sqrt{2v_1}}{\sigma^2} \right) dv_1 \right] \\ & \times \left[\int_0^{V_T} \frac{1}{2\sigma^2} \exp\left[\frac{-v_2}{2\sigma^2} \right] dv_2 \right]^{M-1}. \end{aligned} \tag{6.37}$$

Letting $\sqrt{v_1} = x\sigma$ and $\sqrt{v_2} = x\sigma$ and defining $V_T = 2\alpha A_c{}^2$, where $0 < a < 1$, in (6.37), we derive

$$\begin{aligned} p_e = & \left[\int_0^{\sqrt{2\alpha \frac{E_s}{N_0}}} x \exp\left[-\left(\frac{x^2}{2} + \frac{E_s}{N_0} \right) \right] I_0\left(\sqrt{2\frac{E_s}{N_0}}\, x \right) dx \right] \\ & \times \left[1 - \exp\left[\frac{-V_T}{2\sigma^2} \right] \right]^{M-1}. \end{aligned} \tag{6.38}$$

Since

$$\left[1 - \exp\left[\frac{-V_T}{2\sigma^2} \right] \right]^{M-1} = \sum_{n=0}^{M-1} (-1)^n \binom{M-1}{n} \exp\left[\frac{-n\alpha E_s}{N_0} \right] \tag{6.39}$$

(6.38) can be written as

$$\begin{aligned} p_e = & \left[\int_0^{\sqrt{2\alpha \frac{E_s}{N_0}}} x \exp\left[-\left(\frac{x^2}{2} + \frac{E_s}{N_0} \right) \right] I_0\left(\sqrt{2\frac{E_s}{N_0}}\, x \right) dx \right] \\ & \times \sum_{n=0}^{M-1} (-1)^n \binom{M-1}{n} \exp\left[\frac{-n\alpha E_s}{N_0} \right]. \end{aligned} \tag{6.40}$$

From (6.40), the probability of channel erasure with (*n, k*) RS coding with code rate r is

$$p_e = \left[\int_0^{\sqrt{2\alpha\frac{rE_s}{N_0}}} x \exp\left[-\left(\frac{x^2}{2}+\frac{rE_s}{N_0}\right)\right] I_0\left(\sqrt{2\frac{rE_s}{N_0}}x\right)dx\right] \times\sum_{n=0}^{M-1}(-1)^n\binom{M-1}{n}\exp\left[\frac{-n\alpha rE_s}{N_0}\right]. \tag{6.41}$$

In terms of E_b / N_o, (6.41) can be expressed as

$$p_e = \left[\int_0^{\sqrt{2\alpha\frac{rmE_b}{N_0}}} x \exp\left[-\left(\frac{x^2}{2}+\frac{rmE_b}{N_0}\right)\right] I_0\left(\sqrt{2\frac{rmE_b}{N_0}}x\right)dx\right] \times\sum_{n=0}^{M-1}(-1)^n\binom{M-1}{n}\exp\left[\frac{-n\alpha rmE_b}{N_0}\right]. \tag{6.42}$$

Next, we derive an expression for the probability of correct symbol detection. From (6.26), we have

$$p_c = \int_{V_T}^{\infty}\left[\int_0^{v_1}\int_0^{v_1}\cdots\int_0^{v_1} f_{V_1V_2\ldots V_M}\left(v_1,v_2,\ldots,v_M \mid 1\right)dv_2dv_3\ldots dv_M\right]dv_1 . \tag{6.43}$$

Since the random variables V_m, where $m=1,2,\ldots,M$, are independent. (6.43) can be written as

$$p_c = \int_{V_T}^{\infty} f_{V_1}\left(v_1 \mid 1\right)\times\left[\int_0^{v_1} f_{V_2}\left(v_2 \mid 1\right)dv_2\int_0^{v_1} f_{V_3}\left(v_3 \mid 1\right)dv_3\ldots\int_0^{v_1} f_{V_M}\left(v_M \mid 1\right)dv_M\right]dv_1 \tag{6.44}$$

Using (6.30) in (6.44), we get

$$p_c = \int_{V_T}^{\infty} f_{V_1}\left(v_1 \mid 1\right)\left[\int_0^{v_1} f_{V_2}\left(v_2 \mid 1\right)dv_2\right]^{M-1}dv_1 . \tag{6.45}$$

Finally, substituting (6.32) and (6.33) into (6.45), we get

$$p_c = \int_{V_T}^{\infty}\frac{1}{2\sigma^2}\exp\left[\frac{-\left(v_1+2A_c^{\,2}\right)}{2\sigma^2}\right]I_0\left(\frac{A_c\sqrt{2v_1}}{\sigma^2}\right)\left[\int_0^{v_1}\frac{1}{2\sigma^2}\exp\left[\frac{-v_2}{2\sigma^2}\right]dv_2\right]^{M-1}dv_1 \tag{6.46}$$

which can be partially evaluated to obtain

$$p_c = \int_{V_T}^{\infty}\frac{1}{2\sigma^2}\exp\left[\frac{-\left(v_1+2A_c^{\,2}\right)}{2\sigma^2}\right]I_0\left(\frac{A_c\sqrt{2v_1}}{\sigma^2}\right)\left[1-\exp\left[\frac{-v_1}{2\sigma^2}\right]\right]^{M-1}dv_1 . \tag{6.47}$$

Substituting (6.39) into (6.47), we get

$$\begin{aligned} p_c = & \int_0^{\infty} \frac{1}{2\sigma^2}\exp\left[\frac{-\left(v_1+2A_c^2\right)}{2\sigma^2}\right] I_0\left(\frac{A_c\sqrt{2v_1}}{\sigma^2}\right)\left[\sum_{n=0}^{M-1}(-1)^n\binom{M-1}{n}\exp\left[\frac{-nv_1}{2\sigma^2}\right]\right]dv_1 \\ & -\int_0^{V_T}\frac{1}{2\sigma^2}\exp\left[\frac{-\left(v_1+2A_c^2\right)}{2\sigma^2}\right] I_0\left(\frac{A_c\sqrt{2v_1}}{\sigma^2}\right)\left[1-\exp^{-\left(\frac{x^2}{2}\right)}\right]^{M-1} dv_1 \end{aligned} \tag{6.48}$$

Using (6.36) in (6.48) and interchanging the order of integration and summation, we get

$$\begin{aligned} p_c = & \sum_{n=0}^{M-1}\frac{(-1)^n}{n+1}\binom{M-1}{n}\exp\left[\frac{-nE_s}{(n+1)N_0}\right] \\ & -\left[\int_0^{\sqrt{\frac{2\alpha_i E_s}{N_0}}} x\exp^{-\left(\frac{x^2}{2}+\frac{E_s}{N_0}\right)} I_0\left(\sqrt{\frac{2E_s}{N_0}}x\right)\left[1-\exp^{-\left(\frac{x^2}{2}\right)}\right]^{M-1} dx\right]. \end{aligned} \tag{6.49}$$

From (6.49), the probability of correct channel detection with FEC coding expressed in terms of E_b / N_o and code rate r is

$$\begin{aligned} p_c = & \sum_{n=0}^{M-1}\frac{(-1)^n}{n+1}\binom{M-1}{n}\exp\left[\frac{-nrmE_b}{(n+1)N_0}\right] \\ & -\left[\int_0^{\sqrt{\frac{2\alpha_i rmE_b}{N_0}}} x\exp^{-\left(\frac{x^2}{2}+\frac{rmE_b}{N_0}\right)} I_0\left(\sqrt{\frac{2rmE_b}{N_0}}x\right)\left[1-\exp^{-\left(\frac{x^2}{2}\right)}\right]^{M-1} dx\right]. \end{aligned} \tag{6.50}$$

As with coherent detection, the probability of block error is obtained by substituting (6.27), (6.42) and (6.50) into (6.24).

The performance for 32-ary orthogonal signaling with a (31, 15) RS code and EED in AWGN for different values of α is shown in Figures 33 and 34. From Figures 33 and 34, we see that performance degrades for large α $(\alpha > 0.6)$. There is not much difference in performance for α less than 0.4, and, at $P_b = 10^{-5}$, there is a slight improvement relative to $\alpha = 0.0$ when $\alpha = 0.5$.

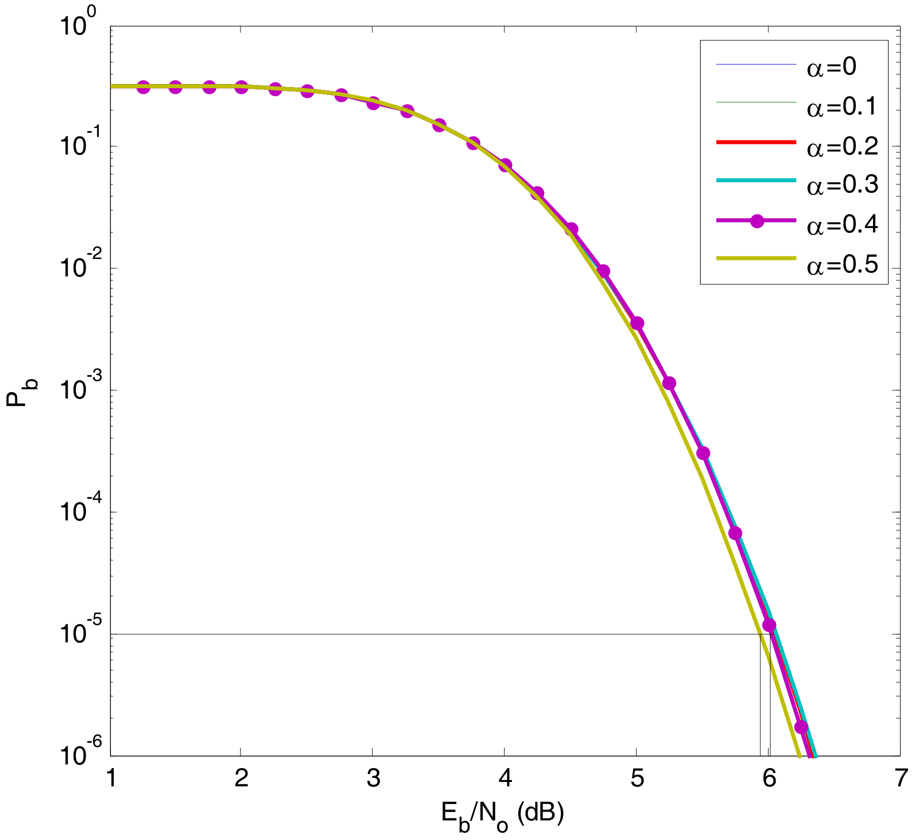

Figure 33. The performance of 32-ary orthogonal signaling with a (31, 15) RS code and EED in AWGN for different values of α for noncoherent demodulation.

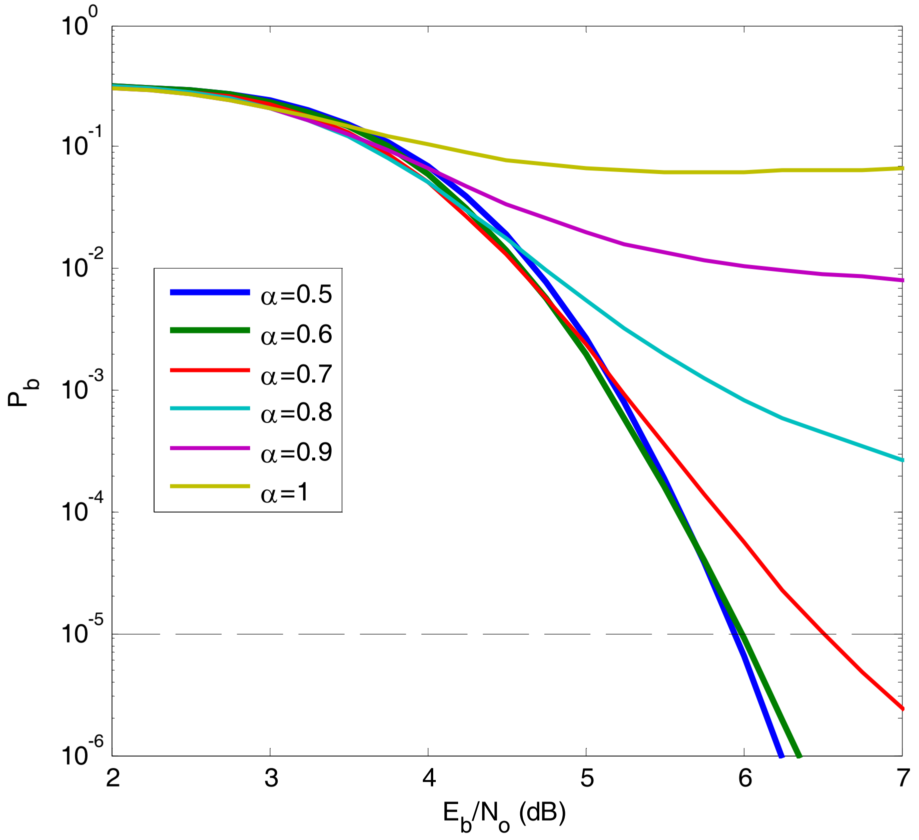

Figure 34. The performance of 32-ary orthogonal signaling with a (31, 15) RS code and EED in AWGN for different values of α for noncoherent demodulation.

C. COHERENT DEMODULATION IN AWGN AND PNI

The probability of channel erasure with FEC and EED in the presence of PNI is obtained from (2.13), (2.15) and (6.15) as

$$\begin{aligned} p_e = \rho\left[\left[1-Q\left((\alpha-1)\sqrt{\frac{2rm}{\frac{N_o}{E_b}+\frac{1}{\rho}\frac{N_I}{E_b}}}\right)\right]\times\left[1-Q\left(\alpha\sqrt{\frac{2rm}{\frac{N_o}{E_b}+\frac{1}{\rho}\frac{N_I}{E_b}}}\right)\right]^{M-1}\right] \\ +(1-\rho)\left[\left[1-Q\left((\alpha-1)\sqrt{\frac{2rmE_b}{N_o}}\right)\right]\times\left[1-Q\left(\alpha\sqrt{\frac{2rmE_b}{N_o}}\right)\right]^{M-1}\right]. \end{aligned} \tag{6.51}$$

Expressing (6.51) in terms of $\gamma_T = \left[1/\left(\gamma_b{}^{-1} + \left(\rho\gamma_I\right)^{-1}\right)\right]$ and γ_b, we get

$$p_e = \rho\left[\left[1-Q\left(\left(\alpha-1\right)\sqrt{2rm\gamma_T}\right)\right]\left[1-Q\left(\alpha\sqrt{2rm\gamma_T}\right)\right]^{M-1}\right] \\ +\left(1-\rho\right)\left[\left[1-Q\left(\left(\alpha-1\right)\sqrt{2rm\gamma_b}\right)\right]\left[1-Q\left(\alpha\sqrt{2rm\gamma_b}\right)\right]^{M-1}\right]. \tag{6.52}$$

Similarly, the probability of correct channel detection when PNI is present is given by

$$p_c = \rho\left[\frac{1}{\sqrt{2\pi}}\int_{-(1-\alpha)\sqrt{2rm\gamma_T}}^{\infty} e^{\left(\frac{-u^2}{2}\right)}\left[1-Q\left(u+\sqrt{2rm\gamma_T}\right)\right]^{M-1} du\right] \\ +\left(1-\rho\right)\left[\frac{1}{\sqrt{2\pi}}\int_{-(1-\alpha)\sqrt{2rm\gamma_b}}^{\infty} e^{\left(\frac{-u^2}{2}\right)}\left[1-Q\left(u+\sqrt{2rm\gamma_b}\right)\right]^{M-1} du\right]. \tag{6.53}$$

The probability of channel symbol error with EED and the probability of block error are now obtained as before when only AWGN was present.

The performance of 32-ary orthogonal signaling with (31, 15) RS coding for different α where $\rho = 0.1$ ($E_b / N_0 = 10$ dB) in the presence of AWGN and PNI is shown in Figure 35. We observe that $0.0 \le \alpha \le 0.5$ provides almost the same performance at $P_b = 10^{-5}$, while $\alpha = 0.6$ gives poorer performance. For $\alpha \ge 0.7$, the performance worsens significantly. Since $\alpha = 0.0$ implies no EED, we conclude that there is very little improvement in the performance of the alternative JTIDS waveform when EED is used in the presence of AWGN and PNI.

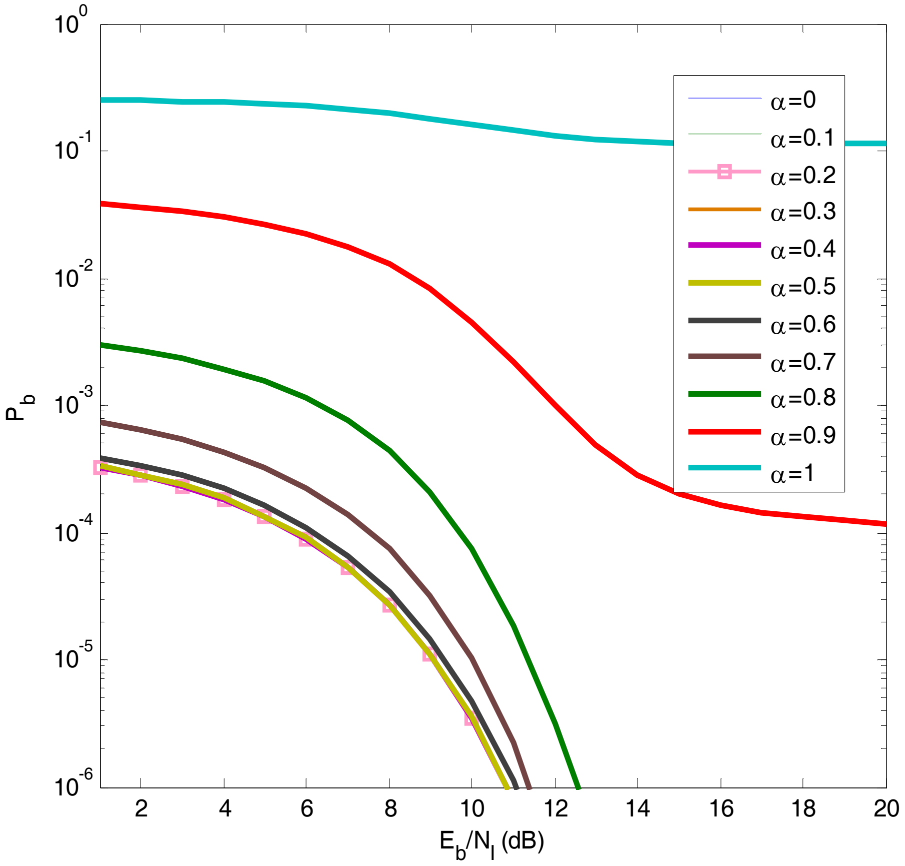

Figure 35. The performance of 32-ary orthogonal signaling with EED in AWGN and PNI for different values of α with $\rho = 0.1$ for coherent demodulation when $E_b / N_0 = 10$ dB.

The performance of 32-ary orthogonal signaling with (31, 15) RS coding for different α where $\rho = 0.2$ ($E_b / N_0 = 10$ dB) in the presence of AWGN and PNI is shown in Figure 36. We observe that now $0.0 \leq \alpha \leq 0.7$ provides almost the same performance at $P_b = 10^{-5}$, while for $\alpha \geq 0.7$, performance worsens significantly.

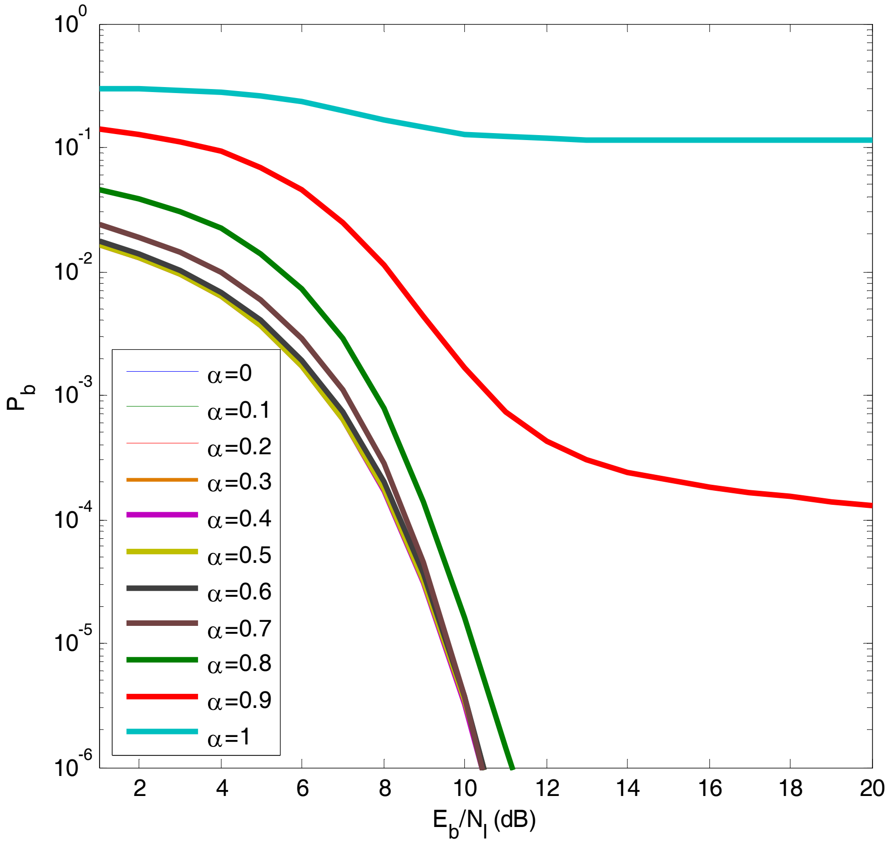

Figure 36. The performance of 32-ary orthogonal signaling with EED in AWGN and PNI for different values of α with $\rho = 0.2$ for coherent demodulation when $E_b / N_0 = 10$ dB.

The performance of 32-ary orthogonal signaling with (31, 15) RS coding for different α where $\rho = 1$ ($E_b / N_0 = 10$ dB) in the presence of AWGN and PNI is shown in Figure 37. As previously, when $\rho < 1$, we observe that $0.0 \le \alpha < 0.7$ provides almost the same performance at $P_b = 10^{-5}$, while for $\alpha \ge 0.7$, performance worsens significantly.

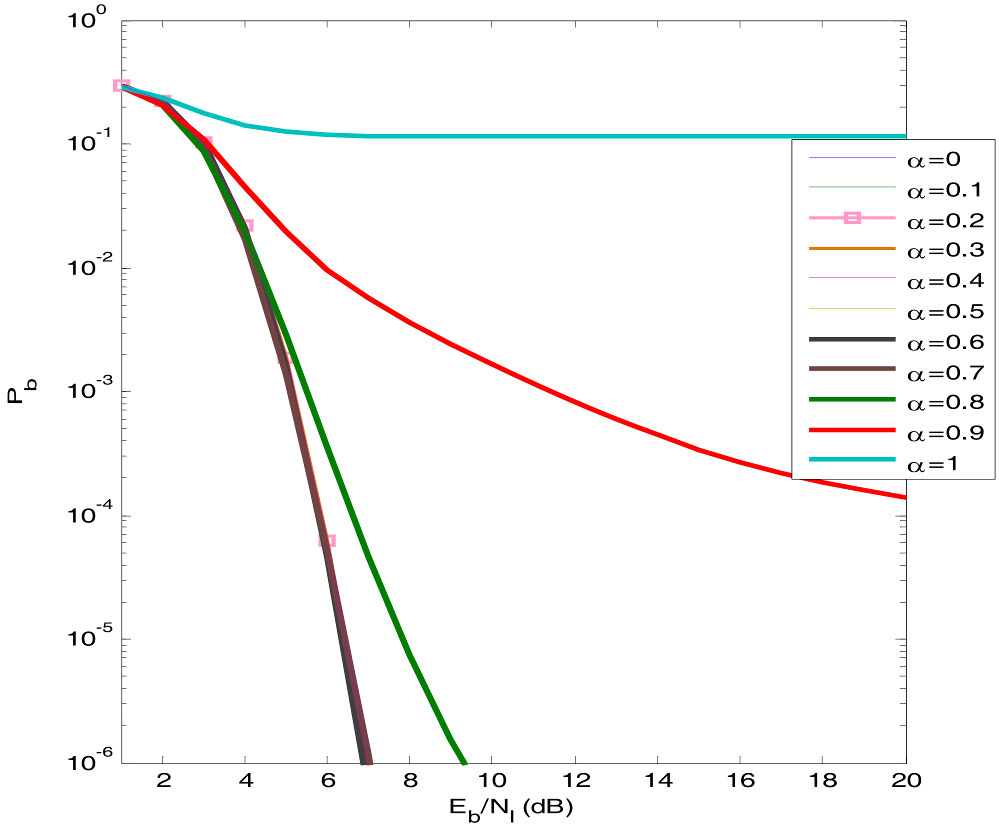

Figure 37. The performance of 32-ary orthogonal signaling with EED in AWGN and PNI for different values of α with $\rho = 1$ for coherent demodulation when $E_b / N_0 = 10$ dB.

Next, we investigate the performance of the alternative waveform with EED for different ρ when $\alpha = 0.5$ since this results in slightly better performance at $P_b = 10^{-5}$. The performance of 32-ary orthogonal signaling with (31, 15) RS coding with EED in a PNI environment for various values of ρ with $\alpha = 0.5$ and $E_b / N_0 = 10$ dB is shown in Figure 38. We observe that at $P_b = 10^{-5}$, as ρ decreases, performance is degraded, but the degradation is limited to about 3.0 dB.

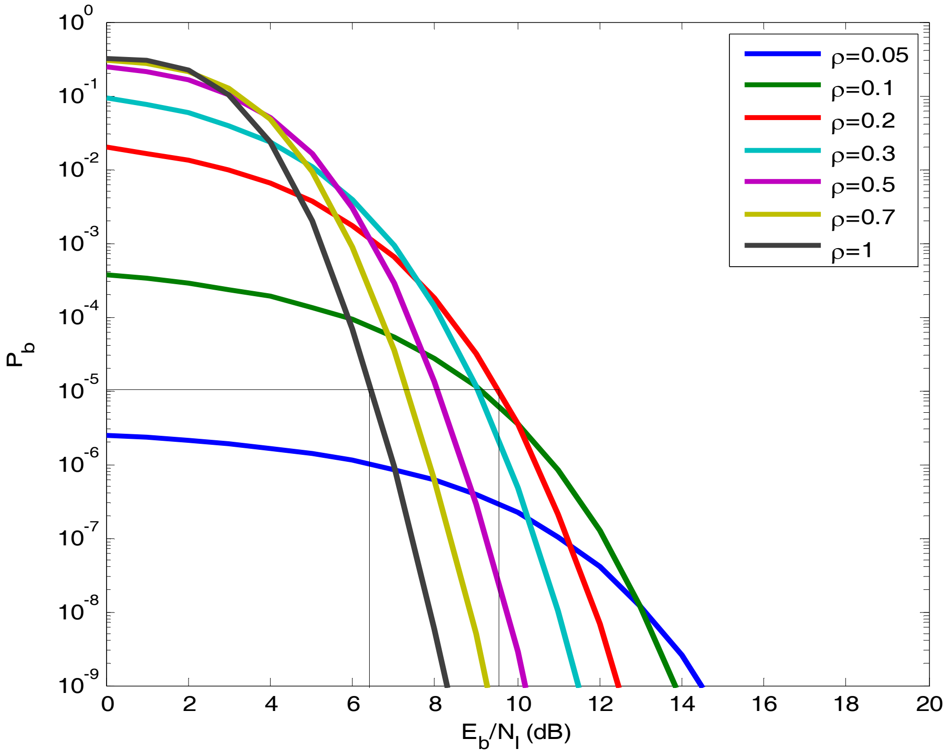

Figure 38. The performance of 32-ary orthogonal signaling with EED in AWGN and PNI with $\alpha = 0.5$ and $E_b / N_0 = 10$ dB for different values of ρ for coherent demodulation.

Comparing the results from Figures 8 and 9 ($E_b / N_0 = 10\,\text{dB}$ and $\alpha = 0.0$) with those from Figure 38 ($E_b / N_0 = 10\,\text{dB}$ and $\alpha = 0.5$), we see that for $P_b = 10^{-5}$ and $0.2 \le \rho \le 1$, performance is about the same or even slightly worse when EED is used.

Next, we investigate the performance of 32-ary orthogonal signaling with (31, 15) RS coding for different α where $\rho = 0.1$ and $E_b / N_0 = 6.8$ dB in the presence of AWGN and PNI is shown in Figure 39. We observe that $0.0 \le \alpha \le 0.4$ provides almost the same performance at $P_b = 10^{-5}$, while $\alpha = 0.5$ gives slightly poorer performance. For $\alpha \ge 0.6$, the performance worsens significantly. Since $\alpha = 0.0$ implies no EED, we conclude that there is very little improvement in the performance of the alternative JTIDS waveform when EED is used in the presence of AWGN and PNI regardless of whether E_b / N_0 is large or not.

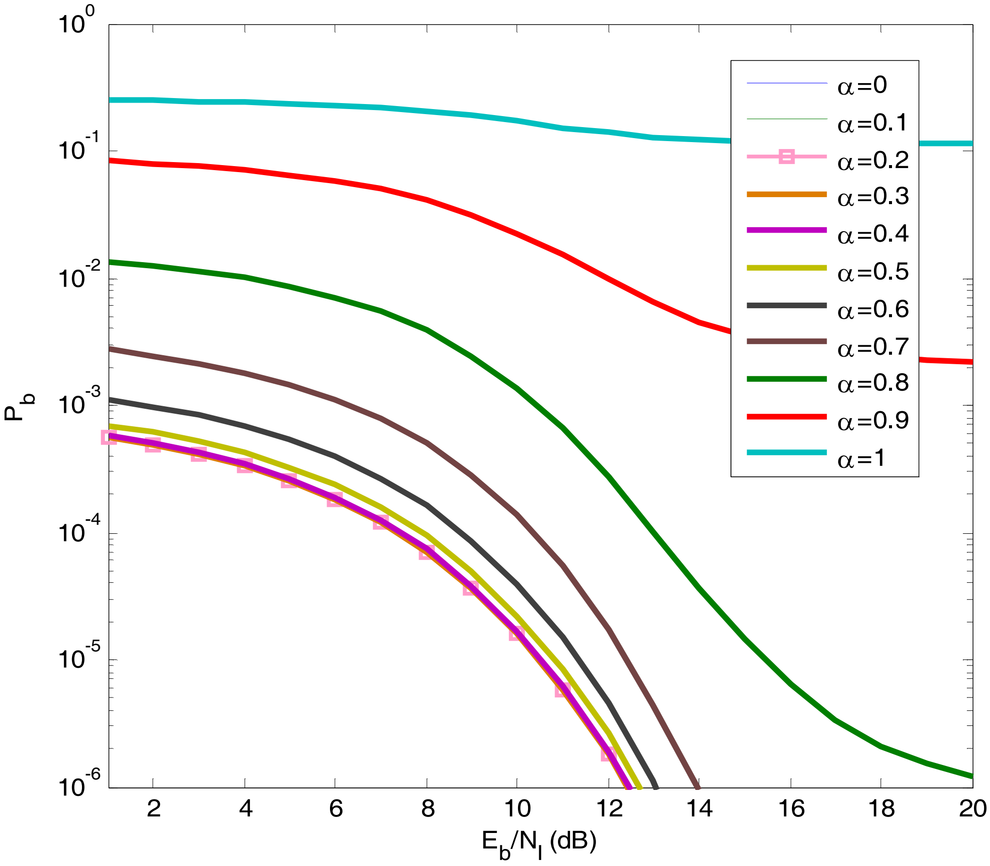

Figure 39. The performance of 32-ary orthogonal signaling with EED in AWGN and PNI for different values of α with $\rho = 0.1$ for coherent demodulation when $E_b / N_0 = 6.8$ dB.

As previously, the performance of 32-ary orthogonal signaling with (31, 15) RS coding for different α where $\rho = 0.2$ ($E_b / N_0 = 6.8$ dB) in the presence of AWGN and PNI is shown in Figure 40. We observe that $0.0 \le \alpha \le 0.4$ provides almost the same performance at $P_b = 10^{-5}$. For $\alpha > 0.6$, performance worsens significantly.

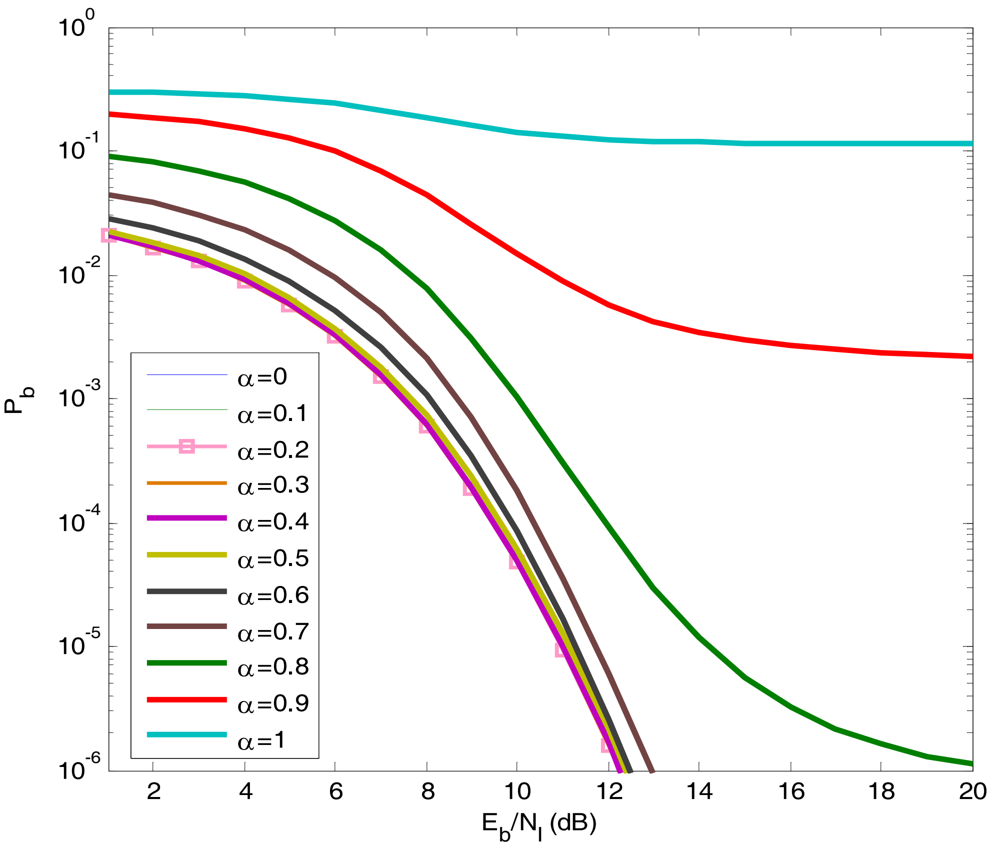

Figure 40. The performance of 32-ary orthogonal signaling with EED in AWGN and PNI for different values of α with $\rho = 0.2$ for coherent demodulation when $E_b / N_0 = 6.8$ dB.

Additionally, the performance of 32-ary orthogonal signaling with (31, 15) RS coding for different α where $\rho = 1$ ($E_b / N_0 = 6.8$ dB) in the presence of AWGN and PNI is shown in Figure 41. As previously, when $\rho < 1$, we observe that $0.0 \le \alpha < 0.5$ provides almost the same performance at $P_b = 10^{-5}$, while for $\alpha \ge 0.7$, performance worsens significantly.

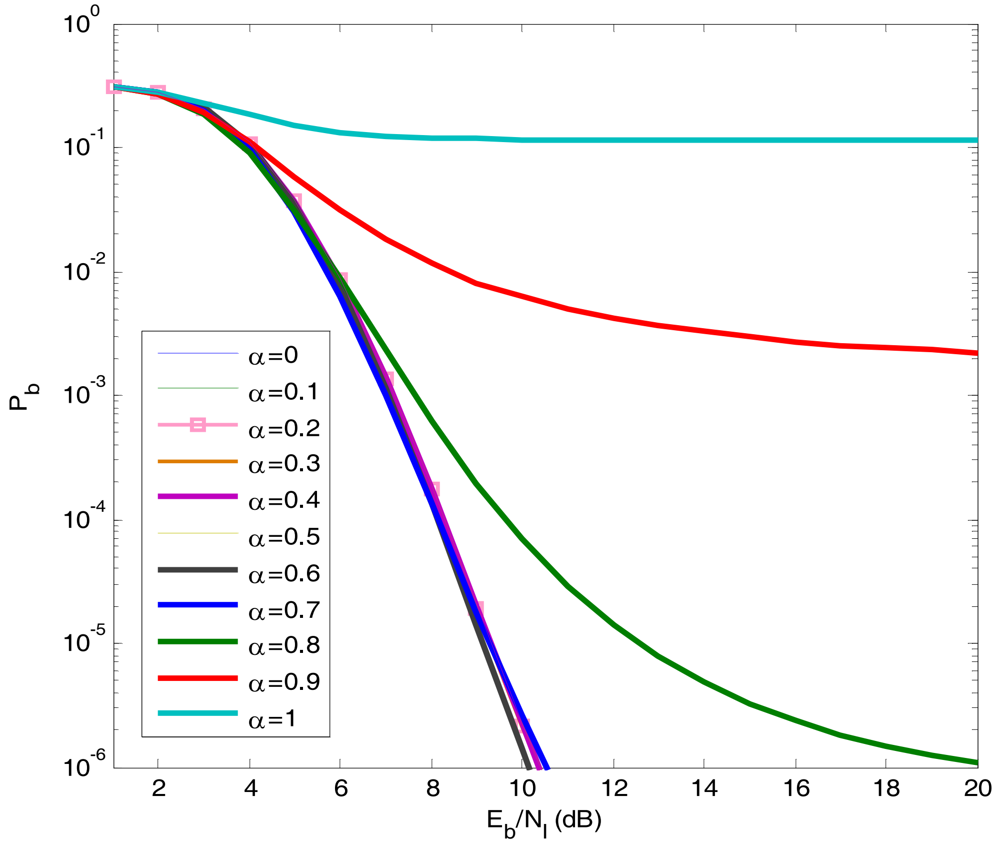

Figure 41. The performance of 32-ary orthogonal signaling with EED in AWGN and PNI for different values of α with $\rho = 1$ for coherent demodulation when $E_b / N_0 = 6.8$ dB.

Finally, we investigate the performance of the alternative waveform with EED for different ρ when $\alpha = 0.3$ since this results in slightly better performance at $P_b = 10^{-5}$. The performance of 32-ary orthogonal signaling with (31, 15) RS coding with EED in a PNI environment for various values of ρ with $\alpha = 0.3$ and $E_b / N_0 = 6.8$ dB is shown in Figure 42. We observe that at $P_b = 10^{-5}$, as ρ decreases, performance is degraded, but the degradation is limited to about 1.7 dB.

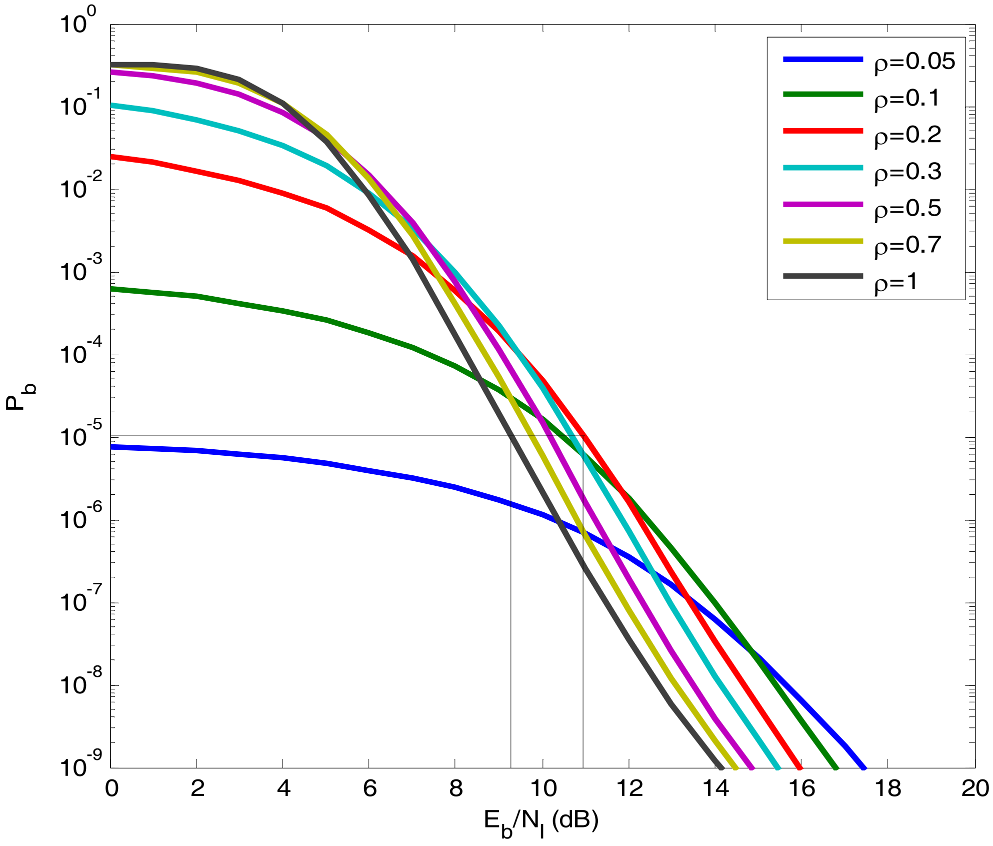

Figure 42. The performance of 32-ary orthogonal signaling with EED in AWGN and PNI with $\alpha = 0.3$ and $E_b / N_0 = 6.8$ dB for different values of ρ for coherent demodulation.

Again, comparing the results from Figures 8 and 9 ($E_b / N_0 = 6.8$dB and $\alpha = 0.0$) with those from Figure 42 ($E_b / N_0 = 6.8$dB and $\alpha = 0.3$), we see that for $P_b = 10^{-5}$ and $0.2 \le \rho \le 1$, performance is about the same or even slightly worse, just as when E_b / N_0 is larger. As a result, we conclude that EED provides no additional benefit when coherent detection is used.

D. NONCOHERENT DEMODULATION IN AWGN AND PNI

The probability of channel erasure with FEC and EED in the presence of PNI is obtained from (2.13), (2.15) and (6.42) as

$$p_e = \rho\left[\left[\int_0^{\sqrt{2\alpha\frac{rm}{\frac{N_o}{E_b}+\frac{1}{\rho}\frac{N_I}{E_b}}}} x\exp\left[-\left(\frac{x^2}{2}+\frac{rm}{\frac{N_o}{E_b}+\frac{1}{\rho}\frac{N_I}{E_b}}\right)\right] I_0\left(\sqrt{2\frac{rm}{\frac{N_o}{E_b}+\frac{1}{\rho}\frac{N_I}{E_b}}}x\right)dx\right]\sum_{n=0}^{M-1}(-1)^n\binom{M-1}{n}\exp\left[\frac{-n\alpha rm}{\frac{N_o}{E_b}+\frac{1}{\rho}\frac{N_I}{E_b}}\right]\right] \tag{6.54}$$

$$+(1-\rho)\left[\left[\int_0^{\sqrt{2\alpha\frac{rmE_b}{N_0}}} x\exp\left[-\left(\frac{x^2}{2}+\frac{rmE_b}{N_0}\right)\right] I_0\left(\sqrt{2\frac{rmE_b}{N_0}x}\right)dx\right]\sum_{n=0}^{M-1}(-1)^n\binom{M-1}{n}\exp\left[\frac{-n\alpha rmE_b}{N_0}\right]\right].$$

Expressing (6.54) in terms of $\gamma_T = \left[1/\left(\gamma_b^{-1}+\left(\rho\gamma_I\right)^{-1}\right)\right]$ and γ_b, we get

$$p_e = \rho\left[\left[\int_0^{\sqrt{2\alpha rm\gamma_T}} x\exp\left[-\left(\frac{x^2}{2}+rm\gamma_T\right)\right] I_0\left(\sqrt{2rm\gamma_T x}\right)dx\right]\sum_{n=0}^{M-1}(-1)^n\binom{M-1}{n}\exp\left[-n\alpha rm\gamma_T\right]\right] \tag{6.55}$$

$$+(1-\rho)\left[\left[\int_0^{\sqrt{2\alpha rm\gamma_b}} x\exp\left[-\left(\frac{x^2}{2}+rm\gamma_b\right)\right] I_0\left(\sqrt{2rm\gamma_b x}\right)dx\right]\sum_{n=0}^{M-1}(-1)^n\binom{M-1}{n}\exp\left[-n\alpha rm\gamma_b\right]\right]$$

In a similar manner, the probability of correct channel detection with FEC and EED in the presence of PNI is obtained by adapting (6.50) to get

$$p_c = \rho\left[\sum_{n=0}^{M-1}\frac{(-1)^n}{n+1}\binom{M-1}{n}\exp\left(-\frac{nrm\gamma_T}{n+1}\right)-\int_{-\infty}^{\sqrt{2r\alpha m\gamma_T}} xe^{-\left(\frac{x^2}{2}+rm\gamma_T\right)}\left[1-\exp\left(-\tfrac{x^2}{2}\right)^{M-1}\right]I_0\left(\sqrt{2rm\gamma_T x}\right)dx\right]$$
$$+(1-\rho)\left[\sum_{n=0}^{M-1}\frac{(-1)^n}{n+1}\binom{M-1}{n}\exp\left(-\frac{nrm\gamma_b}{n+1}\right)-\int_{-\infty}^{\sqrt{2r\alpha m\gamma_b}} xe^{-\left(\frac{x^2}{2}+rm\gamma_b\right)}\left[1-\exp\left(-\tfrac{x^2}{2}\right)^{M-1}\right]I_0\left(\sqrt{2rm\gamma_b x}\right)dx\right] \tag{6.56}$$

The probability of channel symbol error with EED and the probability of block error are now obtained as before when only AWGN was present.

The performance of 32-ary orthogonal signaling with (31, 15) RS coding for different α where $\rho = 0.1$ ($E_b/N_0 = 10$ dB) in the presence of AWGN and PNI is shown in Figure 43. We observe that, for $P_b = 10^{-5}$, $0.0 \le \alpha \le 0.3$ provides almost the same performance. For $\alpha > 0.4$, the performance worsens significantly. Since $\alpha = 0.0$ implies no EED, we conclude that there is very little improvement in the performance of the alternative JTIDS waveform from using EED in the presence of AWGN and PNI.

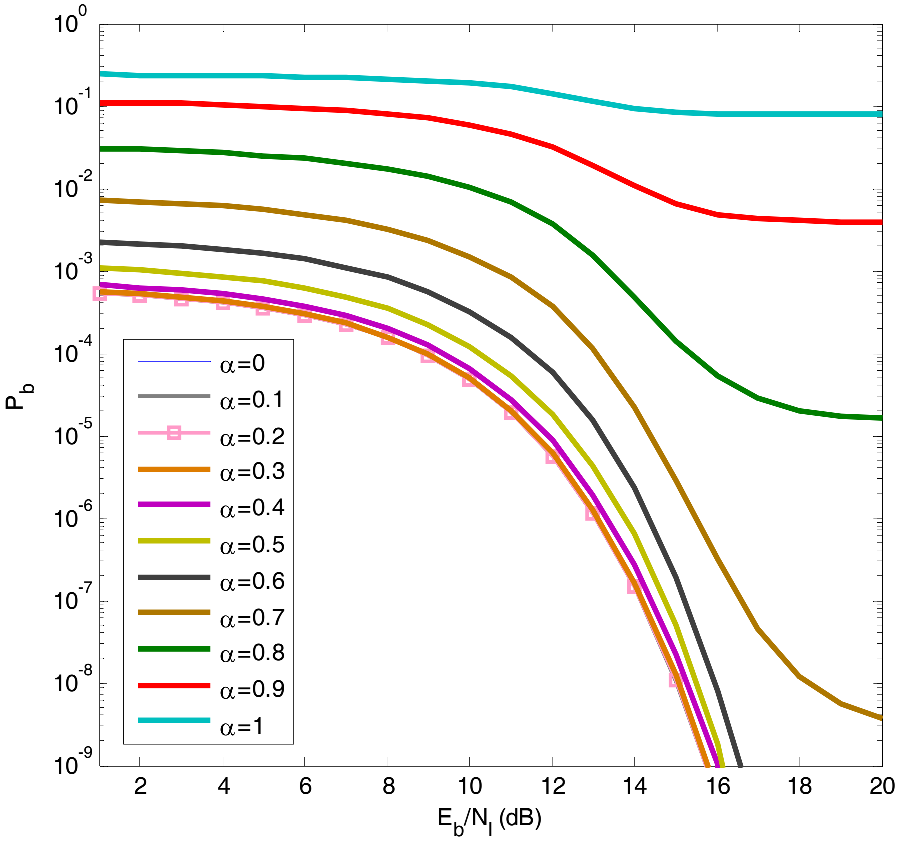

Figure 43. The performance of 32-ary orthogonal signaling with EED in AWGN and PNI for different values of α with $\rho = 0.1$ and for noncoherent demodulation when $E_b / N_0 = 10$ dB.

The performance of 32-ary orthogonal signaling with (31, 15) RS coding for different α where $\rho = 0.2$ ($E_b / N_0 = 10$ dB) in the presence of AWGN and PNI is shown in Figure 44. We observe that for $P_b = 10^{-5}$, $0.0 \le \alpha \le 0.4$ provides almost the same performance. For $\alpha \ge 0.6$, performance worsens significantly.

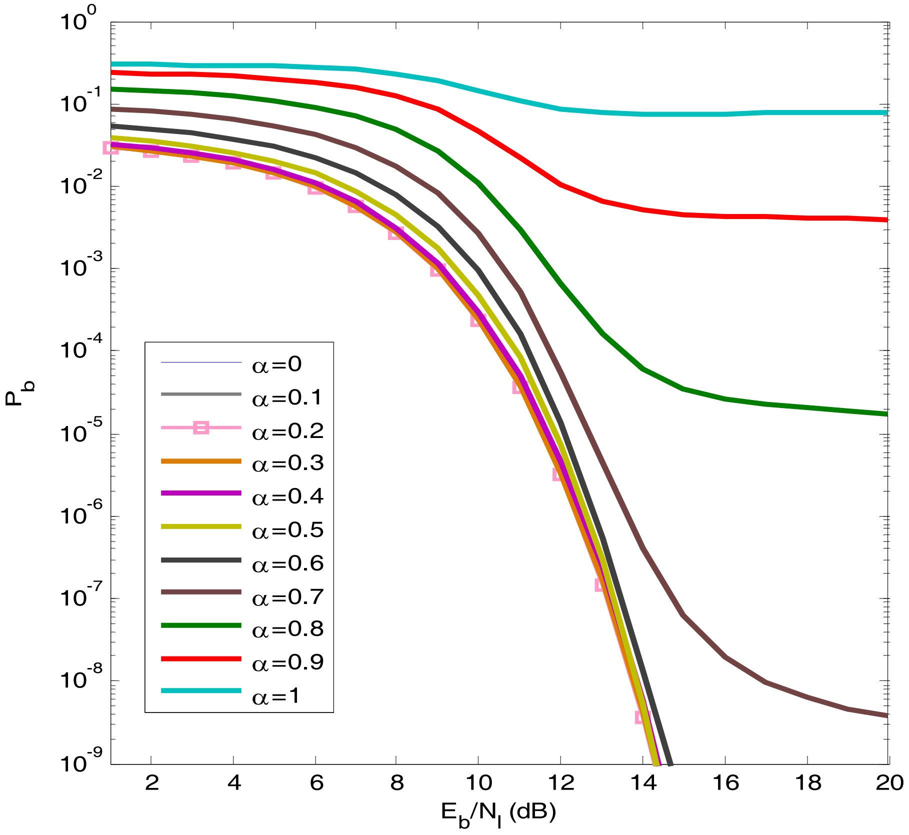

Figure 44. The performance of 32-ary orthogonal signaling with EED in AWGN and PNI for different values of α with $\rho = 0.2$ and for noncoherent demodulation when $E_b / N_0 = 10$ dB.

The performance of 32-ary orthogonal signaling with (31, 15) RS coding for different values of α where $\rho = 1$ ($E_b / N_0 = 10$ dB) in the presence of AWGN and PNI is shown in Figure 45. We observe that $0.0 \le \alpha \le 0.6$ provides almost the same performance at $P_b = 10^{-5}$, but $\alpha = 0.5$ gives slightly better performance than $\alpha = 0.0$. For $\alpha > 0.6$, performance worsens significantly.

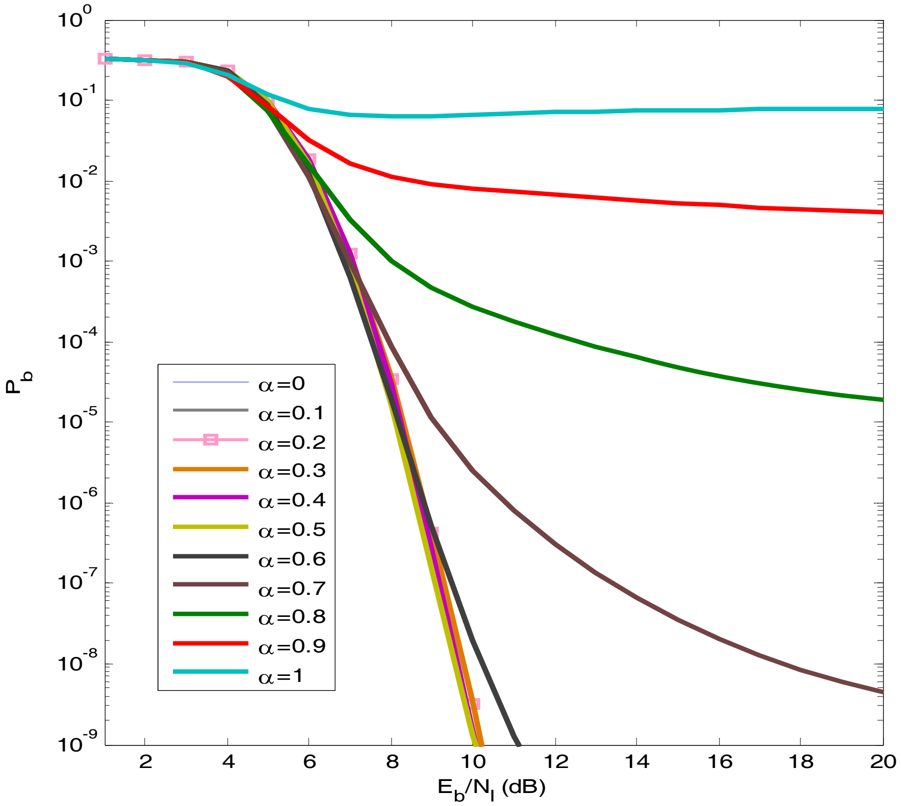

Figure 45. The performance of 32-ary orthogonal signaling with EED in AWGN and PNI for different values of α with $\rho = 1$ and for noncoherent demodulation when $E_b / N_0 = 10$ dB.

Next, we investigate the performance of the alternative waveform with EED for different ρ when $\alpha = 0.3$ since performance is slightly better for $P_b = 10^{-5}$. The performance of 32-ary orthogonal signaling with (31, 15) RS coding with EED in a PNI environment for various values of ρ with $\alpha = 0.3$ and $E_b / N_0 = 10$ dB is shown in Figure 46. We observe that, for $P_b = 10^{-5}$, as ρ decreases, performance is degraded, but the degradation is limited to about 3.0 dB.

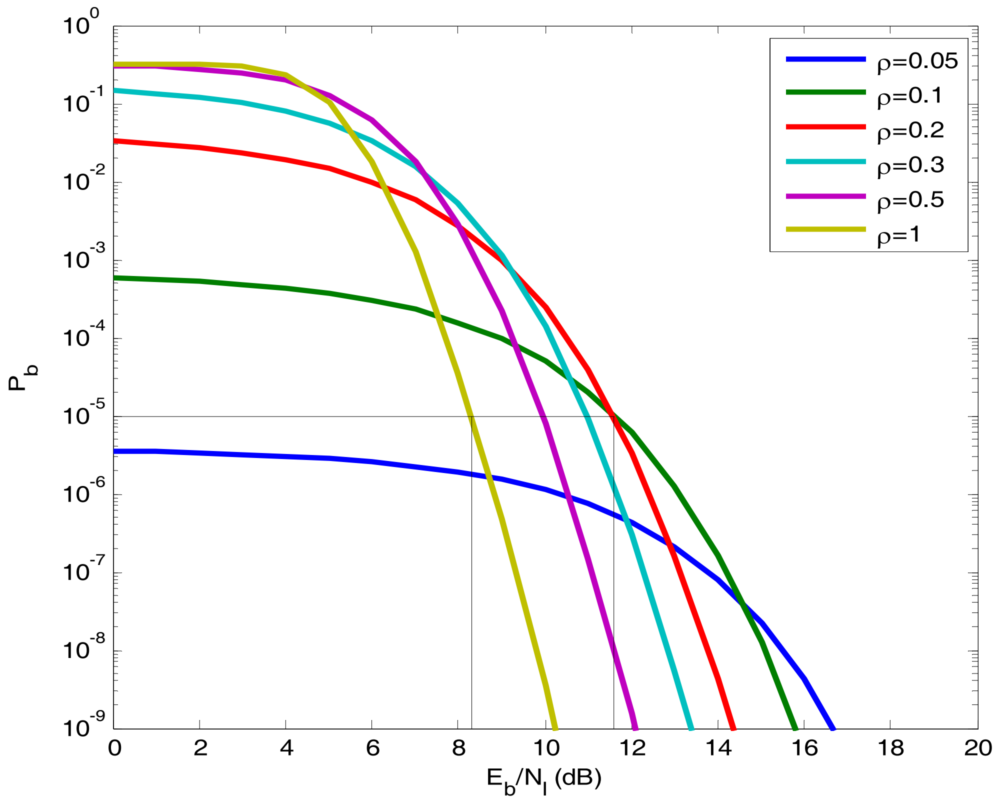

Figure 46. The performance of 32-ary orthogonal signaling with EED in AWGN and PNI with $\alpha = 0.3$ and $E_b / N_0 = 10$ dB for and different values of ρ for noncoherent demodulation.

Comparing the results of Figures 8 and 9 ($E_b / N_0 = 10\,\text{dB}$ and $\alpha = 0.0$) with those of Figure 46 ($E_b / N_0 = 10\,\text{dB}$ and $\alpha = 0.3$), we see that for $P_b = 10^{-5}$ and $0.1 \leq \rho \leq 1$, performance is not improved by EED.

Next, the performance of 32-ary orthogonal signaling with (31, 15) RS coding for different α where $\rho = 0.1$ and $E_b / N_0 = 6.8$ dB in the presence of AWGN and PNI is shown in Figure 47. We observe that $0.0 \leq \alpha \leq 0.4$ provides almost the same performance at $P_b = 10^{-5}$, while $\alpha = 0.5$ and $\alpha = 0.6$ give poorer performance. For $\alpha > 0.6$, the performance worsens significantly. Since $\alpha = 0.0$ implies no EED, we conclude that there is very little improvement in the performance of the alternative JTIDS waveform when EED is used in the presence of AWGN and PNI.

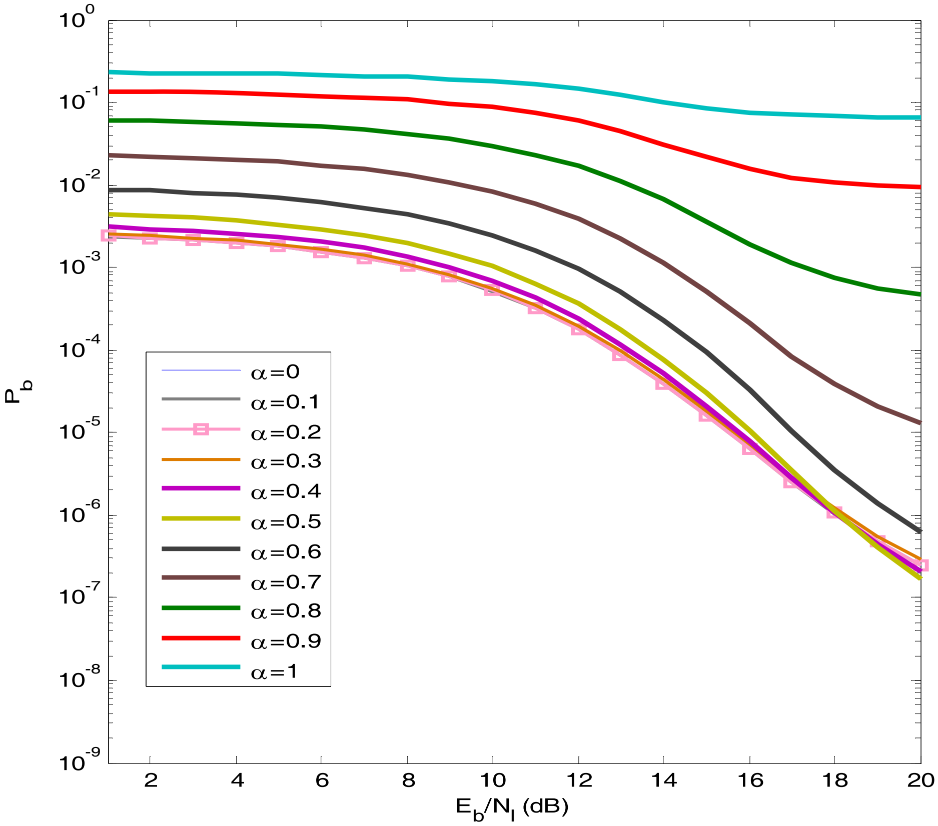

Figure 47. The performance of 32-ary orthogonal signaling with EED in AWGN and PNI for different values of α with $\rho = 0.1$ and for noncoherent demodulation when $E_b / N_0 = 6.8$ dB.

As previously, the performance of 32-ary orthogonal signaling with (31, 15) RS coding for different α where $\rho = 0.2$ ($E_b / N_0 = 6.8$ dB) in the presence of AWGN and PNI is shown in Figure 48. We observe that, for $P_b = 10^{-5}$, $0.0 \le \alpha \le 0.5$ provides almost the same performance. For $\alpha \ge 0.6$, performance worsens significantly.

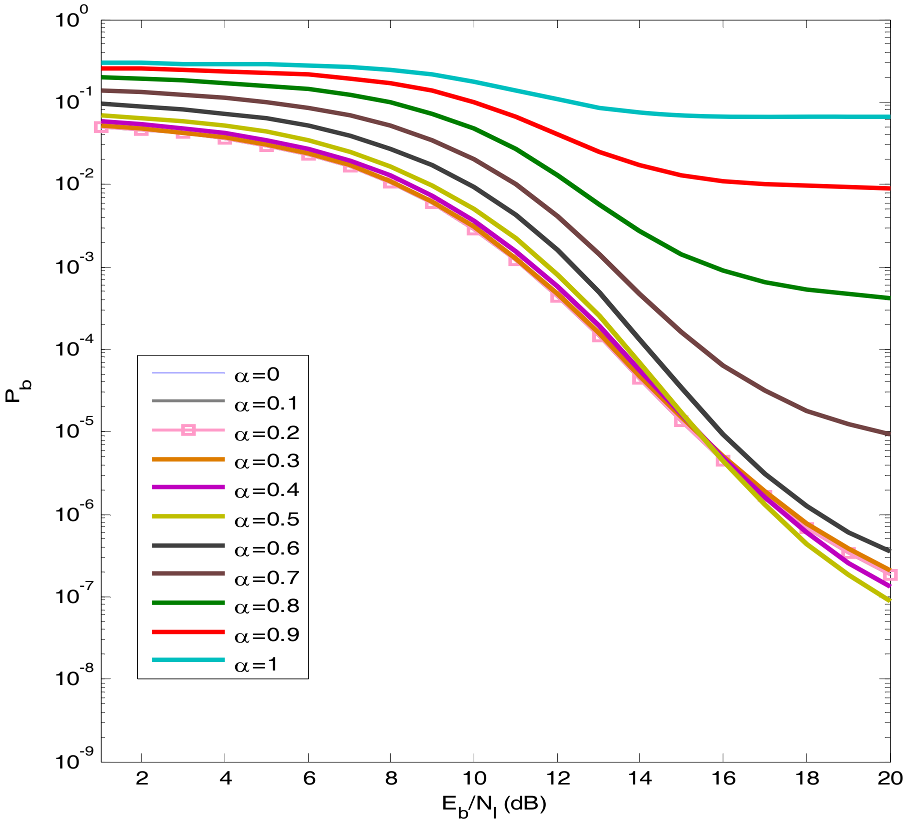

Figure 48. The performance of 32-ary orthogonal signaling with EED in AWGN and PNI for different values of α with $\rho = 0.2$ and for noncoherent demodulation when $E_b / N_0 = 6.8$ dB.

Finally, the performance of 32-ary orthogonal signaling with (31, 15) RS coding for different values of α where $\rho = 1$ ($E_b / N_0 = 6.8$ dB) in the presence of AWGN and PNI is shown in Figure 49. We observe that $\alpha = 0.2$ and $\alpha = 0.4$ provide almost the same performance at $P_b = 10^{-5}$, while $\alpha = 0.5$ and $\alpha = 0.6$ give slightly better performance than $\alpha = 0.0$. For $\alpha \geq 0.7$, performance worsens significantly.

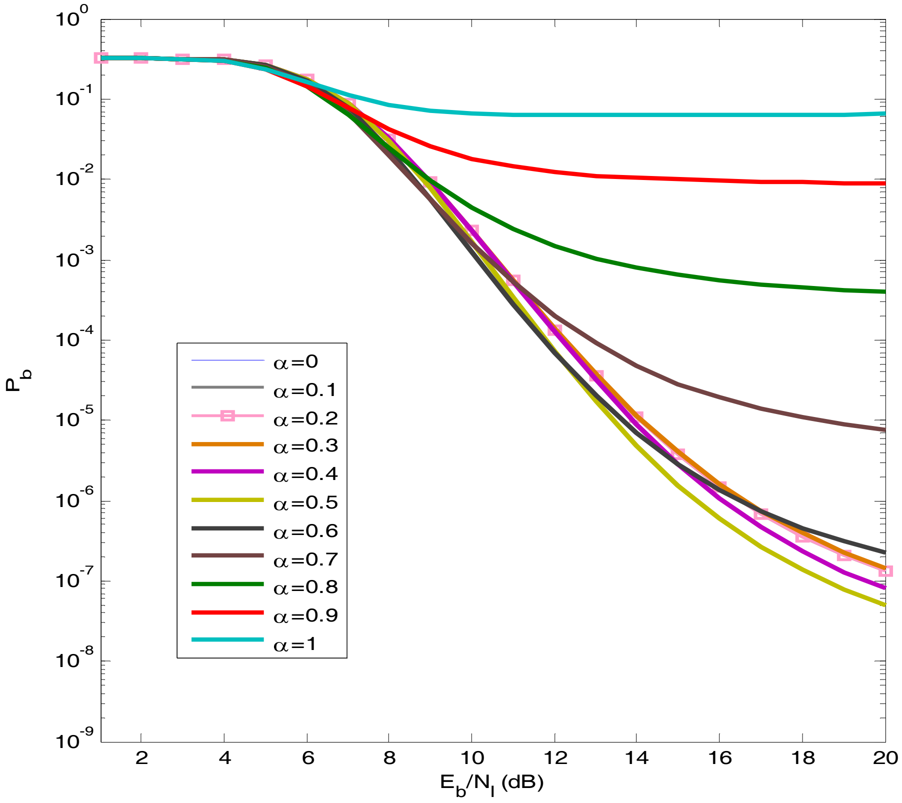

Figure 49. The performance of 32-ary orthogonal signaling with EED in AWGN and PNI for different values of α with $\rho = 1$ and for noncoherent demodulation when $E_b / N_0 = 6.8$ dB.

Now, we consider the performance of the alternative waveform with EED for different ρ when $\alpha = 0.3$ since performance is slightly better for $P_b = 10^{-5}$. The performance of 32-ary orthogonal signaling with (31, 15) RS coding with EED in a PNI environment for various values of ρ with $\alpha = 0.3$ and $E_b / N_0 = 6.8$ dB is shown in Figure 50. We observe that, for $P_b = 10^{-5}$, as ρ decreases, performance is degraded, but the degradation is limited to about 1.4 dB.

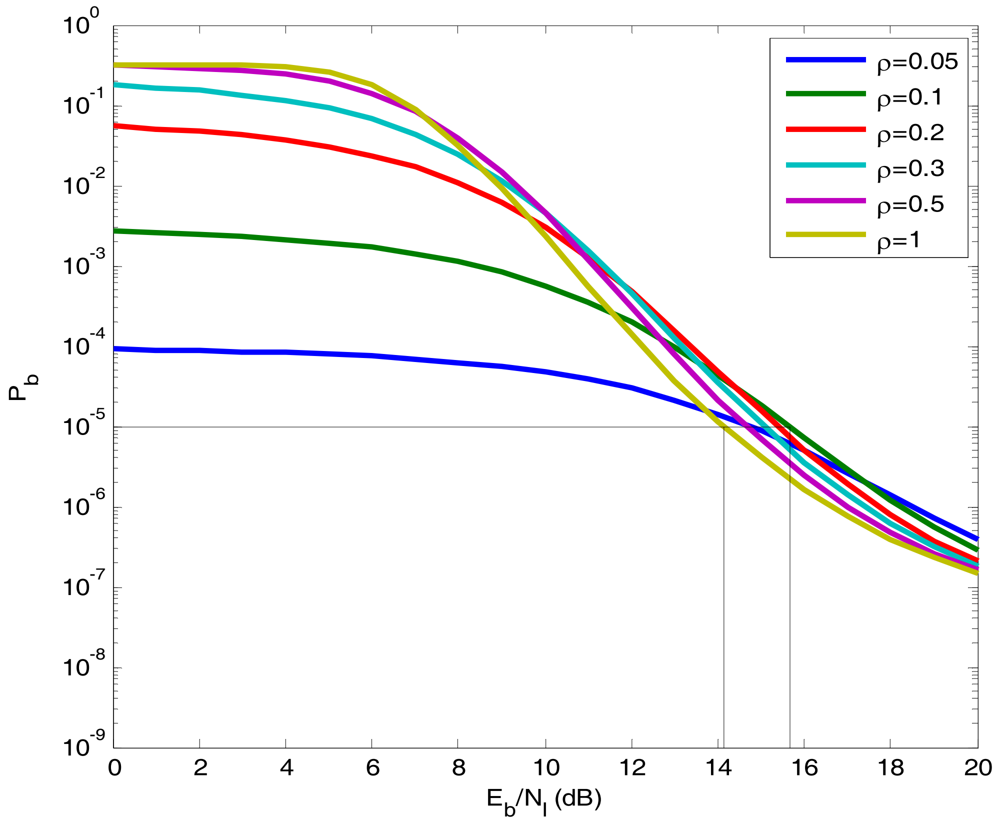

Figure 50. The performance of 32-ary orthogonal signaling with EED in AWGN and PNI with $\alpha = 0.3$ and $E_b / N_0 = 6.8$ dB for and different values of ρ for noncoherent demodulation.

gain, comparing the results from Figures 8 and 9 ($E_b / N_0 = 6.8$dB and $\alpha = 0.0$) with those from Figure 50 ($E_b / N_0 = 6.8$dB and $\alpha = 0.3$), we see that for $P_b = 10^{-5}$ and $0.1 \le \rho \le 1$, performance is not improved by using EED.

E. CHAPTER SUMMARY

In this chapter, the performance of the alternative JTIDS waveform with EED in AWGN only as well as AWGN and PNI for both coherent and noncoherent demodulation was examined. In the next chapter, the findings of this thesis are summarized.

VII. CONCLUSIONS AND FUTURE WORK

A. CONCLUSIONS

This thesis presented an alternative JTIDS/Link-16 waveform, 32-ary orthogonal signaling with (31, 15) RS coding, to the JTIDS/Link-16 waveform. Both coherent and noncoherent demodulation of the proposed waveform were analyzed, and subsequently the performance obtained was compared with that for the existing JTIDS/Link-16 waveform for AWGN as well as PNI. When only AWGN is present, the alternative waveform outperforms the JTIDS/Link-16 waveform by 1.7 dB and 1.4 dB for coherent and noncoherent detection, respectively, when $P_b = 10^{-5}$. When PNI is also present, the maximum degradation of the alternative waveform is 2.8 dB and 3.1 dB at $\rho = 0.2$ for coherent and noncoherent detection, respectively, when $P_b = 10^{-5}$ and $E_b / N_0 = 10 \text{ dB}$. For the same conditions, the JTIDS/Link-16 waveform suffers a further degradation of 3.1 dB and 4.2 dB for coherent and noncoherent detection, respectively. When E_b / N_0 is reduced, the absolute improvement in performance obtained with the alternative waveform is smaller.

We found very little benefit to EED for the alternative waveform since there is only a small improvement in performance as compared to errors-only decoding regardless of whether detection is coherent or noncoherent. This result is rather surprising since EED usually improves the performance of a waveform when PNI is present.

B. FUTURE RESEARCH AREAS

We examined an alternative JTIDS/Link-16 waveform that consists of 32-ary orthogonal signaling with (31,15) RS coding and provides an improvement in performance over the existing JTIDS/Link-16 waveform.

The performance of either the original or the alternative waveform might be further improved by using either a concatenated code or a non-binary convolutional code. The alternative waveform should also be evaluated assuming differential encoding. In this thesis, the alternative waveform is compared only to the JTIDS/Link-16 single-pulse waveform. The alternative waveform should be evaluated as a double-pulse waveform and compared to the JTIDS/Link-16 double-pulse waveform. Finally, the alternative waveform should be analyzed when channel fading is a factor.

LIST OF REFERENCES

[1] Dr. Carlo Kopp, "Network Centric Warfare Fundamentals – Part 3" [Online]. Available at: http://www.ausairpower.net/NCW-101-3.pdf.

[2] Michael B. Pursley, Thomas C. Royster, IV, and Michael Y. Tan, "High-Rate Direct- Sequence Spread Spectrum" *Proc. IEEE MILCOM*, vol. 2, pp. 1101-1106, Clemson University, SC, Oct 2003.

[3] Michael B. Pursley, and Thomas C. Royster, IV, "High-Rate Direct-Sequence Spread Spectrum With Error-Control Coding," *IEEE Transactions on Communications*, vol. 54, No.9, pp. 1693-1702, September 2006.

[4] Hua Wang, Jingming Kuang, Zheng Wang, Hui Xu, "Transmission Performance Evaluation of JTIDS", *Proc. IEEE MILCOM*, vol. 4, pp. 2264 – 2268, October 2005.

[5] Chi-Han Kao, "Performance Analysis of JTIDS/Link-16-type Waveform Subject to Narrowband Waveform over Slow, Flat Nakagami Fading Channels," *Proc. IEEE MILCOM*, Nov 2008, submitted for publication.

[6] R. C. Robertson, class notes for EC4550 (M-ary Digital Communication Systems), Naval Postgraduate School, Monterey, CA, 2007 (unpublished).

[7] R. C. Robertson, class notes for EC4580 (Error Correction Coding), Naval Postgraduate School, Monterey, CA, 2007 (unpublished).

[8] Northrop Grumman Corporation, Information Technology Communication & Information Systems Division, *Understanding Link-16: A Guidebook for New Users*, NCTSI, San Diego, CA, Sept 2001 (Prepared, April 1994, First Revision, September 1998; Second Revision, December 1998; Third Revision, September 2001).

THIS PAGE INTENTIONALLY LEFT BLANK

INITIAL DISTRIBUTION LIST

1. Defense Technical Information Center
Ft. Belvoir, Virginia

2. Dudley Knox Library
Naval Postgraduate School
Monterey, California

3. Chairman, Code IS
Department of Information Sciences
Naval Postgraduate School
Monterey, California

4. Chairman, Code EC
Department of Electrical and Computer Engineering
Naval Postgraduate School
Monterey, California

5. Professor R. Clark Robertson, Code EC/Rc
Department of Electrical and Computer Engineering
Naval Postgraduate School
Monterey, California

6. Professor Tri Ha, Code EC/Ha
Department of Electrical and Computer Engineering
Naval Postgraduate School
Monterey, California

7. Embassy of Greece
Office of Naval Attaché
Washington, District of Columbia

8. LT Lekkakos Dimitrios
Hellenic Navy General Staff
Athens, Greece